

LAPLACIAN GROWTH & SANDPILES ON THE SIERPINSKI GASKET: LIMIT SHAPE UNIVERSALITY AND EXACT SOLUTIONS

JOE P. CHEN AND JONAH KUDLER-FLAM

ABSTRACT. We establish quantitative spherical shape theorems for rotor-router aggregation and abelian sandpile growth on the graphical Sierpinski gasket (SG) when particles are launched from the corner vertex.

In particular, the abelian sandpile growth problem is exactly solved via a recursive construction of self-similar sandpile tiles. We show that sandpile growth and patterns exhibit a $(2 \cdot 3^n)$ -periodicity as a function of the initial mass. Moreover, the cluster explodes—increments by more than 1 in radius—at periodic intervals, a phenomenon not seen on \mathbb{Z}^d or trees. We explicitly characterize all the radial jumps, and use the renewal theorem to prove the scaling limit of the cluster radius, which satisfies a power law modulated by log-periodic oscillations. In the course of our proofs we also establish structural identities of the sandpile groups of subgraphs of SG with two different boundary conditions, notably the corresponding identity elements conjectured by Fairchild, Haim, Setra, Strichartz, and Westura.

Our main theorems, in conjunction with recent results of Chen, Huss, Sava-Huss, and Teplyaev, establish SG as a positive example of a state space which exhibits “limit shape universality,” in the sense of Levine and Peres, among the four Laplacian growth models: divisible sandpiles, abelian sandpiles, rotor-router aggregation, and internal diffusion-limited aggregation (IDLA). We conclude the paper with conjectures about radial fluctuations in IDLA on SG , possible extensions of limit shape universality to other state spaces, and related open problems.

CONTENTS

1. Introduction and main results	2
1.1. Sierpinski gasket graph (SG)	3
1.2. Laplacian growth models and shape theorems on SG	4
1.3. Limit shape universality on SG	7
1.4. Key ideas behind the proofs	8
2. Rotor-router aggregation on SG : Proof of Theorem 1	17
2.1. Abelian stack model and the Friedrich-Levine algorithm	17
2.2. Divisible sandpile odometer	19
2.3. Rotor-router cluster and odometer	20
3. Abelian sandpile growth on SG : Proofs of Theorems 2, 4, 5, and 6	22
3.1. Sandpile cluster is an exact ball	22
3.2. Toppling identities & the identity element of the sandpile group	23
3.3. A reflection and a rotation lemma	28
3.4. Explosions in sandpile growth	29
3.5. Enumeration of radial jumps (I): analysis of sandpile tiles	32

Date: July 29, 2021.

2010 Mathematics Subject Classification. 05C20, 05C81, 05E18, 28A80, 31A15, 37B15, 60K05, 82C24.

Key words and phrases. Laplacian growth, rotor-router aggregation, divisible sandpiles, abelian sandpiles, sandpile group, internal diffusion-limited aggregation, harmonic measure, analysis on fractals, Sierpinski arrowhead curve, self-similarity, limit shapes, exact renormalization.

This project was initiated while JKF was an undergraduate at Colgate University. It has been supported in part by the Research Council of Colgate University, the Simons Foundation (Collaboration Grant for Mathematicians #523544), and the National Science Foundation (DMS-1855604).

3.6. Enumeration of radial jumps (II): analysis of traps along the space-filling curve	38
3.7. Recursive formula for the cluster radius	43
3.8. Cluster growth asymptotically follows a power law modulated by log-periodic oscillations	43
3.9. Geometric estimate of sandpile growth	45
4. Fluctuations of the IDLA cluster on SG	47
5. Open questions	48
Acknowledgements	51
References	51

1. INTRODUCTION AND MAIN RESULTS

Internal aggregation models—such as internal diffusion-limited aggregation (IDLA) and rotor-router aggregation—and the abelian sandpile model have a long history in the statistical physics and the mathematics literature. For reasons to be explained shortly, we prefer to call them **Laplacian growth models**, to emphasize their close association with the **combinatorial graph Laplacian**, which is defined on a connected, locally finite, undirected graph $G = (V(G), E(G))$ by the non-positive symmetric matrix

$$\Delta_G(x, y) = \begin{cases} -\deg(x), & \text{if } x = y, \\ \mathbf{N}_{xy}, & \text{if } x \neq y, \end{cases} \quad (x, y \in V(G))$$

where \mathbf{N}_{xy} is the number of edges connecting x and y . It is also convenient to introduce the graph Laplacian normalized by the vertex degree, $\Delta(x, y) := \frac{1}{\deg(x)} \Delta_G(x, y)$, sometimes also called the **probabilistic graph Laplacian**.

The present work is devoted to the solutions of two Laplacian growth models—rotor-router aggregation and the abelian sandpile growth model—on the graphical Sierpinski gasket (SG , see Figure 1), when particles (or “chips”) are launched from the corner vertex of SG . In particular, we solve the abelian sandpile growth problem exactly via a renormalization scheme involving self-similar sandpile configurations, or sandpile “tiles,” on subgraphs of SG .

The motivations for our study are twofold:

(1) *The limit shape universality conjecture.* A folklore conjecture in the sandpile community is that on a fixed state space, the growing clusters associated with the four Laplacian growth models—IDLA, rotor-router aggregation, divisible sandpiles, and abelian sandpiles—have the same limit shape. This “limit shape universality” conjecture does not hold in general. In fact, exhibiting even a positive example of a state space beyond \mathbb{Z} is difficult. On \mathbb{Z}^d , it has been proven that the first three models have Euclidean balls as limit shapes [44, 48], but numerical evidence strongly suggests that the limit shape in the abelian sandpile model on \mathbb{Z}^2 is closer to a polygon than an Euclidean ball, see Figure 2. Table 1 summarizes the state of the art on \mathbb{Z}^d . See the excellent survey [50] of Levine and Peres for an overview of the basic mechanisms behind each of the Laplacian growth models and the lack of limit shape universality on \mathbb{Z}^d .

We will show that limit shape universality holds on SG , see Theorem 3 below.

(2) *From “fractals in a sandpile” to “sandpile on a fractal.”* The abelian sandpile model, introduced by Bak, Tang, and Wiesenfeld [5, 6], exhibits nontrivial fractal patterns on the Euclidean lattice \mathbb{Z}^d , see Figure 2 again. While the fractal nature of the sandpile patterns has been long recognized, rigorous proofs did not arrive until recently. In an important breakthrough, Pegden and Smart [57] showed that the scaling limit of the patterns exists in the sense of weak- $*$ $L^\infty(\mathbb{R}^d)$ convergence. Shortly after, the seminal works of Levine, Pegden, and Smart [46, 47] established the existence of the Apollonian structure in the sandpile patterns on \mathbb{Z}^2 , via the analysis of \mathbb{Z} -valued superharmonic matrices. (See Figure 3 for a picture of an Apollonian gasket.)

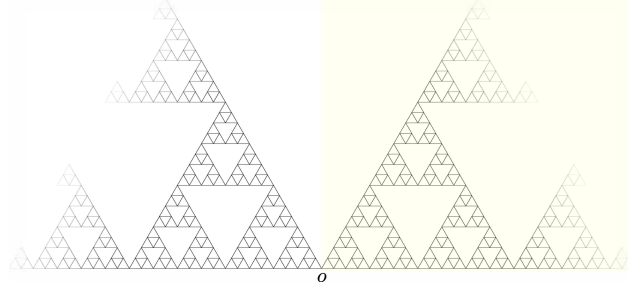


FIGURE 1. The double-sided Sierpinski gasket graph SG . The single-sided gasket graph (shaded) is just one half of the double-sided one. The vertex o is the source vertex from which particles are launched.

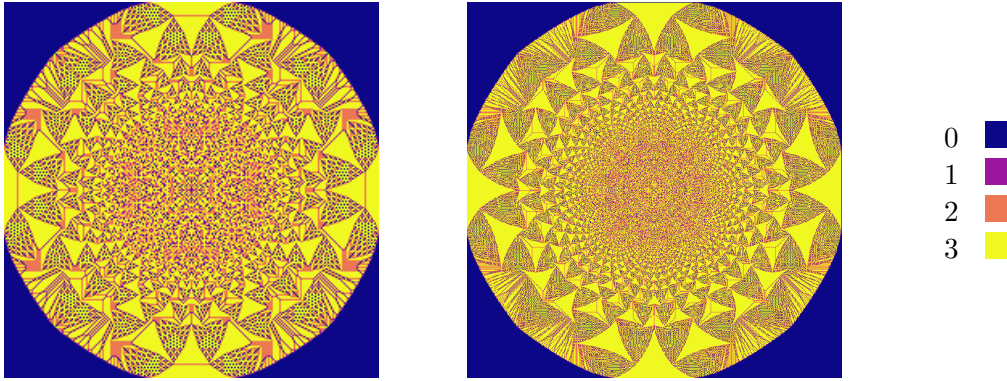


FIGURE 2. Abelian sandpile cluster on \mathbb{Z}^2 starting with 10^5 chips (left) and 10^6 chips (right) at the origin. Each vertex is colored according to the number of chips there.

Inspired by the “analysis of fractals in sandpiles,” and following the lead of Strichartz, we are prompted to study “analysis of sandpiles on fractals.” We are grateful to Strichartz and his undergraduate students for making several key numerical findings and conjectures in [22]. Indeed, the exact renormalization scheme we present here stems from an insight which appeared in [22], namely, Dhar’s multiplication by identity test applied to cut points on a nested fractal graph. This is the key mechanism behind the production of self-similar sandpile tiles on SG , which enables us to establish the identity element of the sandpile groups of subgraphs of SG (Theorem 4), and to solve the sandpile growth problem exactly (Theorems 5 and 6). Let us mention that the notion of sandpile tiles has also appeared in the Euclidean setting [12, 58], and its connection to curves in tropical geometry has been explored in [37].

Notation. Throughout the paper, unless noted otherwise, a graph $G = (V(G), E(G))$ is assumed to be undirected, locally finite, and connected. When $xy \in E(G)$ we write $x \sim y$. Let $d : V(G) \times V(G) \rightarrow \mathbb{N}_0$ be the graph metric on G , and $B_x(r) := \{y \in V(G) : d(x, y) \leq r\}$ be the closed ball of radius r centered at x . The cardinality of a finite set S is denoted $|S|$.

1.1. Sierpinski gasket graph (SG). We define the Sierpinski gasket and the associated pre-fractal graph. Let $a_0 = (0, 0) =: o$, $a_1 = (\frac{1}{2}, \frac{\sqrt{3}}{2})$, and $a_2 = (1, 0)$ be the vertices of a unit equilateral triangle in \mathbb{R}^2 , and \mathfrak{G}_0 be the complete graph on the vertex set $V_0 = \{a_0, a_1, a_2\}$, as shown on the left in Figure 4. We introduce three contracting similitudes $\Psi_i : \mathbb{R}^2 \rightarrow \mathbb{R}^2$, $\Psi_i(x) = \frac{1}{2}(x - a_i) + a_i$ for each $i \in \{0, 1, 2\}$. The Sierpinski gasket fractal K is the unique nonempty compact set K such

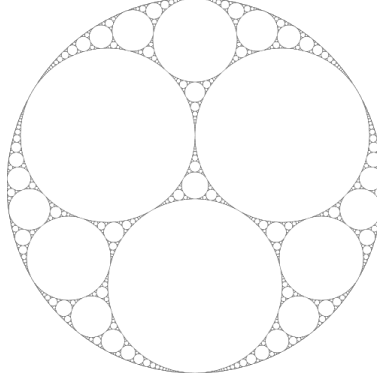


FIGURE 3. An Apollonian gasket. Picture by Time3000, https://commons.wikimedia.org/wiki/File:Apollonian_gasket.svg [GFDL or CC BY-SA 4.0], from Wikimedia Commons.

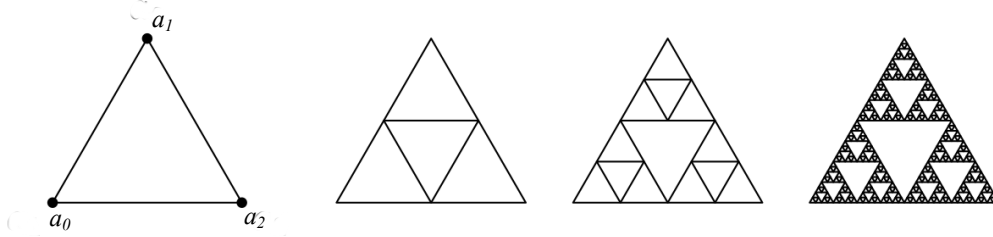


FIGURE 4. The pre-fractal Sierpinski gasket graphs of level 0, 1, 2, and 5.

that $K = \bigcup_{i=0}^2 \Psi_i(K)$. To obtain the associated level- n pre-fractal graph \mathfrak{G}_n , $n \geq 1$, we define by induction $\mathfrak{G}_n = \bigcup_{i=0}^2 \Psi_i(\mathfrak{G}_{n-1})$; see Figure 4. To make all edges of the graph have unit length, we consider $G_n := 2^n \mathfrak{G}_n$, where for $\alpha > 0$ and $S \subset \mathbb{R}^2$ we denote $\alpha S := \{\alpha x : x \in S\}$. The one-sided Sierpinski gasket graph SG is then defined to be the infinite graph $G_\infty := \bigcup_{n=0}^\infty G_n$, and the double-sided gasket graph, $G_\infty \cup \mathfrak{R}(G_\infty)$, where \mathfrak{R} is the reflection about $x_1 = 0$; see Figure 1.

Given a set $U \subset \mathbb{R}^n$, let $\text{diam}(U) := \sup\{|x - y| : x, y \in U\}$ denote the diameter of U in the Euclidean metric. The Hausdorff dimension of a set $F \subset \mathbb{R}^n$ is defined as

$$(1) \quad d_H(F) := \inf\{s \geq 0 : \mathcal{H}^s(F) = 0\} \stackrel{\text{or}}{=} \sup\{s \geq 0 : \mathcal{H}^s(F) = \infty\},$$

where

$$(2) \quad \mathcal{H}^s(F) := \liminf_{\delta \downarrow 0} \left\{ \sum_{i=1}^{\infty} [\text{diam}(U_i)]^s \mid \{U_i\}_i \text{ is a } \delta\text{-cover of } F \right\}$$

is the s -dimensional Hausdorff measure of F . See *e.g.* [24, Chapter 2] for more details. It is well known that the Hausdorff dimension of the Sierpinski gasket K is $\frac{\log 3}{\log 2}$.

1.2. Laplacian growth models and shape theorems on SG . We now define the Laplacian growth models under study. All of them belong to the so-called *abelian networks* introduced by Bond and Levine [10]; for the rationale behind the abelian property we refer the reader to [10, 20, 31, 50].

In this subsection, G is the one-sided gasket graph SG , and the “origin” o is the corner vertex of SG ; see again Figure 1. Propositions 1.1 and 1.2, which are the main theorems of [15] and [33], respectively, were proved on the double-sided SG . It is straightforward to modify the proof to work on the one-sided SG , which results in no change in the statement.

1.2.1. *Internal diffusion-limited aggregation (IDLA)*. Launch m particles successively from o , and let each of them perform i.i.d. random walks until reaching a site previously unvisited. Recall that a random walk on G is a Markov chain on the state space $V(G)$ with infinitesimal generator Δ . The resulting (random) set of occupied vertices is called an IDLA cluster, denoted $\mathcal{I}(m)$.

Proposition 1.1 (Shape theorem for IDLA on SG [15, Theorem 1.1]). *For all $\epsilon > 0$, we have*

$$B_o(n(1 - \epsilon)) \subset \mathcal{I}(|B_o(n)|) \subset B_o(n(1 + \epsilon))$$

for all n sufficiently large, with probability 1.

1.2.2. *Divisible sandpiles*. Divisible sandpiles were introduced by [48]. Start with m amount of sand at the origin o . Whenever the amount of sand $s(x)$ at vertex x exceeds 1, we topple the excess amount $s(x) - 1$ and distribute it equally among the neighboring vertices $y \sim x$, i.e., the resulting configuration is $s' = s + \max(s(x) - 1, 0) \Delta(x, \cdot)$. Continue this procedure until the amount of sand is ≤ 1 for all $x \in V(G)$, in which case we say that the sandpile has stabilized.

Let $\mathcal{D}(m)$ denote the set of vertices which have toppled in the process, which we refer to as the *divisible sandpile cluster*. Let $\mathbf{b}_n := |B_o(n)| - \frac{1}{2}|\partial_I B_o(n)|$, where $\partial_I A = \{x \in A : \exists y \in A^c \text{ with } x \sim y\}$ is the inner boundary of a set $A \subset V(G)$.

Proposition 1.2 (Shape theorem for divisible sandpiles on SG [33, Theorem 1.1]). *Let $n_m = \max\{k \geq 0 : \mathbf{b}_k \leq m\}$. Then $B_o(n_m - 1) \subset \mathcal{D}(m) \subset B_o(n_m)$.*

1.2.3. *Rotor-router aggregation*. A rotor(-router) walk on a graph, introduced by Propp, is a de-randomized version of a random walk on a graph. To begin, each vertex, x , is equipped with an arrow (rotor) which targets its neighboring vertices in a periodic sequence. This periodic sequence is called a *rotor mechanism*. A rotor mechanism is said to be *simple* if each neighbor of x occurs exactly once in a period. A particle performing rotor walk first changes the rotor at the current position to point to the next neighbor, according to the simple periodic rotor mechanism, and then moves to the neighboring vertex the rotor points towards. The rotor-router action ρ on a particle configuration on G is governed by the **stack Laplacian** Δ_ρ which, unlike the usual Laplacian Δ , is a *nonlinear* operator. See Definition 2.1 below.

In rotor-router aggregation, we launch m rotor walks successively from the origin o , and let each of them perform rotor walks until reaching a site previously unvisited. We assume that each vertex carries a rotor mechanism which is periodic and simple. Let $\mathcal{R}(m)$ and $\sigma(m)$ denote, respectively, the set of vertices which have fired and the set of vertices occupied by the rotor walkers.

Theorem 1 (Shape theorem for rotor-router aggregation on SG). *Let $n_m = \max\{k \geq 0 : \mathbf{b}_k \leq m\}$. Then for any periodic simple rotor mechanism,*

$$B_o(n_m - 2) \subset \mathcal{R}(m) \subset B_o(n_m) \quad \text{and} \quad B_o(n_m - 1) \subset \sigma(m) \subset B_o(n_m + 1)$$

for all $m \in \mathbb{N}$.

Remark 1.3. When considered over all possible periodic simple rotor mechanisms, our Theorem 1 is sharp, namely, that the difference between the out-radius and the in-radius may equal, but never exceeds, 2. This has been confirmed by our simulations, see Figure 5. In fact, simulations indicate that the cluster growth tends to fill up the sphere of radius n before entering the sphere of radius $n + 1$, with occasional exceptions resulting in (temporary) outer–inner radial difference of 2. Moreover, the second-named author has numerical evidence [40] that starting from a nearly symmetric rotor configuration, assigning to all vertices the clockwise (resp. counter-clockwise) rotor mechanisms, the radial difference appears never to exceed 1.

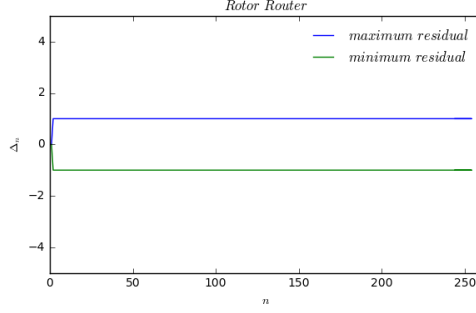


FIGURE 5. Fluctuations of the rotor-router cluster $\sigma(|B_o(n)|)$ about the expected radius n , as a function of $n \in \{1, 2, \dots, 256\}$. For each n , 1000 instances of the rotor-router cluster associated with random initial rotor configurations were generated. The data points indicate the smallest possible out-radius (blue) and the largest possible in-radius (green) among the 1000 samples.

1.2.4. *The abelian sandpile (or chip-firing) model.* Start with m chips at the origin o . Whenever the number of chips $\eta(x)$ at vertex x equals or exceeds $\deg(x)$, we **topple** or **fire** at x by sending one chip to each of the neighboring vertices $y \sim x$. Put in another way, toppling at x on the sandpile configuration $\eta : V(G) \rightarrow \mathbb{N}_0$ produces the new configuration $\eta' = \eta + \Delta_G(x, \cdot)$. Continue this procedure until the number of chips at x is fewer than $\deg(x)$ for all $x \in V(G)$, in which case we say that the sandpile has stabilized. It is well-known that the order of topplings does not affect the stable configuration, which leads to the term “abelian” in the abelian sandpile model.

Note that for the one-sided gasket graph, since $\deg(o) = 2$, the sandpile configurations at mass $2k$ and $2k + 1$, $k \in \mathbb{N}_0$, only differ at the origin o (which carries 0 and 1 chip, respectively). Therefore it suffices to study the growing sandpile cluster starting with an even number of chips at o .

Let $S(m)$ be the set of all vertices which have received at least a chip during the toppling process, which we refer to as the **receiving set**. This is to be distinguished from the **firing set** $A(m)$, the set of vertices which have fired at least once. Trivially $A(m) \subset S(m)$.

Recall $d_H = \frac{\log 3}{\log 2} = 1.58496\dots$ is the Hausdorff dimension of SG .

Theorem 2 (Shape theorem for the abelian sandpile cluster on SG). *The following hold for the abelian sandpile cluster on SG with initial configuration $m\mathbb{1}_o$:*

- (1) *For every $m \in \mathbb{N}$, there exists a radius $r_m \in \mathbb{N}_0$ such that $B_o(r_m - 1) \subset A(m) \subset B_o(r_m) = S(m)$. (It is understood that $B_o(-1) = \emptyset$.)*
- (2) *Let $r : [0, \infty) \rightarrow [0, \infty)$ be defined by $r(x) = r_{\lfloor x \rfloor}$. Then*

$$(3) \quad r(x) = x^{1/d_H} [\mathcal{G}(\log x) + o(1)] \quad \text{as } x \rightarrow \infty,$$

where \mathcal{G} is a nonconstant $(\log 3)$ -periodic function having a finite number of well-defined discontinuities within each period (see Theorems 5 and 6, and Figure 9 below). In particular, when $x \in [\frac{10}{9}, \frac{4}{3})$,

$$(4) \quad \mathcal{G}(\log x) = \frac{1}{2} x^{-1/d_H} \in (0.4170, 0.4679).$$

We also have the global estimate

$$(5) \quad 0.3871 \leq \left(\frac{2}{9}\right)^{1/d_H} \leq \mathcal{G}(\log x) \leq \frac{3}{4},$$

Figure 6 shows the radius-to-mass scaling of Theorem 2.

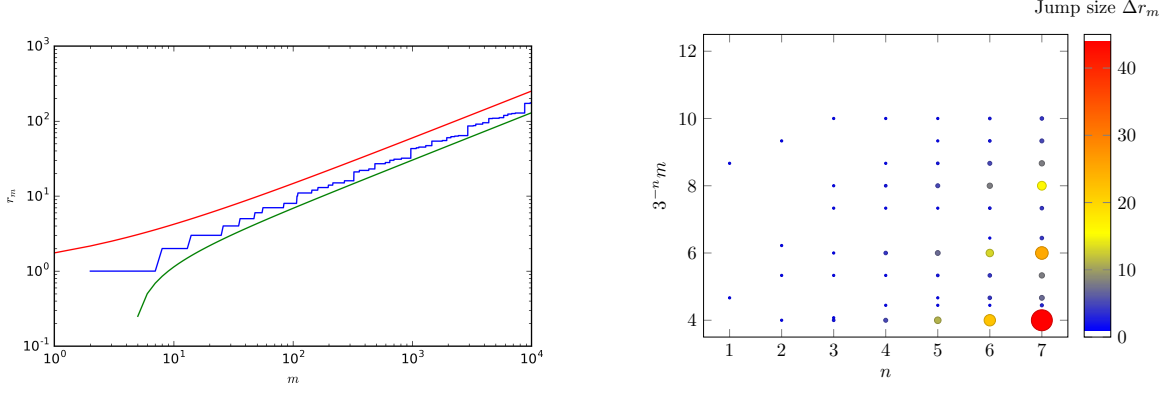


FIGURE 6. (Left) The radius r_m of the abelian sandpile cluster $(m\mathbb{1}_o)^\circ$ as a function of the initial mass m . Upper and lower bounds are given by the global estimate (5). (Right) Jumps in r_m , cf. Table 3. Enumeration of the radial jumps is given in Theorems 5 and 6; see also Figure 9.

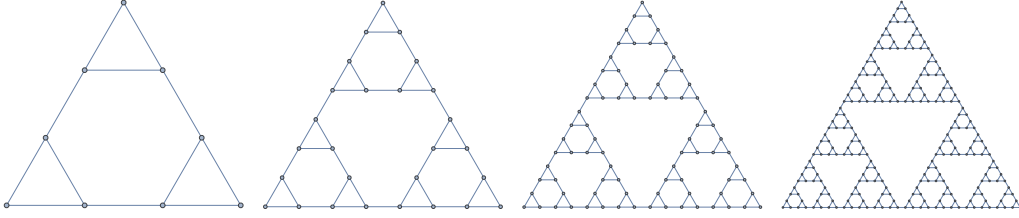


FIGURE 7. The Hanoi-tower graphs of level 1, 2, 3, and 4.

Remark 1.4. As alluded to earlier, there have been previous works on the abelian sandpile model on SG (or its variant). One type of problem is to study sandpile dynamics under stationarity (*a.k.a.* sandpile Markov chains) and obtain critical exponents of sandpile avalanches. This was the focus of the numerical works [17, 18, 41] in the late 90s. A rigorous analysis of sandpile height correlations was carried out by Matter [55, Chapter 5] on the Hanoi tower graph (Figure 7), which is a different approximation of the Sierpinski gasket fractal. The other type of problem is deterministic single-source sandpile growth, which was studied by Fairchild, Haim, Setra, Strichartz, and Westura [22] and is the main focus of the present work.

An expected feature appearing in both types of problems is that the relevant observable (be it the number of avalanche events, the cluster radius, etc.) asymptotically follows a **power law modulated by log-periodic oscillations**. This is a phenomenon expected on state spaces that possess discrete scale invariance, SG being a prime example, although to our best knowledge there has been no rigorous proof prior to the present work.

In terms of cluster radial asymptotics, it was proved in [22] that $r_m = \mathcal{O}(m^{1/d_H})$. Our Theorem 2 improves upon this result by showing rigorously that the radius follows a power law (with exponent $1/d_H$) modulated by a nonconstant log-periodic function \mathcal{G} . This \mathcal{G} function has a Fourier series representation with explicit Fourier coefficients, cf. (41), and we can evaluate it in certain intervals of x , cf. (4).

1.3. Limit shape universality on SG . Propositions 1.1 and 1.2 and Theorems 1 and 2 together imply the following “limit shape universality” result on SG , summarized in Table 2.

Theorem 3 (Limit shape universality on SG). *On SG , the four single-source Laplacian growth models—IDLA, rotor-router aggregation, divisible sandpiles, and abelian sandpiles—launched from the corner vertex o all fill balls in the graph metric centered at o .*

<i>Growth model</i>	<i>Shape theorem/conjecture</i>
IDLA	In/out-radius $\left\{ \begin{array}{ll} n \pm \mathcal{O}(\log n), & d = 2 \\ n \pm \mathcal{O}(\sqrt{\log n}), & d \geq 3 \end{array} \right\}$ [2, 3, 35, 36, 43, 44]
Rotor-router aggregation	In-radius $n - c \log n$, out-radius $n + c' \log n$ [48, 50] (c, c' indep of n)
Divisible sandpiles	In-radius $n - c$, out-radius $n + c'$ [48] (c, c' indep of n)
Abelian sandpiles	Limit shape is not spherical, appears to be a polygon Rigorous outer/inner spherical bounds (with a gap) [25, 48]

TABLE 1. A summary of shape results for Laplacian growth models on \mathbb{Z}^d , starting with $|B_o(n)|$ particles at the origin o .

<i>Growth model</i>	<i>Initial # of chips</i>	<i>Shape theorem/conjecture</i>
IDLA	$ B_o(n) $	In/out-radius $n \pm \mathcal{O}(\sqrt{\log n})$ [15], $[\diamond]$
Rotor-router aggregation	m	In-radius $n_m - 2$, out-radius n_m $[\diamond]$
Divisible sandpiles	m	In-radius $n_m - 1$, out-radius n_m [33]
Abelian sandpiles	m	Receiving set $S(m) = B_o(r_m)$ $r_m = m^{1/d_H} [\mathcal{G}(\log m) + o(1)]$ as $m \rightarrow \infty$ $[\diamond]$ (\mathcal{G} is an explicit $(\log 3)$ -periodic function)

TABLE 2. A summary of shape results for Laplacian growth models on SG , with a single source at the origin o . $[\diamond]$ denotes results addressed in the present paper. Here $n_m = \max\{k \geq 0 : |B_o(k)| - \frac{1}{2}|\partial_I B_o(k)| \leq m\}$, where $\partial_I A = \{x \in A : \exists y \in SG \setminus A, y \sim x\}$ denotes the inner boundary of $A \subset SG$.

As far as we are aware, this is the first non-tree state space whereupon the limit shapes of all four Laplacian growth models have been rigorously proven to coincide. The fact that the abelian sandpile cluster on SG is a ball is not entirely trivial, but nonetheless can be established easily via induction. On other lattices and graphs the sandpile limit shape problem is largely open.

1.4. Key ideas behind the proofs. Our proof methods combine ideas and tools from analysis, probability, algorithms, combinatorics, algebra, and geometry. For the reader's convenience we summarize the key elements of our proofs in this subsection.

1.4.1. From divisible sandpiles to IDLA and rotor-router aggregation. Let $(X_t)_{t \geq 0}$ be a continuous-time random walk on G with infinitesimal generator Δ , and \mathbb{P}_o denote its law started at o . Given a bounded subset $D \ni o$ of $V(G)$ which has boundary ∂D , one would like to estimate the hitting distribution of X_t on ∂D as it exits D . This is known as the **harmonic measure** ν on ∂D :

$$\nu(S) = \mathbb{P}_o[X_\tau \in S] \quad (S \subset \partial D)$$

where $\tau = \inf\{t > 0 : X_t \in \partial D\}$.

In Laplacian growth models, the first particle occupies o , and inductively the m th particle is launched from o and occupies the first vertex upon exiting the cluster $\Omega(m-1)$ formed by the first $m-1$ particles. So the analysis involves the harmonic measure on the boundary $\partial\Omega(m-1)$, which

evolves with m . We need to make an educated guess of $\Omega(m)$ at special values of m , for example, when $m = |B_o(n)|$.

The strategy suggested by Levine and Peres [48] is to first solve the divisible sandpile problem, *i.e.*, the variational problem

$$(6) \quad u_\infty(x) = \inf \{w(x) \mid w : V(G) \rightarrow [0, \infty) \text{ satisfies } m\mathbb{1}_o + \Delta w \leq 1\},$$

also known as the *least action principle* for divisible sandpiles. Here u_∞ is the divisible sandpile **odometer function** associated with the initial configuration $m\mathbb{1}_o$, $\sigma_\infty = m\mathbb{1}_o + \Delta u_\infty$ is the final configuration, and the divisible sandpile cluster $D(m)$ is the support of u_∞ . See [50, §2] for a discussion.

In [33] Huss and Sava-Huss solved the divisible sandpile problem on SG . Specifically they showed that at $m = \mathbf{b}_n$, the odometer function u_∞ is the unique solution of a Dirichlet problem on the ball $D(\mathbf{b}_n) = B_o(n)$ with boundary $\partial_I B_o(n)$. See [33, Theorem 4.2] or Lemma 2.4 below.

The key philosophy to follow is that the divisible sandpile cluster gives a very good approximation of the bulk of the cluster in rotor-router aggregation and in IDLA. This is best illustrated by the exact algorithm of Friedrich and Levine [28] for fast simulations of large-scale growth models, see Algorithm 2.1 below. In this algorithm, one can input any odometer function to produce an (incorrect) configuration, and then correct it by successive firings and unfirings and reverse cycle-popping. By using the divisible sandpile odometer u_∞ as the input odometer, the ensuing error corrections predominantly involve rotors near the boundary of the putative cluster.

This idea, combined with the fact that the harmonic measure on spheres in SG is uniform, is central to our proof of the rotor-router shape Theorem 1. At $m = \mathbf{b}_n$, we use the corresponding divisible sandpile odometer u_∞ as the input to the Friedrich-Levine algorithm, and obtain an outer bound for the rotor-router cluster $\mathcal{R}(\mathbf{b}_n)$. We then take advantage of the structure of SG and the constancy of u_∞ along the cluster boundary $\partial_I B_o(n-1)$ to carry out the error corrections exactly, leading to the inner bound.

Computationally this algorithm can also be implemented for IDLA, but analytically it appears not as useful. Indeed, one has to take into account randomization of rotors in calculating the *random* approximate odometer, and then carry out the *random* error corrections, neither of which is straightforward to analyze. To our best knowledge, the best techniques for analyzing IDLA are still based on those in [43, 44], combined with properties of random walks on graphs (Green's function estimates, elliptic Harnack inequality). In particular one needs to prove a mean-value inequality for the Dirichlet Green's function over balls, which can be obtained from solving the divisible sandpile problem. In [15] the first-named author, Huss, Sava-Huss, and Teplyaev adopted this idea to prove the inner bound of the IDLA cluster (Proposition 1.1); see [15, Section 3.1]. The inner bound was then used to prove a matching outer bound using arguments similar to [21].

1.4.2. Abelian sandpile growth. The analysis of the abelian sandpile model is carried out differently from the other three growth models. Since the model is predicated upon the **integrality** of the sandpile configuration (or height function), $\eta : V(G) \rightarrow \mathbb{N}_0$, we cannot directly apply tools from analysis of real-valued functions on fractals [7, 38, 64]. Instead, we analyze integer-valued functions on subgraphs of SG endowed with suitable boundary conditions (sinks), which brings us to the notion of a **sandpile group**. For a modern introduction to this subject, see the excellent surveys [34] and [59], as well as references therein.

A quick primer on the sandpile group. Let $G = (V \cup \{s\}, E)$ be a finite, connected, undirected graph with a distinguished vertex s (or possibly a set of distinguished vertices identified together) called the **sink**. A sandpile configuration on G is a map $\eta : V \rightarrow \mathbb{N}_0$. **Toppling** the configuration η at the vertex $x \in V$ produces the new configuration $\eta' = \eta + \Delta'_G(x, \cdot)$, where Δ'_G is the combinatorial

graph Laplacian:

$$(7) \quad \Delta'_G(x, y) = \begin{cases} -\deg_G(x), & \text{if } x = y \in V, \\ N_{xy}, & \text{if } x \neq y, x, y \in V. \end{cases}$$

Here $\deg_G(x)$ is the degree of the vertex x in G . Note that the sink s plays a distinguished role in that chips that fall into s are lost and do not return to V . Accordingly the Laplacian Δ'_G is endowed with Dirichlet boundary condition on s , and is notated differently from the aforementioned Laplacian Δ_G . (That said, in our proofs to follow, it is necessary to keep track of the number of chips received by the sink after stabilization.)

A configuration η is **stable** if $\eta(x) < \deg_G(x)$ for all $x \in V$. Denote Ω_G as the set of all stable configurations on G . If η is unstable, we can stabilize it by executing successive (legal) topplings until it reaches a unique stable configuration $\eta^\circ \in \Omega_G$. This is guaranteed by the existence of the sink s . Let us define the binary operation of pointwise addition of two stable configurations followed by stabilization

$$\oplus : \Omega_G \times \Omega_G \rightarrow \Omega_G, \quad \eta \oplus \xi = (\eta + \xi)^\circ.$$

This makes (Ω_G, \oplus) into a commutative monoid.

Now define a Markov chain on Ω_G with transitions

$$\eta \rightarrow \eta \oplus \mathbb{1}_x \quad \text{with probability } p(x),$$

where $p(x) > 0$ for all $x \in V$ and $\sum_{x \in V} p(x) = 1$. Using the standard Markov chain language, we say that $\eta \in \Omega_G$ is **recurrent** if starting from η , the Markov chain returns to η with probability 1. The following facts are well-known [34, §2]: there is exactly one recurrent communication class \mathcal{R}_G in Ω_G , and that $\eta \in \mathcal{R}_G$ if and only if for any sandpile σ , there exists a sandpile ζ such that $\eta = \sigma \oplus \zeta$. One may check membership in \mathcal{R}_G using the **burning test** of Dhar and Majumdar [19, 54], see *e.g.* [34, §4.1] for description of the **burning bijection** between recurrent configurations in \mathcal{R}_G and spanning trees on G rooted at s .

Taking \mathbb{Z}^V as an abelian group, the integer row span $\mathbb{Z}^V \Delta'_G$ of Δ'_G forms a subgroup of \mathbb{Z}^V . Put in another way, we define an equivalence relation on \mathbb{Z}^V by declaring that

$$\xi \sim \zeta \iff \xi - \zeta \in \mathbb{Z}^V \Delta'_G,$$

that is, two configurations are equivalent if one can be obtained from the other via successive (possibly illegal) topplings. The equivalence classes under \sim form an abelian group $K_G := \mathbb{Z}^V / \mathbb{Z}^V \Delta'_G$, which is called the **sandpile group** of G . Each equivalence class in K_G corresponds to one and exactly one recurrent configuration in \mathcal{R}_G . In other words, (\mathcal{R}_G, \oplus) , which is the minimal ideal of (Ω_G, \oplus) , forms an abelian group which is isomorphic to K_G . As a finite abelian group, K_G can be expressed as the direct sum of cyclic groups. For a systematic discussion of the sandpile group, including its computation via the Smith normal form of Δ'_G , see [9, 53].

Dhar's multiplication by identity test and its application. The next result is due to Dhar [19].

Lemma 1.5 (Multiplication by identity test). *Let $\eta \in \mathcal{R}_G$. Then $\eta \oplus \sum_{y \in V} N_{sy} \mathbb{1}_y = \eta$, and each vertex topples exactly once upon stabilization.*

Proof. Using (7) we have that for each $y \in V$,

$$N_{sy} + \sum_{x \in V} \Delta'_G(x, y) = N_{sy} + \left(\sum_{\substack{x \in V \\ x \neq y}} N_{xy} - \deg_G(y) \right) = 0.$$

This implies that on a recurrent configuration η , after we add N_{sy} chips to each vertex $y \in V$, and then topple once at every vertex, the same configuration η is returned. \square

We now explain how Lemma 1.5 is applied to the state space SG (the same idea also works on other nested fractal graphs, see [22]). Let G_n be the level- n pre-fractal Sierpinski gasket graph; see Figure 4, and observe the three corner vertices o (origin), x , and y . We denote by $\partial G_n = \{x, y\}$ the set of two non-origin corner vertices which are distance 2^n from o in the graph metric. The two types of sinked graphs we consider are: $G_n^{(s)}$, where we designate ∂G_n as the sink; and $G_n^{(o)}$, where we designate o as the sink. We denote the set of recurrent configurations on $G_n^{(s)}$ (resp. $G_n^{(o)}$) by $\mathcal{R}_n^{(s)}$ (resp. $\mathcal{R}_n^{(o)}$).

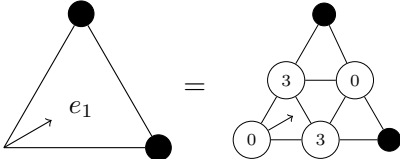
In the process of stabilizing $m\mathbb{1}_o$, chips will occupy the graph G_n for some n . Instead of stabilizing all vertices in SG at once, we can use the abelian property to stabilize only the vertices in $G_n \setminus \partial G_n$, and pause any excess chips on ∂G_n . (By the axial symmetry of the initial configuration, an equal number of chips will reach x and y .) This creates a recurrent configuration $\eta \in \mathcal{R}_n^{(s)}$ on $G_n^{(s)}$. Now we topple at the two cut vertices x and y in ∂G_n —think of them as sinks of $G_n^{(s)}$, but sources for producing the “tail” configuration in $(G_n)^c$ —which leads to 1 chip being added to each vertex adjacent to ∂G_n . By Lemma 1.5, we can then topple at every vertex in $G_n \setminus \partial G_n$, and this results in no change in the configuration η on $G_n^{(s)}$. Overall, x and y each loses 2 chips to the vertices in the “tail” $(G_n)^c$. Continue this process until a stable configuration is reached.

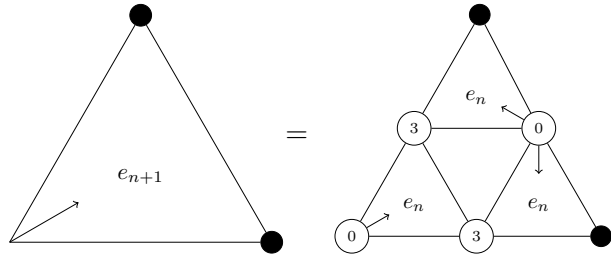
In summary, we obtain the fundamental diagram

$$(8) \quad (m\mathbb{1}_o)^\circ = \left(\begin{array}{c} \text{triangle with } m' \text{ chips at } x \text{ and } y \\ \text{and } \eta \in \mathcal{R}_n^{(s)} \text{ on } G_n^{(s)} \end{array} \right)^\circ \subseteq G_{n+1}.$$

which means that the cluster first fills G_n with m' chips paused at each vertex in ∂G_n , and then upon full stabilization the cluster fills a subset of G_{n+1} . Based on (8), we prove in Proposition 3.2 below that the receiving set of $(m\mathbb{1}_o)^\circ$ is always a ball $B_o(r_m)$, and for $m \geq 12$, $r_m = 2^n + r_{m'-2}$.

Structural theorems on the sandpile groups of subgraphs of SG . Using the preceding ideas we obtain, via induction on n , a number of structural results on the sandpile groups $\mathcal{R}_n^{(s)}$ and $\mathcal{R}_n^{(o)}$. In the diagrams to follow throughout the paper, \bullet represents a sink vertex, and long arrows (or long dashed lines) are used as visual devices for indicating orientations.

Definition 1.6. Let  , and for each $n \geq 1$, e_{n+1} is constructed by gluing three copies of e_n according to the rule



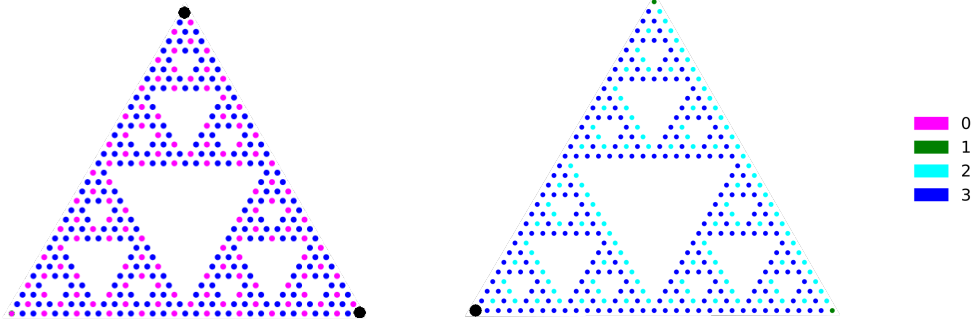
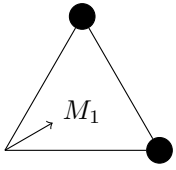
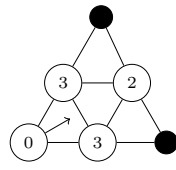
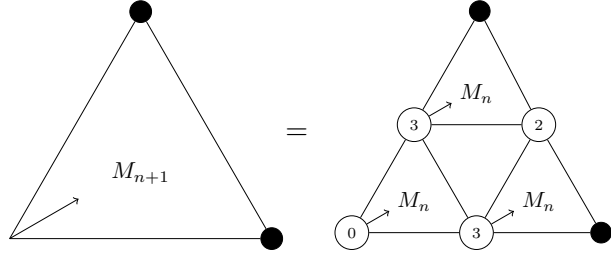


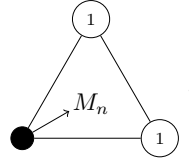
FIGURE 8. The identity elements $e_5 \in \mathcal{R}_5^{(s)}$ and $e_5^{(o)} \in \mathcal{R}_5^{(o)}$.

Definition 1.7. Let $M_1 =$  $=$  , and for each $n \geq 1$, M_{n+1} is constructed

by gluing three copies of M_n according to the rule



Let $e_n^{(o)}$ denote the configuration



Theorem 4. We have the following identities:

- (1) e_n and $e_n^{(o)}$ are, respectively, the identity element of $(\mathcal{R}_n^{(s)}, \oplus)$ and $(\mathcal{R}_n^{(o)}, \oplus)$.
- (2) For every $\eta \in \mathcal{R}_n^{(s)}$, $\eta \oplus (2 \cdot 3^n) \mathbb{1}_o = \eta$.
- (3) Let $\partial G_n = \{x, y\}$. For every $\eta \in \mathcal{R}_n^{(o)}$,

$$\eta \oplus 3^n (\mathbb{1}_x + \mathbb{1}_y) = \eta, \quad \eta \oplus 3^{n+1} \mathbb{1}_x = \eta, \quad \text{and} \quad \eta \oplus 3^{n+1} \mathbb{1}_y = \eta.$$

See Figure 8 for pictures of the identity elements, and observe the tiling construction.

Remark 1.8. In [22] the authors numerically obtained the identity elements e_n for $n = 1, 2, 3$ via an application of Lemma 1.5 to ∂G_n . They also computed the sandpile group of G_n for $n = 1, 2, 3$, with all three corner vertices $\{o, x, y\}$ identified as sink.

Remark 1.9. Since Theorem 4 suffices for our purposes, we do not pursue a full characterization of the sandpile group in the present work, though it is of interest to further investigate the underlying self-similar structure.

Radial explosions, periodicity, and the exact solution of the sandpile growth problem. A somewhat surprising feature on SG is that the configurations M_n and e_n appear in the stabilizations of $m \mathbb{1}_o$ periodically in m . We will show in §3.4 below that

$$((4 \cdot 3^n - 2)\mathbb{1}_o)^\circ = \begin{array}{c} \textcircled{1} \\ \diagup \quad \diagdown \\ M_n \\ \diagdown \quad \diagup \\ \textcircled{1} \end{array} \quad ; \text{ and}$$

$$((4 \cdot 3^n)\mathbb{1}_o)^\circ = \left(\begin{array}{c} \textcircled{b_n} \\ \diagup \quad \diagdown \\ e_n \\ \diagdown \quad \diagup \\ \textcircled{b_n} \end{array} \right)^\circ, \text{ where } b_n = |V(G_{n-1})| = \frac{3}{2}(3^{n-1} + 1).$$

The proof of M_n is not difficult. The proof of e_n , on the other hand, is subtle, and uses the cut point structure and the axial symmetry of SG . See the axial reflection lemma in §3.3.

The significance of this result is that the sandpile cluster “explodes”—the cluster radius increments by more than 1—at mass $4 \cdot 3^n$. Using the toppling identities stated in Theorem 4, we further deduce radial explosions at mass $6 \cdot 3^n$, $8 \cdot 3^n$, and $10 \cdot 3^n$, *i.e.*, the $(2 \cdot 3^n)$ -periodicity which is evident from Figure 6. Details are given in §3.4.

Remark 1.10. The $(2 \cdot 3^n)$ -periodicity of sandpile growth on SG was already conjectured by the authors of [22]; see their Conjecture 16, where they stated the $(4 \cdot 3^n)$ -periodicity on the double-sided SG . The complete enumeration of radial jumps up to $n = 6$, *cf.* the right-hand diagram in Figure 6, was first obtained numerically by the second-named author. The first-named author then discovered further patterns based on the diagram, as well as the results in [22], to write down the proofs of the periodicity.

To describe all the other radial jumps in Figure 6, we need to identify the function $m \mapsto m'$ in the fundamental diagram (8). This jump function turns out to be well-defined for $m \geq 4 \cdot 3^3$.

Theorem 5. For $n \geq 3$ and $m \in [4 \cdot 3^n, 4 \cdot 3^{n+1})$, $(m\mathbb{1}_o)^\circ = \left(\begin{array}{c} \textcircled{m'} \\ \diagup \quad \diagdown \\ \eta \in \mathcal{R}_n^{(s)} \\ \diagdown \quad \diagup \\ \textcircled{m'} \end{array} \right)^\circ \subseteq G_{n+1}$, where

$m \mapsto m'$ is a piecewise constant right-continuous function which has jumps indicated in the following table:

m	m'	Location of statement & proof
$(4 + 2p) \cdot 3^n$	$b_n + p \cdot 3^n$	“4” (Prop. 3.14)
$(4 + 2p) \cdot 3^n + 2$	$(b_n + 1) + p \cdot 3^n$	“ $e + 2$ ” (Prop. 3.26), “ $4\frac{4}{9}$ ” (Prop. 3.28)
$(4\frac{4}{9} + 2p) \cdot 3^n$	$2 \cdot 3^{n-1} + 1 + p \cdot 3^n$	“ $4\frac{4}{9}$ ” (Prop. 3.23), “ $4\frac{2}{3}$ ” (Prop. 3.20)
$(4\frac{2}{3} + 2p) \cdot 3^n$	$2 \cdot 3^{n-1} + 2 + p \cdot 3^n$	“ $4\frac{2}{3}$ ” (Prop. 3.22), “ $5\frac{1}{3}$ ” (Prop. 3.21)
$(5\frac{1}{3} + 2p) \cdot 3^n$	$3^n + 1 + p \cdot 3^n$	“ $5\frac{1}{3}$ ” (Prop. 3.24), “6” (Prop. 3.13)

where $p \in \{0, 1, 2, 3\}$, and $b_n = |V(G_{n-1})| = \frac{3}{2}(3^{n-1} + 1)$.

Remark 1.11. Regarding the statements in the right-most column, “ a^- ” and “ a ” stand for, respectively, “just below the jump at a ” and “at the jump at a .” All statements refer to the case $p = 0$. Once proved, we can establish the case $p \in \{1, 2, 3\}$ easily. We have indicated above where these results are stated and proved in §3.5 and §3.6.

The proof of Theorem 5 is fairly technical, and relies mainly upon the identification of sandpile tiles which, when glued together in a self-similar and symmetric way, produce the sandpile configuration on $G_n^{(s)}$, see Figure 9. In the physics parlance this procedure can be considered an **exact block renormalization**, where the blocks are the sandpile tiles. To our best knowledge

this may be the first time an abelian sandpile problem is exactly solved using renormalization-type arguments. Detailed proofs are provided in §3.5.

That said, there are two exceptions, “ $e + 2$ ” and “ $4\frac{4}{9}^-$,” where the block renormalization idea does not immediately apply. To tackle these two cases, we observe that in the identity element e_n , there is a unique shortest path connecting o to each vertex in ∂G_n along which every vertex carries 3 chips, see Figure 10. This path is the concatenation of the first n iterations of the **Sierpinski arrowhead curve** [62], and fills up half of SG . Toppling once at o triggers a chain of topplings down the path, and results in each vertex in ∂G_n receiving an extra chip, which proves “ $e + 2$.” We then analyze the landscape of “traps” resulting from “ $e + 2$ ” along the path, and show that it requires adding at least $4 \cdot 3^{n-2}$ chips at o to deliver extra chips to ∂G_n , thereby establishing “ $4\frac{4}{9}^-$.” See §3.6 for details.

Remark 1.12 (A take-home message). In essence, we have just described two ways in which *fractals* manifest themselves in the “sandpile on a *fractal*”: via self-similar tilings (block renormalization) and via the Sierpinski arrowhead curve. It will be helpful to examine Figures 9 and 10 while reading the proofs in §3.5 and §3.6. We suspect the self-similar tiling idea should be applicable to sandpile growth on other fractal graphs. But the appearance of the Sierpinski arrowhead curve in the identity element e_n , and the role it plays in the proofs below, seems to be unique to SG .

As a historical aside, Sierpinski introduced the arrowhead curve [62] as a model of space-filling curves (which differ from those constructed by Peano [56] and Hilbert [30], respectively) prior to his eponymous gasket. It is a surprising coincidence that we rediscovered his arrowhead curve through the abelian sandpile identity element on his gasket.

From Theorem 5, we obtain a family of recursive formulae for the cluster radii, which completely explains the results shown in Figure 6, and is used in conjunction with the renewal theorem to prove Theorem 2, Part (2). This is the content of our final Theorem 6, which is understood mnemonically using Figure 11.

Theorem 6. *The following recursions hold for a and b belonging to the respective intervals:*

$r_{a \cdot 3^n} = 2^n + r_{b \cdot 3^{n-2}}$	$(n \geq 4)$	$r_{a \cdot 3^n} = 2^n + r_{b \cdot 3^{n-1}}$	$(n \geq 3)$
$\begin{array}{cc} a & b \\ \hline [4, 4\frac{4}{9}) & [4\frac{4}{9}, 4\frac{2}{3}) \\ [4\frac{4}{9}, 4\frac{2}{3}) & [5\frac{1}{3}, 6) \\ [4\frac{2}{3}, 5\frac{1}{3}) & [6, 6\frac{4}{9}) \\ [5\frac{1}{3}, 6) & [8\frac{2}{3}, 9\frac{1}{3}) \end{array}$		$\begin{array}{cc} a & b \\ \hline [6, 6\frac{4}{9}) & [4\frac{4}{9}, 4\frac{2}{3}) \\ [6\frac{4}{9}, 7\frac{1}{3}) & [4\frac{2}{3}, 5\frac{1}{3}) \\ [7\frac{1}{3}, 8) & [5\frac{1}{3}, 6) \\ [8, 8\frac{2}{3}) & [7\frac{1}{3}, 8) \end{array}$	$\begin{array}{cc} a & b \\ \hline [8\frac{2}{3}, 9\frac{1}{3}) & [8, 8\frac{2}{3}) \\ [9\frac{1}{3}, 10) & [8\frac{2}{3}, 9\frac{1}{3}) \\ [10, 12) & [10, 12) \end{array}$

In particular, for $n \geq 4$, the restriction of the function $r : [0, \infty) \rightarrow [0, \infty)$ to $[4 \cdot 3^n, 4 \cdot 3^{n+1})$ is piecewise constant on each of the following intervals:

$$\begin{aligned}
& \left[4 \cdot 3^n, 4\frac{4}{9} \cdot 3^n\right), \left[4\frac{4}{9} \cdot 3^n, 4\frac{2}{3} \cdot 3^n\right), \left[4\frac{2}{3} \cdot 3^n, 5\frac{1}{3} \cdot 3^n\right), \left[5\frac{1}{3} \cdot 3^n, 6 \cdot 3^n\right), \\
& \left[6 \cdot 3^n, 6\frac{4}{9} \cdot 3^n\right), \left[6\frac{4}{9} \cdot 3^n, 7\frac{1}{3} \cdot 3^n\right), \left[7\frac{1}{3} \cdot 3^n, 8 \cdot 3^n\right), \\
& \left[8 \cdot 3^n, 8\frac{2}{3} \cdot 3^n\right), \left[8\frac{2}{3} \cdot 3^n, 9\frac{1}{3} \cdot 3^n\right), \left[9\frac{1}{3} \cdot 3^n, 10 \cdot 3^n\right), \\
& [10 \cdot 3^n, 4 \cdot 3^{n+1}).
\end{aligned}$$

The rest of the paper is organized as follows. Theorem 1 is proved in §2. Theorems 2, 4, 5, and 6 are proved in §3. In §4, we provide strong numerical evidence suggesting sublogarithmic

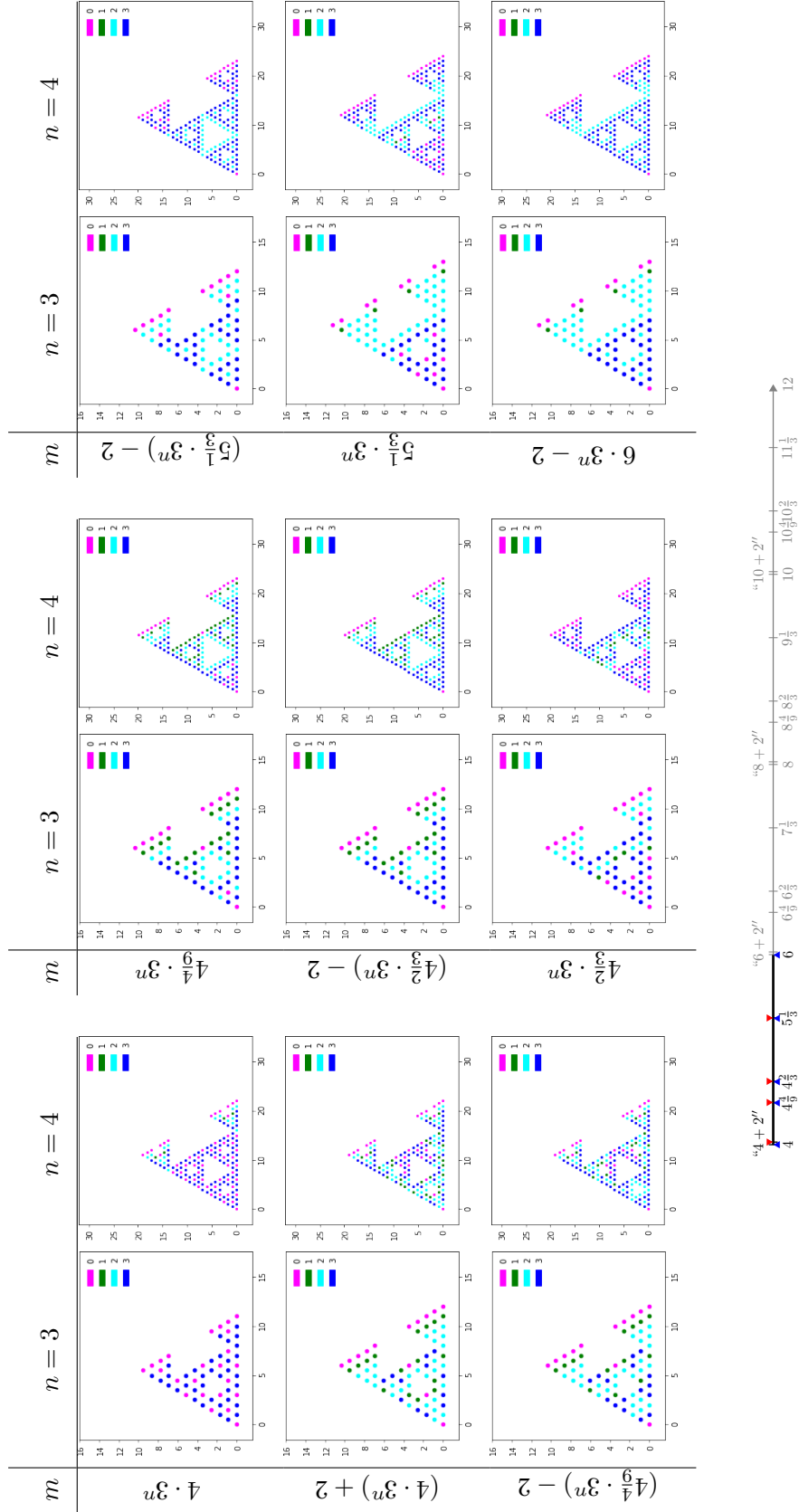


FIGURE 9. The “periodic table” of single-source sandpile on SG : $(m\mathbb{1}_0)^\circ$ at special values of m . We only present the patterns for $m \in [4 \cdot 3^n, 6 \cdot 3^n)$. Using the $(2 \cdot 3^n)$ periodicity (Theorem 4, Item (2)), we can infer patterns for $m \in [6 \cdot 3^n, 12 \cdot 3^n)$, as the timeline suggests.

$\frac{m}{3^n}$	m	m'	$m - 2m'$	Δr_m	$\frac{m}{3^n}$	m	m'	$m - 2m'$	Δr_m	$\frac{m}{3^n}$	m	m'	$m - 2m'$	Δr_m
	2	1	0	1	8	216	69	78	1	$6\frac{2}{3}$	1620	407	806	
	8	4	0	1	$8\frac{2}{27}$	218	70	78		$7\frac{1}{3}$	1782	487	808	1
n = 1					$8\frac{4}{9}$	228	73	82		8	1944	609	726	5
4	12	3	6		$8\frac{2}{3}$	234	74	86		$8\frac{2}{35}$	1946	610	726	
$4\frac{2}{3}$	14	4	6	1	$9\frac{1}{3}$	252	82	88		$8\frac{4}{9}$	2052	649	754	
6	18	6	6		10	270	96	78	1	$8\frac{2}{3}$	2106	650	806	2
$6\frac{2}{3}$	20	7	6		$10\frac{2}{27}$	272	97	78		$9\frac{1}{3}$	2268	730	808	1
8	24	9	6		$10\frac{4}{9}$	282	100	82		10	2430	852	726	1
$8\frac{2}{3}$	26	10	6	1	$10\frac{2}{3}$	288	101	86		$10\frac{2}{35}$	2432	853	726	
10	30	12	6		$11\frac{1}{3}$	306	109	88		$10\frac{4}{9}$	2538	892	754	
$10\frac{2}{3}$	32	13	6		n = 4					$10\frac{2}{3}$	2592	893	806	
n = 2					4	324	42	240	5	$11\frac{1}{3}$	2754	943	808	
4	36	6	24	1	$4\frac{2}{81}$	326	43	240		n = 6				
$4\frac{2}{9}$	38	7	24		$4\frac{4}{9}$	360	55	250	1	4	2916	366	2184	22
$4\frac{2}{3}$	42	8	26		$4\frac{2}{3}$	378	56	266		$4\frac{2}{36}$	2918	367	2184	
$5\frac{1}{3}$	48	10	28	1	$5\frac{1}{3}$	432	82	268	1	$4\frac{4}{9}$	3240	487	2266	1
6	54	15	24		6	486	123	240	4	$4\frac{2}{3}$	3402	488	2426	4
$6\frac{2}{9}$	56	16	24	1	$6\frac{2}{81}$	488	124	240		$5\frac{1}{3}$	3888	730	2428	4
$6\frac{2}{3}$	60	17	26		$6\frac{4}{9}$	522	136	250		6	4374	1095	2184	13
$7\frac{1}{3}$	66	19	28		$6\frac{2}{3}$	540	137	266		$6\frac{2}{36}$	4376	1096	2184	
8	72	24	24		$7\frac{1}{3}$	594	163	268	1	$6\frac{4}{9}$	4698	1216	2266	1
$8\frac{2}{9}$	74	25	24		8	648	204	240	2	$6\frac{2}{3}$	4860	1217	2426	
$8\frac{2}{3}$	78	26	26		$8\frac{2}{81}$	649	205	240		$7\frac{1}{3}$	5346	1459	2428	2
$9\frac{1}{3}$	84	28	28	1	$8\frac{4}{9}$	684	217	250		8	5832	1824	2184	8
10	90	33	24		$8\frac{2}{3}$	702	218	266	1	$8\frac{2}{36}$	5834	1825	2184	
$10\frac{2}{9}$	92	34	24		$9\frac{1}{3}$	756	244	268		$8\frac{4}{9}$	6156	1945	2266	
$10\frac{2}{3}$	96	35	26		10	810	285	240	1	$8\frac{2}{3}$	6318	1946	2426	5
$11\frac{1}{3}$	102	37	28		$10\frac{2}{81}$	812	286	240		$9\frac{1}{3}$	6804	2188	2428	2
n = 3					$10\frac{4}{9}$	846	298	250		10	7290	2553	2184	2
4	108	15	78	2	$10\frac{2}{3}$	864	299	266		$10\frac{2}{36}$	7292	2554	2184	
$4\frac{2}{27}$	110	16	78	1	$11\frac{1}{3}$	918	325	268		$10\frac{4}{9}$	7614	2674	2266	
$4\frac{4}{9}$	120	19	82		n = 5					$10\frac{2}{3}$	7766	2675	2426	
$4\frac{2}{3}$	126	20	86		4	972	123	726	11	$11\frac{1}{3}$	8262	2917	2428	
$5\frac{1}{3}$	144	28	88	1	$4\frac{2}{35}$	974	124	726		n = 7				
6	162	42	78	1	$4\frac{4}{9}$	1080	163	754	1	4	8748	1095	6558	44
$6\frac{2}{27}$	164	43	78		$4\frac{2}{3}$	1134	164	806	1	$4\frac{2}{37}$	8750	1096	6558	
$6\frac{4}{9}$	174	46	82		$5\frac{1}{3}$	1296	244	808	2	$4\frac{4}{9}$	9720	1459	6802	3
$6\frac{2}{3}$	180	47	86		6	1458	366	726	7	$4\frac{2}{3}$	10206	1460	7286	7
$7\frac{1}{3}$	198	55	88	1	$6\frac{2}{35}$	1460	367	726		$5\frac{1}{3}$	11664	2188	7288	8
					$6\frac{4}{9}$	1566	406	754		6	13122	3282	6558	25

Legend: $(m\mathbb{1}_o)^\circ = \left(\begin{array}{c} \text{triangle with } m' \text{ at top and } m' \text{ at bottom} \\ \eta \in \mathcal{R}_n^{(s)} \end{array} \right)^\circ \subseteq G_{n+1}; \quad \#\{\text{chips in } \eta\} = m - 2m'.$

TABLE 3. Periodic structure of the single-source sandpile cluster on SG . See Legend for explanation of m , m' , and n . We only list values of m at which m' changes. $\Delta r_m := r_m - r_{m-1}$ is the jump in the cluster radius. Special values of m are: $4 \cdot 3^n$, $6 \cdot 3^n$, $8 \cdot 3^n$, $10 \cdot 3^n$.

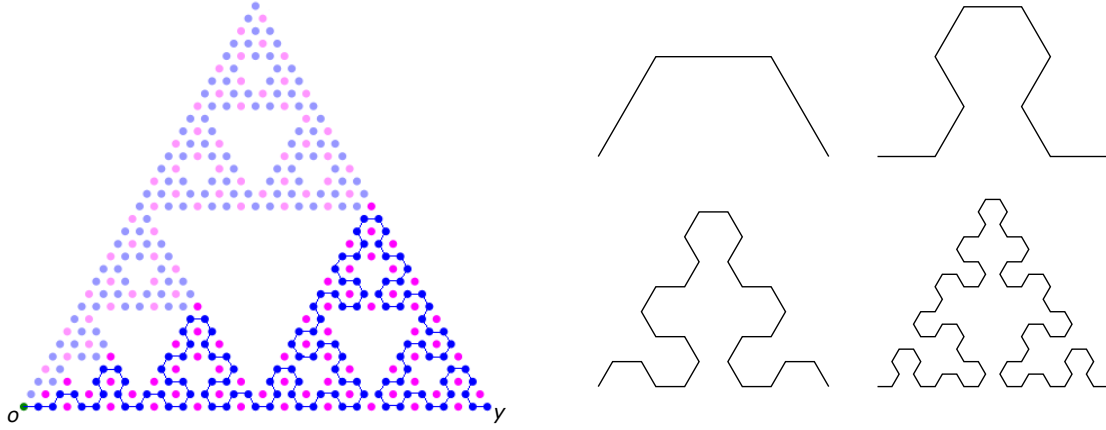


FIGURE 10. The configuration e_5 (left). Indicated in blue is the space-filling curve connecting o to the sink vertex $y \in \partial G_5$ along which every vertex carries 3 chips. It is formed by the concatenation of the first 4 iterations of the Sierpinski arrowhead curve (right).

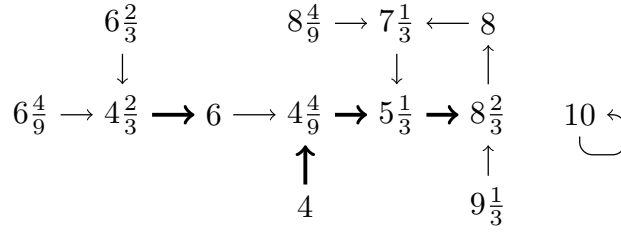


FIGURE 11. Mnemonic for Theorem 6. $a \rightarrow b$ means $r_{a \cdot 3^n} = 2^n + r_{b \cdot 3^{n-1}}$, while $a \xrightarrow{\text{thick}} b$ (with a thick arrow) means $r_{a \cdot 3^n} = 2^n + r_{b \cdot 3^{n-2}}$.

fluctuations in the radius of the IDLA cluster, and investigate a potential central limit theorem (CLT). Possible extensions to nested fractals, as well as related open questions, are discussed in §5.

2. ROTOR-ROUTER AGGREGATION ON SG : PROOF OF THEOREM 1

Let us first summarize the overall strategy in the proof of Theorem 1.

- Solving the rotor-router problem is equivalent to solving the *least action principle* for the model (see Proposition 2.2).
- A fast exact simulation algorithm for rotor-router aggregation based on this least action principle was devised by Friedrich and Levine (see Algorithm 2.1). The algorithm involves an initial approximation step followed by two error-correcting steps, and produces the correct rotor-router configuration and odometer function.
- It turns out that on SG , we have an excellent candidate for the initial approximation using the divisible sandpile odometer, which was solved by Huss and Sava-Huss [33]; see §2.2 for key facts needed for our proof. By an inductive argument described in §2.3, we can carry out precise error corrections in the Friedrich-Levine algorithm to arrive at the true rotor-router odometer.

2.1. Abelian stack model and the Friedrich-Levine algorithm. In this subsection we describe a more general aggregation model called the **abelian stack model**, which includes rotor-router aggregation and IDLA as special cases. The description follows [28] closely.

Fix a directed graph $G = (V, E)$ which is locally finite and strongly connected, that is, given any vertices $x, y \in V$ there are directed paths from x to y and from y to x . A directed edge is denoted $e = (\mathbf{s}(e), \mathbf{t}(e))$, where $\mathbf{s}(e)$ and $\mathbf{t}(e)$ are the source and target vertices, respectively. A rotor configuration $\rho : V \rightarrow E$ is an assignment of an edge $\rho(x) \in E$ to the vertex $x \in V$, with $\mathbf{s}(\rho(x)) = x$.

In the abelian stack model, we equip each vertex $x \in V$ with a *stack* of rotors $\{\rho_k(x)\}_{k=0}^\infty$, where each $\rho_k(x)$ is an edge with source vertex x . A finite number of indistinguishable chips are assigned to V according to some initial configuration. For each $x \in V$, the first chip to visit x is absorbed there and does not move again. Each subsequent chip arriving at x first shifts the stack at x to become $(\rho_{k+1}(x))_k$. After shifting the stack, the chip moves from x to the target of the new rotor on top, $y = \mathbf{t}(\rho_1(x))$. This procedure is called a **firing** of the vertex x . It can be readily seen that the k th chip fired from x travels along the edge $\rho_k(x)$.

Given a directed edge e and a nonnegative integer n , define

$$R_\rho(e, n) = \#\{1 \leq k \leq n : \rho_k(\mathbf{s}(e)) = e\}$$

to be the number of times e occurs among the first n rotors in the stack at the vertex $\mathbf{s}(e)$. In the case of rotor-router aggregation with simple periodic rotor mechanism, one can show that

$$(9) \quad R_\rho(e, n) = \left\lfloor \frac{n + d_{\text{out}}(\mathbf{s}(e)) - j(e)}{d_{\text{out}}(\mathbf{s}(e))} \right\rfloor,$$

where $j(e)$ is the minimum positive integer such that $\rho_j(\mathbf{s}(e)) = e$, and $d_{\text{out}}(v)$ is the out-degree of vertex v .

Definition 2.1. The **stack Laplacian** of a function $u : V \rightarrow \mathbb{N}$ is the function $\Delta_\rho u : V \rightarrow \mathbb{Z}$ given by

$$\Delta_\rho u(x) = \sum_{\mathbf{t}(e)=x} R_\rho(e, u(\mathbf{s}(e))) - u(x),$$

where the sum runs over all edges e with target vertex x .

The role of the stack Laplacian is as follows. Starting from a chip configuration σ_0 , we perform $u(x)$ firings at each vertex $x \in V$. It is direct to verify that the resulting configuration is $\sigma_0 + \Delta_\rho u$. We denote by

$$\text{Top}_\rho(u)(x) = \rho_{u(x)}(x) \quad (x \in V)$$

the rotor configuration on the tops of the stacks after the firings.

The main question in the abelian stack model is to identify the odometer function u_* which produces the final stable configuration σ_* from σ_0 . The solution to this question is given by the following *least action principle*.

Proposition 2.2 ([28, Theorem 1]). *Let G be a directed graph, ρ a collection of rotor stacks on G , and σ_0 a chip configuration on G . Fix $u_* : V \rightarrow \mathbb{N}$, and let $A_* = \text{supp}(u_*)$. Let $\sigma_* = \sigma_0 + \Delta_\rho u_*$. Suppose that*

- $\sigma_* \leq 1$.
- A_* is finite.
- $\sigma_*(x) = 1$ for all $x \in A_*$.
- $\text{Top}_\rho(u_*)$ is acyclic on A_* .

Then there exists a finite complete legal firing sequence for σ_0 , and its odometer function is u_ .*

Based on Proposition 2.2, Friedrich and Levine established a three-step algorithm which produces u_* exactly [28], as described in Algorithm 2.1 below. Step 1 of the algorithm takes in any function $u_1 : V \rightarrow \mathbb{N}_0$ and returns the resulting approximate configuration σ_1 . Following it are two error-correcting steps, annihilation and reverse cycle-popping, which correct the errors in the particle

configuration and the rotor configuration, respectively. Readers interested in the computational costs associated with this algorithm may consult [28, §4–§6].

Algorithm 2.1: Computing the abelian stack odometer [28]

Inputs : Initial chip configuration σ_0 and approximate odometer u_1

Outputs: Final chip configuration σ_2 and exact odometer u_3

```

1 (Step 1) Approximation: return  $\sigma_1 = \sigma_0 + \Delta_\rho u_1$ ;
2 (Step 2) Annihilation: Set  $u_2 = u_1$  and  $\sigma_2 = \sigma_1$ ;
3 foreach  $x \in V$  do
4   if  $\sigma_2(x) > 1$  then
5     call  $x$  a hill, fire it by moving one chip from  $x$  to  $\mathbf{t}(\text{Top}(u_2)(x))$  and incrementing  $u_2(x)$ 
      by 1;
6   else if  $\sigma_2(x) < 0$ , or  $\sigma_2(x) = 0$  and  $u_2(x) > 0$  then
7     call  $x$  a hole, unfire it by moving one chip from  $\mathbf{t}(\text{Top}(u_2)(x))$  to  $x$  and decrementing
       $u_2(x)$  by 1;
8 end
9 return  $\sigma_2$  and  $u_2$ ;
10 (Step 3) Reverse cycle-popping: Set  $u_3 = u_2$  and  $A_3 = \text{supp}(u_3) := \{x \in V : u_3(x) > 0\}$ ;
11 if  $\text{Top}(u_3)$  is not acyclic on  $A_3$  then
12   pick a cycle and unfire each of its vertices once. (This does not change  $\sigma_2$ .) Update  $u_3$  and
       $A_3$ ;
13 end
14 return  $u_3$ 

```

2.2. Divisible sandpile odometer. While the Friedrich-Levine algorithm was devised for fast simulation purposes, it turns out to work well on SG from the analytic point-of-view, when we choose the divisible sandpile odometer as the input function u_1 .

Recall the description of the divisible sandpile problem in §1.2.2. Consider an initial configuration $\sigma_0 : V(G) \rightarrow [0, \infty)$. We would like to stabilize it to a final configuration σ_∞ where $\sigma_\infty \leq 1$ everywhere, and identify the corresponding odometer function $u_\infty : V(G) \rightarrow [0, \infty)$, where $u_\infty(x)$ represents the amount of mass emitted from x during the stabilization. The solution to this problem is given in variational form by (6). On a general state space it is difficult to solve (6). Instead we can use an alternative formulation which is analogous to that for the abelian stack model, Proposition 2.2 above.

Proposition 2.3. *Let $u_* : V(G) \rightarrow [0, \infty)$ be a function, $A_* = \{z \in V(G) : u_*(z) > 0\}$ and $\sigma_* = \sigma_0 + \Delta u_*$. Suppose that*

- $\sigma_*(z) = 1$ for all $z \in A_*$.
- A_* is finite.
- $\sigma_* \leq 1$.

Then the divisible sandpile odometer $u_\infty = u_$.*

Proof. See [33, Lemma 3.10] for the proof, which was stated for SG , but works on any infinite, locally finite, connected graph supporting an irreducible random walk process with infinitesimal generator Δ . \square

Let us specialize to SG . Denote the closed ball and the sphere of radius n centered at o by $B_n = \{y \in SG : d(o, y) \leq n\}$ and $S_n = \{y \in SG : d(o, y) = n\}$. Given a subset $A \subset SG$, we define

its inner boundary by $\partial_I A := \{x \in A : \exists y \in A^c, x \sim y\}$. For each $n \geq 1$, set

$$(10) \quad \mathbf{b}_n := |B_n| - \frac{1}{2}|\partial_I B_n| = |B_{n-1}| + |\partial_I B_{n-1}|.$$

For the proof of the latter equality see [33, Lemma 4.1]. The point is that \mathbf{b}_n counts the number of vertices in B_n which also takes into account boundary corrections.

In [33] Huss and Sava-Huss used an inductive procedure and Proposition 2.3 to give an explicit characterization of the divisible sandpile odometer function starting from $\mathbf{b}_n \mathbb{1}_o$. We summarize their main result as follows:

Lemma 2.4. *The following hold for the divisible sandpile odometer u_n^{DS} associated with the initial distribution $\mathbf{b}_n \mathbb{1}_o$:*

- (1) $\text{supp}(u_n^{\text{DS}}) = B_{n-1}$.
- (2) $\Delta u_n^{\text{DS}}(z) = \begin{cases} 1 - \mathbf{b}_n \mathbb{1}_o, & \text{if } z \in B_n \setminus \partial_I B_n, \\ 1/2, & \text{if } z \in \partial_I B_n, \\ 0, & \text{if } z \notin B_n. \end{cases}$
- (3) $u_n^{\text{DS}}(y) = 2$ for each $y \in \partial_I B_{n-1}$.

Proof. Parts (1) and (2) are established in [33, Theorem 4.2]. For Part (3), observe that $y \in \partial_I B_{n-1}$ is connected to two vertices $z_1, z_2 \in S_n$. Take z_1 , which has 4 adjacent vertices y, z_2, w_1, w_2 , where $w_1, w_2 \in S_{n+1}$. By Part (1), $u_n^{\text{DS}}(z_1) = u_n^{\text{DS}}(z_2) = u_n^{\text{DS}}(w_1) = u_n^{\text{DS}}(w_2) = 0$. By Part (2),

$$\Delta u_n^{\text{DS}}(z_1) = \frac{1}{4} (u_n^{\text{DS}}(y) + u_n^{\text{DS}}(z_2) + u_n^{\text{DS}}(w_1) + u_n^{\text{DS}}(w_2)) - u_n^{\text{DS}}(z_1) = \frac{1}{2}.$$

Infer that $u_n^{\text{DS}}(y) = 2$. □

Remark 2.5. Taking together Items (1) and (2), it is not difficult to check that u_n^{DS} solves the Dirichlet boundary-value problem

$$(11) \quad \begin{cases} \Delta u_n^{\text{DS}} = 1 - \mathbf{b}_n \mathbb{1}_o & \text{on } B_{n-1}, \\ u_n^{\text{DS}} = 0 & \text{on } (B_{n-1})^c. \end{cases}$$

Equation (11), and more generally, Poisson's equation on ball subsets of SG , have already been solved by Strichartz [63]. Technically speaking, the divisible sandpile problem is a *free* boundary-value problem. But often its solution can be found by first guessing the support of the odometer, and then solving the *Dirichlet* boundary-value problem on the support set.

2.3. Rotor-router cluster and odometer. In the subsection we show that the divisible sandpile odometer u_n^{DS} makes an excellent approximation of the rotor-router odometer under the same initial configuration $\mathbf{b}_n \mathbb{1}_o$, in the sense that we can perform precise error corrections in the Friedrich-Levine algorithm. Our error-correction proof uses induction on n and consists of two acts: “filling the bulk” and “pulling the marionette.” Upon making the error corrections, we identify the support of the rotor-router cluster and odometer function, thereby proving Theorem 1.

Proposition 2.6. *For any periodic simple rotor mechanism ρ ,*

$$\Delta_\rho u_n^{\text{DS}}(x) \in \begin{cases} \{0\}, & \text{if } x \notin B_n, \\ \{0, 1\}, & \text{if } x \in \partial_I B_n, \\ \{0, 1, 2\}, & \text{if } x \in S_n \setminus \partial_I B_n. \end{cases}$$

Proof. If $x \notin B_n$, then there is no vertex $y \in B_{n-1}$ which is connected to x , so Part (1) of Lemma 2.4 implies that $\Delta_\rho u_n^{\text{DS}}(x) = 0$. If $x \in \partial_I B_n$, then it is connected to 4 vertices y, z, w_1 , and w_2 ,

where $y \in \partial_I B_{n-1}$, $z \in S_n$, and $w_1, w_2 \in S_{n+1}$. By Part (1) of Lemma 2.4, $u_n^{\text{DS}}(x) = u_n^{\text{DS}}(z) = u_n^{\text{DS}}(w_1) = u_n^{\text{DS}}(w_2) = 0$, while by Part (3) we have $u_n^{\text{DS}}(y) = 2$. Therefore

$$\Delta_\rho u_n^{\text{DS}}(x) = R_\rho((y, x), u_n^{\text{DS}}(y)) = R_\rho((y, x), 2) = \begin{cases} 1, & \text{if } (y, x) \in \{\rho_1(y), \rho_2(y)\}, \\ 0, & \text{if } (y, x) \in \{\rho_3(y), \rho_4(y)\}. \end{cases}$$

Finally, if $x \in S_n \setminus \partial_I B_n$, then it is connected to 4 vertices y_1, y_2, x_1 , and x_2 , where $y_1, y_2 \in \partial_I B_{n-1}$ and $x_1, x_2 \in S_n$. Again by Lemma 2.4, $u_n^{\text{DS}}(y_1) = u_n^{\text{DS}}(y_2) = 2$ and $u_n^{\text{DS}}(x) = u_n^{\text{DS}}(x_1) = u_n^{\text{DS}}(x_2) = 0$, so

$$\Delta_\rho u_n^{\text{DS}}(x) = \sum_{i=1}^2 R_\rho((y_i, x), 2) = \begin{cases} 2, & \text{if } (y_1, x) \in \{\rho_1(y_1), \rho_2(y_1)\} \text{ and } (y_2, x) \in \{\rho_1(y_2), \rho_2(y_2)\}, \\ 1, & \text{if } (y_1, x) \in \{\rho_1(y_1), \rho_2(y_1)\} \text{ and } (y_2, x) \in \{\rho_3(y_2), \rho_4(y_2)\}, \\ 1, & \text{if } (y_1, x) \in \{\rho_3(y_1), \rho_4(y_1)\} \text{ and } (y_2, x) \in \{\rho_1(y_2), \rho_2(y_2)\}, \\ 0, & \text{if } (y_1, x) \in \{\rho_3(y_1), \rho_4(y_1)\} \text{ and } (y_2, x) \in \{\rho_3(y_2), \rho_4(y_2)\}. \end{cases}$$

□

Let u_n^{RR} and σ_n^{RR} denote, respectively, the rotor-router odometer and the final chip configuration associated with the initial configuration $\mathbf{b}_n \mathbb{1}_o$.

Proposition 2.7. $B_{n-2} \subset \text{supp}(u_n^{\text{RR}}) \subset B_{n-1}$ and $B_{n-1} \subset \text{supp}(\sigma_n^{\text{RR}}) \subset B_n$.

Proof. We prove this by induction on n . When $n = 1$, $\mathbf{b}_1 = 2$, and the claim clearly holds. Now assume the claim holds for n . Then we have $\text{supp}(\sigma_{n+1}^{\text{RR}}) \supset B_{n-1}$, i.e., B_{n-1} is fully occupied. To complete the induction, we need to settle the remaining $\mathbf{b}_{n+1} - |B_{n-1}|$ chips, and show that they fill S_n and do not overrun B_{n+1} .

We apply Algorithm 2.1, using the divisible sandpile odometer u_{n+1}^{DS} as the approximate odometer in Step 1. Let u'_{n+1} and $\sigma'_{n+1} = \mathbf{b}_{n+1} \mathbb{1}_o + \Delta_\rho u_{n+1}^{\text{DS}}$ be, respectively, the odometer and the chip configuration which serve as input to Step 2 of Algorithm 2.1. By Lemma 2.4, Part (1), $u'_{n+1}(x) = 0$ for all $x \notin B_n$, so no vertex in $(B_n)^c$ is a hole. Moreover, by Proposition 2.6, if $x \in \partial_I B_{n+1}$ (resp. $x \in (B_{n+1})^c$), then $\sigma'_{n+1}(x) \in \{0, 1\}$ (resp. $\sigma'_{n+1}(x) = 0$), so every vertex in $\partial_I B_{n+1} \cup B_{n+1}^c$ is neither a hill nor a hole.

According to the above rationale, we carry out Step 2 in two acts:

Act 1: Filling the bulk. Fire and unfire vertices in B_{n-1} so as to place 1 chip at each vertex in B_{n-1} , in accordance with the induction hypothesis. This leaves

$$\mathbf{b}_{n+1} - |B_{n-1}| = |B_n| + |\partial_I B_n| - |B_{n-1}| = |S_n| + |\partial_I B_n|$$

chips in $B_{n+1} \setminus B_{n-1}$. In particular, since $u'_{n+1}(x) > 0$ for each $x \in S_n$, we will fire and unfire as many vertices in S_n as needed until 1 chip is placed at each vertex in S_n . This is carried out in the next act.

Act 2: Pulling the marionette. According to Proposition 2.6, there exists (many) a rotor configuration ρ_{\max} which places the maximal number of chips on S_{n+1} after Act 1, namely:

$$\sigma'_{n+1}(x) = \begin{cases} 1, & \text{if } x \in \partial_I B_{n+1}, \\ 2, & \text{if } x \in S_{n+1} \setminus \partial_I B_{n+1}. \end{cases}$$

The ensuing analysis differs depending on whether n is odd or even. See Figure 12.

When n is odd, there are $2|S_{n+1}| - |\partial_I B_{n+1}|$ chips on S_{n+1} . Moreover, since $u'_{n+1}(x) = 2$, every vertex $x \in S_n$ carries a rotor which is targeted towards some vertex in S_{n+1} . Since $|S_n| = |\partial_I B_n|$, deduce that S_n carries $(|S_n| + |\partial_I B_n|) - (2|S_{n+1}| - |\partial_I B_{n+1}|) = 2|S_n| - 2|S_{n+1}| + |\partial_I B_{n+1}| = 0$ chips. Therefore we unfire every vertex $x \in S_n$ to pull one chip from its successor vertex $\mathbf{t}(\rho_2(x))$ in S_{n+1} , and then fire the remaining hills on S_{n+1} .

When n is even, observe that $S_{n+1} = \partial_I B_{n+1}$ and $|\partial_I B_n| = \frac{1}{2}|S_{n+1}|$. Given that every vertex on S_{n+1} carries 1 chip, deduce that S_n carries $(|S_n| + |\partial_I B_n|) - |S_{n+1}| = |S_n| - |\partial_I B_n|$ chips, that

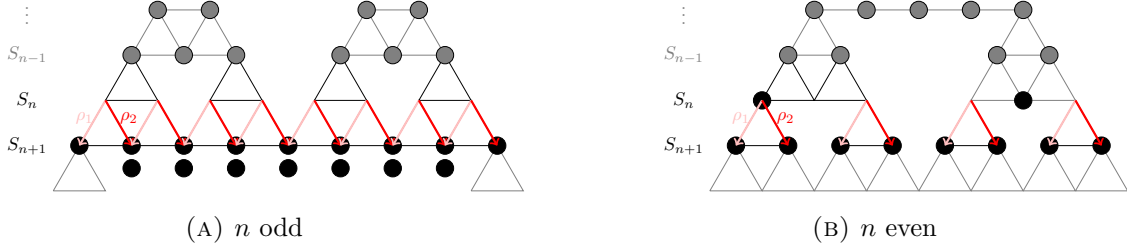


FIGURE 12. The setup for the “marionette” act in the proof of Proposition 2.7.

is, there are at least $|\partial_I B_n|$ holes on S_n . Therefore we fire and unfire as many vertices in B_n as necessary until every vertex in S_n carries 1 chip. In the process $|\partial_I B_n|$ chips will be pulled from S_{n+1} , leaving $|\partial_I B_n|$ chips on S_{n+1} .

In either case, we arrive at a configuration σ''_{n+1} with

$$(12) \quad B_n \subset \text{supp}(\sigma''_{n+1}) \subset B_{n+1}.$$

Using another rotor configuration ρ places no more chips on S_{n+1} , and thus requires no more pulls from S_{n+1} , than ρ_{\max} . Consequently, the resulting configuration σ''_{n+1} will satisfy (12). If u''_{n+1} denotes the corresponding odometer function, we deduce that $B_{n-1} \subset \text{supp}(u''_{n+1}) \subset B_n$. (The inner bound $\text{supp}(\sigma''_{n+1}) \supset B_n$ implies that all vertices in B_{n-1} have fired.) This completes Step 2.

Finally, Step 3 (reverse cycle-popping) involves unfirings only and does not alter the chip configuration. So the final rotor-router cluster σ_{n+1}^{RR} is identical to σ''_{n+1} and satisfies (12), while the support of the odometer cannot increase. In other words, $B_n \subset \text{supp}(\sigma_{n+1}^{\text{RR}}) \subset B_{n+1}$ and $B_{n-1} \subset \text{supp}(u_{n+1}^{\text{RR}}) \subset B_n$. \square

Proof of Theorem 1. For each $m \in \mathbb{N}$, let $n_m = \max\{k \geq 0 : b_k \leq m\}$. Then $b_{n_m} \leq m < b_{n_m+1}$, which implies that $\text{supp}(u_{n_m}^{\text{RR}}) \subset \mathcal{R}(m) \subset \text{supp}(u_{n_m+1}^{\text{RR}})$ and $\text{supp}(\sigma_{n_m}^{\text{RR}}) \subset \sigma(m) \subset \text{supp}(\sigma_{n_m+1}^{\text{RR}})$. Now apply Proposition 2.7 to deduce the theorem. \square

3. ABELIAN SANDPILE GROWTH ON SG : PROOFS OF THEOREMS 2, 4, 5, AND 6

The proofs of the various theorems proceed as follows: Theorem 2, Part (1) \rightarrow Theorem 4 \rightarrow Theorem 5 \rightarrow Theorem 6 \rightarrow Theorem 2, Part (2).

Recall that G_n is the level- n Sierpinski gasket pre-fractal graph, which has three corner vertices o, x, y . Set $\partial G_n = \{x, y\}$. The graph $G_n^{(s)}$ (resp. $G_n^{(o)}$) is the sinked version of G_n with ∂G_n (resp. o) identified as sink. The sandpile group of $G_n^{(s)}$ (resp. $G_n^{(o)}$) is denoted $\mathcal{R}_n^{(s)}$ (resp. $\mathcal{R}_n^{(o)}$).

3.1. Sandpile cluster is an exact ball. In this subsection we prove Theorem 2, Part (1). Given a sandpile configuration η on G and a subgraph $G' \subset G$, we denote the restriction of η to $V(G')$ by $\eta|_{G'}$.

Lemma 3.1. *Let η be an unstable configuration on $\bigcup_{n \geq 1} G_n$ with the property that $\eta|_{G_n^{(s)}} \in \mathcal{R}_n^{(s)}$ for some $n \in \mathbb{N}$. Suppose we stabilize η at all vertices in $G_n^{(s)}$ and obtain a configuration η° (which may be unstable outside $G_n^{(s)}$), and in doing so, each of the two vertices in ∂G_n is toppled k times. Then every vertex in $G_n^{(s)}$ is also toppled k times, and $\eta^\circ|_{G_n^{(s)}} = \eta|_{G_n^{(s)}}$.*

Proof. On η we topple at each of the two vertices in ∂G_n once, and produce the configuration $\eta' = \eta + \sum_{x \in \partial G_n} \Delta'(x, \cdot)$. In the process every vertex y that is connected to ∂G_n receives an extra chip. So $\eta'|_{G_n^{(s)}} = (\eta + \sum_{y \sim s} \mathbb{1}_y)|_{G_n^{(s)}} = \eta|_{G_n^{(s)}} + \sum_{y \in G_n^{(s)}} \mathbb{1}_y$. By Lemma 1.5, we can stabilize $\eta'|_{G_n^{(s)}}$

by toppling at every vertex in $G_n^{(s)}$ exactly once, and return the original configuration $\eta|_{G_n^{(s)}}$. This process can be repeated as many times as needed. \square

Let $A(m)$ and $S(m)$ denote, respectively, the firing set and the receiving set of $(m\mathbb{1}_o)^\circ$. The following result is fundamental to the solution of the sandpile growth problem on SG .

Proposition 3.2. *For each $m \geq 12$, there exists a unique $(n, m') \in \mathbb{N}^2$ with $m' < m/2$ such that*

$$(m\mathbb{1}_o)^\circ = \left(\begin{array}{c} \text{Diagram: A triangle with vertices labeled } m' \text{ (top), } \eta \in \mathcal{R}_n^{(s)} \text{ (bottom-left), and } m' \text{ (bottom-right).} \\ \text{The triangle is enclosed in large parentheses with a superscript } \circ. \end{array} \right)^\circ \subseteq G_{n+1}.$$

Moreover:

- (1) For each $m \in \mathbb{N}$, $B_o(r_m - 1) \subset A(m) \subset S(m) = B_o(r_m)$.
- (2) For each $m \geq 12$, $r_m = 2^n + r_{m'-2}$.

Proof. It is direct to check that for each $m < 12$, $S(m) \subset G_1$, $S(m) = B_o(r_m)$ for some $r_m \in \{0, 1, 2\}$, and $A(m) = B_o(r_m - 1)$, with the understanding that $B_o(-1) = \emptyset$.

If $m \geq 12$, we obtain $(m\mathbb{1}_o)^\circ$ according to the following algorithm. First topple and stabilize at every vertex of $G_n^{(s)}$, but pause any excess chips on ∂G_n . This produces a recurrent configuration $\eta \in \mathcal{R}_n^{(s)}$ in $G_n^{(s)}$. By the axial symmetry of G_n , each of the two cut points in ∂G_n carries the same number of chips m' . If $m' < 4$ (degree of the cut point), we are done. Otherwise, we topple on ∂G_n , but with each toppling we also topple once at every vertex in $G_n^{(s)}$. By Lemma 3.1, this leaves $\eta|_{G_n^{(s)}}$ invariant while additional chips are fired into $G_{n+1} \setminus G_n$. Continue stabilizing at every vertex in $G_{n+1}^{(s)}$ and, if necessary, pause any excess chips on ∂G_{n+1} . If the resulting configuration is stable, we are done. Otherwise, continue the above process into G_{n+2} . This algorithm proves the claimed diagram. The condition $m' < m/2$ follows from Propositions 3.13 and 3.14 below.

Let us make two observations. First, since m is finite, the algorithm terminates. Second, with each simultaneous toppling on G_n , each $x \in \partial G_n$ loses 4 chips to its neighboring vertices, and receives 2 chips back from $y \sim x$, $y \in G_n^{(s)}$, thereby losing a net number of 2 chips while keeping $\eta|_{G_n^{(s)}}$ intact. As a result, upon further toppling and stabilizing on $G_{n+1} \setminus G_n$ (plus any additional simultaneous toppling on G_n), the number of chips at x decrements in steps of 2, until 2 (resp. 3) chips remain if m' is even (resp. odd). This process generates a copy of $((m' - 2)\mathbb{1}_o)^\circ$ (resp. $((m' - 3)\mathbb{1}_o)^\circ$) in each connected component of $G_{n+1} \setminus G_n$.

To prove Part (1), we claim that for every $m \in \mathbb{N}$ such that $S(m) \subset G_n$, there exists $r_m \in \mathbb{N}_0$ such that $B_o(r_m - 1) \subset A(m) \subset S(m) = B_o(r_m)$. When $n = 1$, this claim holds by virtue of the first paragraph of the proof. Now suppose the claim holds at level n . Then for every $m \in \mathbb{N}$ such that $G_n \subsetneq S(m) \subset G_{n+1}$, it follows from the previous paragraph and the induction hypothesis that $S(m) = B_o(r_m)$ for some $r_m \in (2^n, 2^{n+1}]$, and that every vertex in $B_o(r_m - 1)$ has fired, i.e., $A(m) \supset B_o(r_m - 1)$.

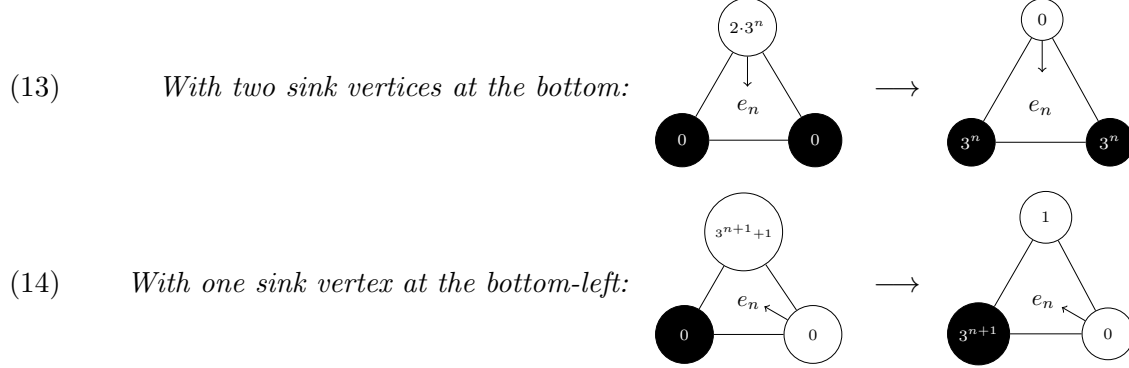
To prove Part (2), we deduce from the diagram and Part (1) that $r_m = 2^n + r_{m'-2}$ (resp. $r_m = 2^n + r_{m'-3}$) if m' is even (resp. odd). Recall (from §1.2.4) that when m is even, $(m\mathbb{1}_o)^\circ$ and $((m+1)\mathbb{1}_o)^\circ$ differs only at the origin o . This implies that $r_{m'-3} = r_{m'-2}$ when m' is odd. \square

Remark 3.3. Both containments in $B_o(r_m - 1) \subset A(m) \subset B_o(r_m)$ are strict in general. For example, both $A(12)$ and $A(14)$ are equal to $G_1 \setminus \partial G_1$ (neither cut point on ∂G_1 topples), which strictly contains $B_o(1)$ and is strictly contained in $B_o(2)$.

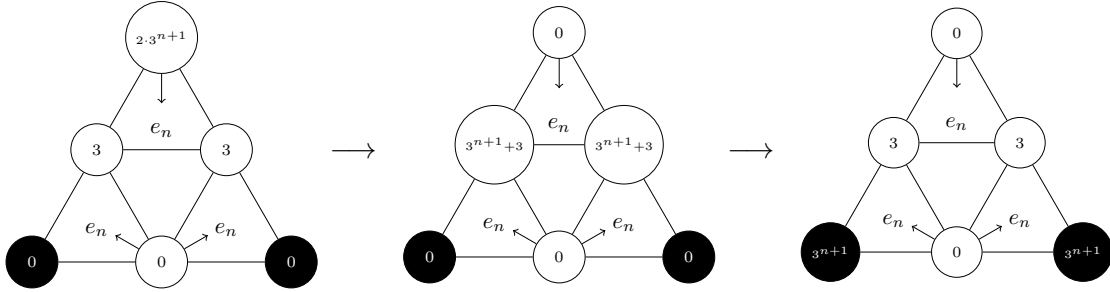
3.2. Toppling identities & the identity element of the sandpile group. In this subsection we prove Theorem 4. Let's begin with the toppling identities. For concreteness, in the proof below

we choose e_n (cf. Definition 1.6) to be the “background” recurrent configuration, and study the toppling patterns over e_n .

Lemma 3.4. *For each $n \in \mathbb{N}$, the following stabilizations hold. (The number at each sink vertex indicates the number of chips absorbed there.)*

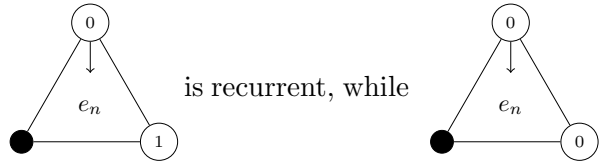


Proof. We prove both results by induction on n . The $n = 1$ case is a direct calculation left for the reader. Now suppose both (13) and (14) hold at level n . To verify the claim at level $n + 1$, recall how e_{n+1} is constructed per Definition 1.6. We then apply the induction hypothesis to each level- n cell as many times as needed, using Lemma 3.1. After each toppling operation over a single (or a pair of adjacent) level- n cells, pause the chips at the cut (or corner) vertices. Then based on the number of the chips available, we carry out further operations until every vertex, except the sinks, carries a nonnegative number of chips fewer than its degree. For (13) the induction step is straightforward:



For (14) the induction step is described in Figure 13. □

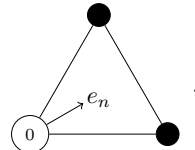
Remark 3.5. For the configuration e_n , we note that



is not recurrent, as can be checked using the burning test and by induction on n .

Next we establish the identity elements.

Proposition 3.6. *The identity element e_n of $(\mathcal{R}_n^{(s)}, \oplus)$ is*



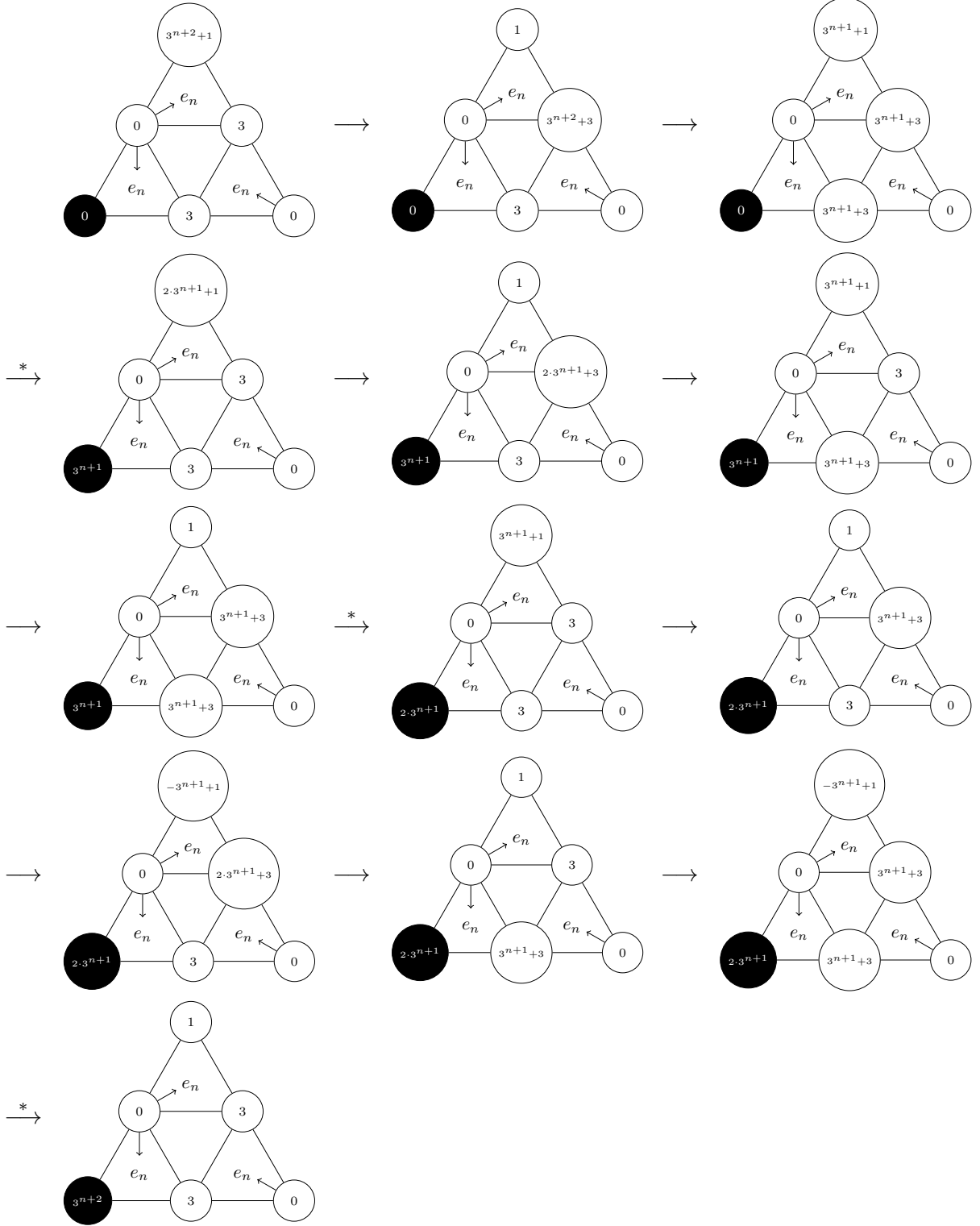
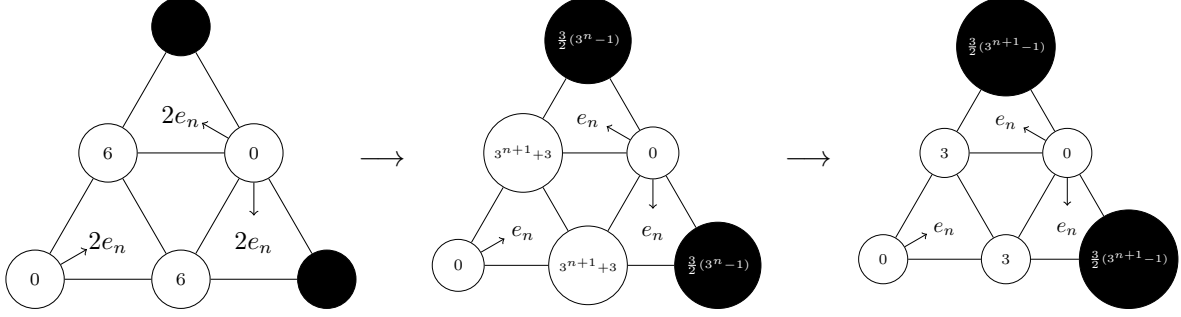


FIGURE 13. The induction step in the stabilization (14) of Lemma 3.4. Arrows with an asterisk * indicate an application of Lemma 3.1.

FIGURE 14. The induction step in the proof of $(2e_n)^\circ = e_n$.

Proof. We prove by induction on n that $(2e_n)^\circ = e_n$, and upon stabilization each sink vertex in ∂G_n absorbs $\frac{3}{2}(3^n - 1)$ chips. (This cardinality makes sense since $3(3^n - 1)$ is the total number of chips in e_n .)

The base case $n = 1$ is a straightforward computation. For the induction step, assume that e_n is the identity element of $\mathcal{R}_n^{(s)}$, and that in the stabilization of $2e_n$, each sink vertex receives $\frac{3}{2}(3^n - 1)$ chips. Let e_{n+1} be constructed according to Definition 1.6. Then we stabilize $2e_{n+1}$ using the induction hypothesis, followed by an application of (14) in Lemma 3.4, as depicted in Figure 14. This proves that e_{n+1} is the identity element of $\mathcal{R}_{n+1}^{(s)}$. \square

Using Proposition 3.6 and the toppling identity (13) we can derive a number of useful consequences.

Proposition 3.7. *For every $\eta \in \mathcal{R}_n^{(s)}$,*

$$(15) \quad \begin{array}{ccc} \bullet & & \bullet \\ & \eta & \\ \circ & & \circ \\ & 2 \cdot 3^n & \end{array} \longrightarrow \begin{array}{ccc} \bullet & & \bullet \\ & \eta & \\ \circ & & \circ \\ & 3^n & \end{array} .$$

Proof. The stabilization (13) in Lemma 3.4 says that $(2 \cdot 3^n) \mathbb{1}_o \oplus e_n = e_n$, with each sink vertex receiving 3^n chips upon stabilization. By the abelian property, $(2 \cdot 3^n) \mathbb{1}_o \oplus \eta = ((2 \cdot 3^n) \mathbb{1}_o \oplus e_n) \oplus \eta = e_n \oplus \eta = \eta$, and each sink vertex still receives 3^n chips upon stabilization. \square

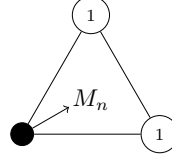
We can also reverse the process (15), which leads to the following stabilization:

Proposition 3.8. *For every $\eta \in \mathcal{R}_n^{(o)}$,*

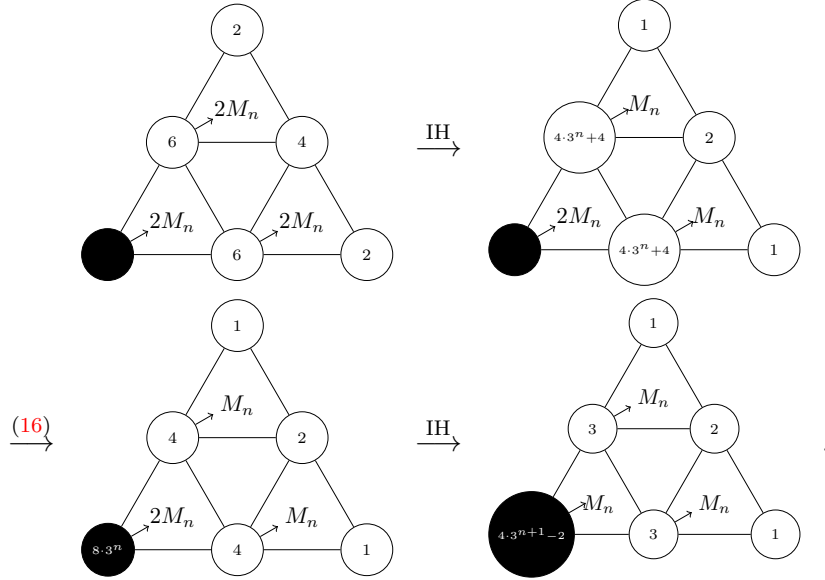
$$(16) \quad \begin{array}{ccc} \circ & & \circ \\ & \eta & \\ \bullet & & \bullet \\ & 3^n & \end{array} \longrightarrow \begin{array}{ccc} \circ & & \circ \\ & \eta & \\ \bullet & & \bullet \\ & 2 \cdot 3^n & \end{array} .$$

We now have all the tools to prove

Proposition 3.9. *The identity element $e_n^{(o)}$ of $(\mathcal{R}_n^{(o)}, \oplus)$ is*



Proof. We prove by induction on n that $(2e_n^{(o)})^\circ = e_n^{(o)}$, and upon stabilization the sink o receives $4 \cdot 3^n - 2$ chips. When $n = 1$ the calculation is straightforward. Suppose the result holds on level n . The induction step for level $n + 1$ proceeds as follows. (From this point onwards, “IH” denotes an application of the induction hypothesis.)



□

Proof of Theorem 4. We already proved Items (1), (2) and the first identity

$$(17) \quad \eta \oplus 3^n(\mathbb{1}_x + \mathbb{1}_y) = \eta$$

in Item (3). It remains to establish that for every $\eta \in \mathcal{R}_n^{(o)}$,

$$(18) \quad \eta \oplus 3^{n+1}\mathbb{1}_x = \eta,$$

$$(19) \quad \eta \oplus 3^{n+1}\mathbb{1}_y = \eta.$$

To prove (18) we combine (14) with the abelian property and proceed *à la* the proof of Proposition 3.7. The identity (19) is equivalent to (18) once we reflect the configuration across the axis of symmetry. □

Remark 3.10 (Nested structure of the identity elements). We pause to make an observation which applies to other nested self-similar fractal graphs: that the sequence of identity elements $(e_n)_n$ is nested in that for every $n \in \mathbb{N}$, $e_{n+1}|_{G_n^{(s)}} = e_n$. Indeed, if e_{n+1} is the identity element of $\mathcal{R}_{n+1}^{(s)}$, then we can stabilize $2e_{n+1}$ by first stabilizing everywhere in $G_n^{(s)}$ to produce $(2e_{n+1}|_{G_n^{(s)}})^\circ$ and pausing excess chips on ∂G_n . Then we fire chips into $G_{n+1}^{(s)} \setminus G_n^{(s)}$ and stabilize every vertex therein, and by Lemma 3.1, this leaves the configuration in $G_n^{(s)}$ invariant. At the end of the stabilization, we recover e_{n+1} , and thus on $G_n^{(s)}$ we have $(2e_{n+1}|_{G_n^{(s)}})^\circ = e_{n+1}|_{G_n^{(s)}}$, i.e., $e_{n+1}|_{G_n^{(s)}} = e_n$. By the same argument, the nested property also holds for the sequence $(e_n^{(o)})_n$.

3.3. A reflection and a rotation lemma. In this subsection we establish two stabilization lemmas on $G_n^{(o)}$, taking advantage of the axial symmetry inherent in the graph. These lemmas play a crucial role in the proof of radial jumps in §3.4 and §3.5.

Lemma 3.11 (Reflection across the axis of symmetry). *Let $\eta \in \mathcal{R}_n^{(o)}$ be such that $\eta = e_n^{(o)} \oplus \alpha \mathbb{1}_x \oplus \beta \mathbb{1}_y$ for some $\alpha, \beta \in \mathbb{N}_0$. Let $k_x, k_y \in \mathbb{N}_0$ solve the system of equations*

$$(20) \quad \begin{cases} \alpha + k_x &= \beta + p_0 \cdot 3^n + p_1 \cdot 3^{n+1} \\ \beta + k_y &= \alpha + p_0 \cdot 3^n + p_2 \cdot 3^{n+1} \end{cases}$$

for some $p_0, p_1, p_2 \in \mathbb{Z}$. Then

$$(21) \quad \begin{array}{c} \begin{array}{ccc} & \textcircled{k_x} & \\ & \downarrow & \\ \bullet & \text{---} \eta \text{---} & \textcircled{k_y} \end{array} & \equiv & \begin{array}{ccc} & \textcircled{} & \\ & \downarrow & \\ \bullet & \text{---} \tilde{\eta} \text{---} & \textcircled{} \end{array} \end{array},$$

where $\tilde{\eta}$ is the reflection of η across the axis of symmetry.

Proof. By the axial symmetry, the reflection of η satisfies $\tilde{\eta} = e_n^{(o)} \oplus \beta \mathbb{1}_x \oplus \alpha \mathbb{1}_y$. We then observe that (21) is implied by the algebraic identity

$$e_n^{(o)} \oplus (\alpha + k_x) \mathbb{1}_x \oplus (\beta + k_y) \mathbb{1}_y = e_n^{(o)} \oplus \beta \mathbb{1}_x \oplus \alpha \mathbb{1}_y.$$

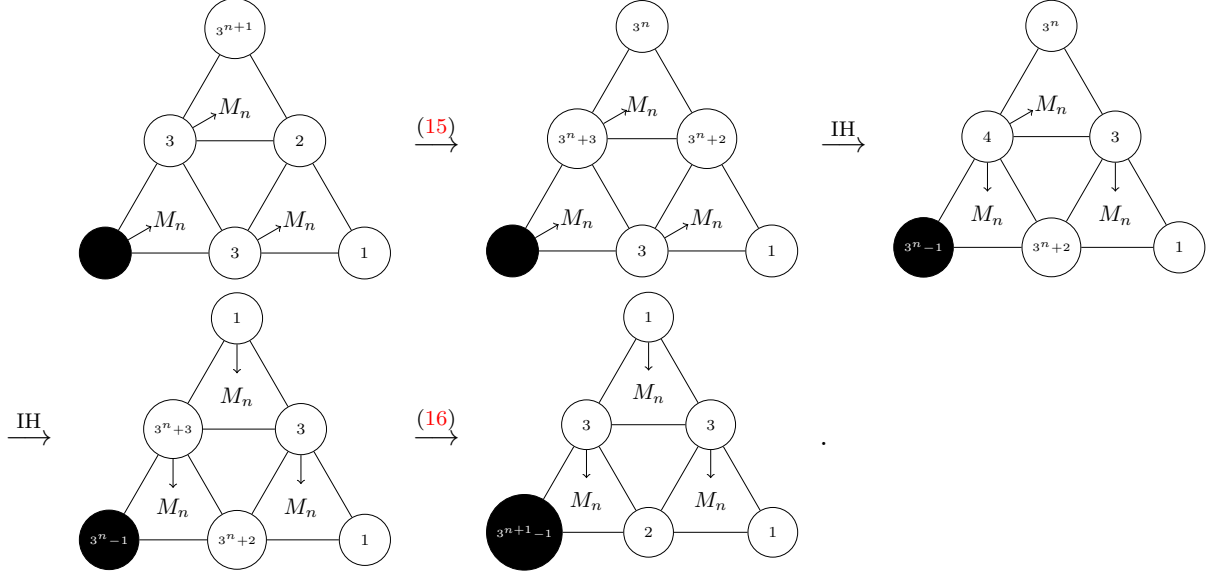
This explains (20) in the special case $p_0 = p_1 = p_2 = 0$. For the general case of (20), we apply the equivalence under the toppling identities (17), (18), and (19). \square

Lemma 3.12 (120°-rotation of M_n). *The following stabilizations hold:*

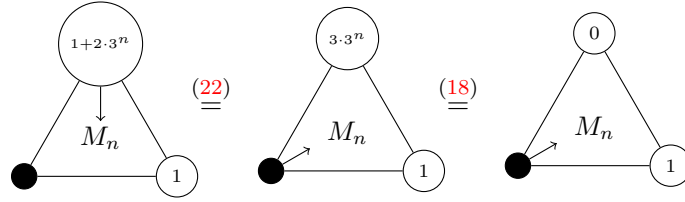
$$(22) \quad \begin{array}{ccc} \begin{array}{ccc} & \textcircled{3^n} & \\ & \downarrow & \\ \bullet & \text{---} M_n \text{---} & \textcircled{1} \end{array} & \longrightarrow & \begin{array}{ccc} & \textcircled{1} & \\ & \downarrow & \\ \bullet & \text{---} M_n \text{---} & \textcircled{1} \end{array} \end{array},$$

$$(23) \quad \begin{array}{ccc} \begin{array}{ccc} & \textcircled{1+2 \cdot 3^n} & \\ & \downarrow & \\ \bullet & \text{---} M_n \text{---} & \textcircled{1} \end{array} & \longrightarrow & \begin{array}{ccc} & \textcircled{0} & \\ & \downarrow & \\ \bullet & \text{---} M_n \text{---} & \textcircled{1} \end{array} \end{array}.$$

Proof. We prove (22) by induction on n . The $n = 1$ case is verified readily. Suppose the stabilization holds at level n . At level $n + 1$ the stabilization proceeds as follows:



Now we can prove (23) using (22) and the toppling identity (18):



The number of chips that the sink receives can be inferred readily. \square

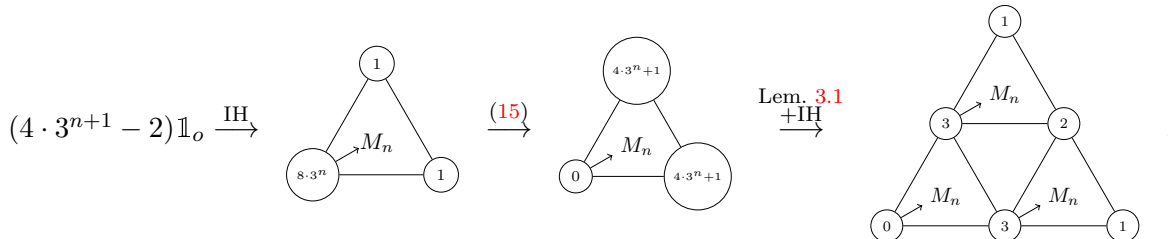
3.4. Explosions in sandpile growth. In this subsection we prove the existence of explosions in the growing cluster, *i.e.*, a radial jump of size > 1 . To be precise, the main explosion, occurring at mass $4 \cdot 3^n$, happens as the configuration transitions from M_n (see Definition 1.7) to e_n (see Definition 1.6).

Proposition 3.13. *For each $n \in \mathbb{N}$,*

$$((4 \cdot 3^n - 2) \mathbb{1}_o)^\circ = \text{triangle with top node 1, bottom nodes 1 and 1, and an arrow labeled } M_n \text{ from top to bottom-left node.}$$

It follows that $r_{4 \cdot 3^n - 2} = 2^n$.

Proof. It is direct to verify the identity for $n = 1$. Suppose the identity holds at level n . Note that $4 \cdot 3^{n+1} - 2 = (4 \cdot 3^n - 2) + 4(2 \cdot 3^n)$. Based on this we carry out the stabilization as follows:



In the last step, we use Lemma 3.1 to topple the $4 \cdot 3^n + 1$ chips at the cut point in ∂G_n . The number of chips decrements in steps of 2 until 3 chips remain, producing a facsimile of $((4 \cdot 3^n - 2)\mathbb{1}_o)^\circ$ that emanates from the cut point. By the induction hypothesis this configuration is M_n . The two copies of M_n merge at the midpoint between the two sinks of $G_{n+1}^{(s)}$, resulting in $1 + 1$ chips at that midpoint. According to Definition 1.7, this is the stable configuration M_{n+1} with 1 chip at each sink of $G_{n+1}^{(s)}$.

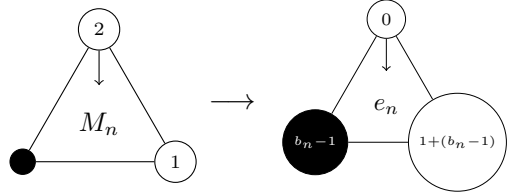
Since M_n has full support in G_n , it follows that $r_{4 \cdot 3^n - 2} = 2^n$. \square

Proposition 3.14. *For each $n \in \mathbb{N}$,*

$$(24) \quad (4 \cdot 3^n \mathbb{1}_o)^\circ = \begin{array}{c} \text{1} \\ \swarrow \quad \searrow \\ \text{ } \quad \quad \text{ } \\ \nearrow \quad \nwarrow \\ \text{ } \quad \quad \text{ } \\ \text{1} \end{array} \xrightarrow{M_n} \oplus 2\mathbb{1}_o = \left(\begin{array}{c} \text{ } \quad \quad \text{ } \\ \swarrow \quad \searrow \\ \text{ } \quad \quad \text{ } \\ \nearrow \quad \nwarrow \\ \text{ } \quad \quad \text{ } \\ \text{ } \quad \quad \text{ } \end{array} \right)^\circ,$$

where $b_n = |V(G_{n-1})| = \frac{3}{2}(3^{n-1} + 1)$. It follows that $r_{4 \cdot 3^n} = 2^n + r_{b_n - 2}$.

Proof. When $n = 1$ the identity is verified directly. Suppose the identity holds at level n . Based on the induction hypothesis we have

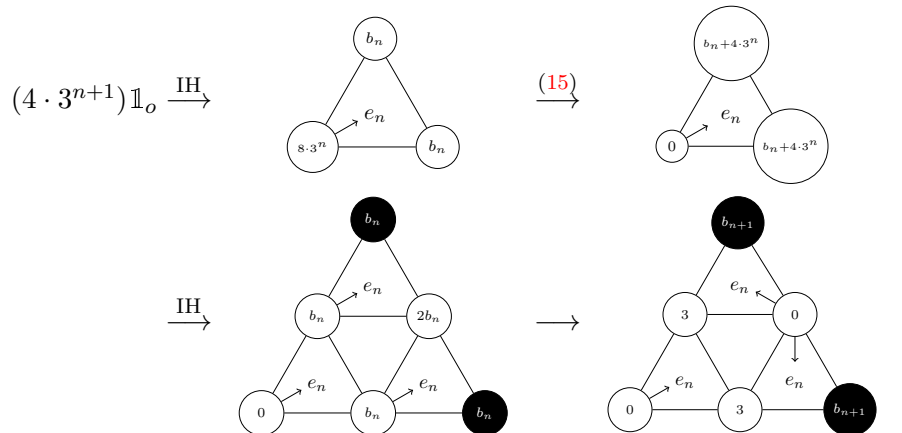


Combine this with the M_n rotation identity (22), infer that

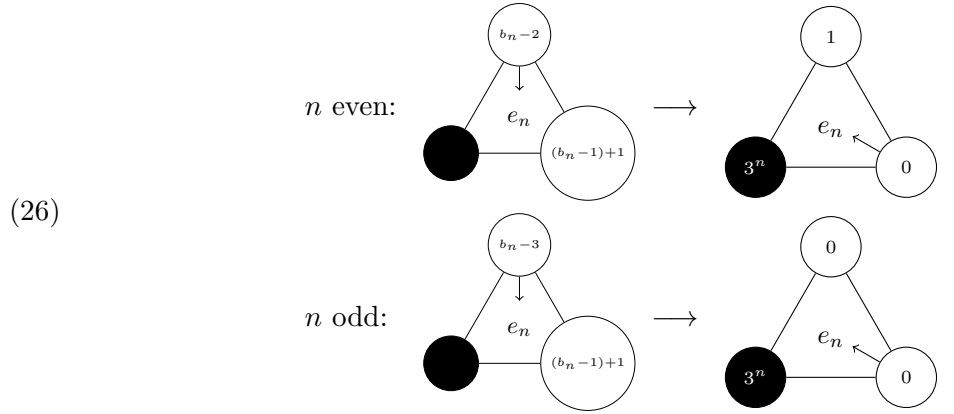
$$(25) \quad \begin{array}{c} \text{0} \\ \swarrow \quad \searrow \\ \text{ } \quad \quad \text{ } \\ \nearrow \quad \nwarrow \\ \text{ } \quad \quad \text{ } \\ \text{ } \quad \quad \text{ } \end{array} \xrightarrow{e_n} = e_n^{(o)} \oplus 3^n \mathbb{1}_x \oplus (1 - b_n) \mathbb{1}_y \stackrel{(17)}{=} e_n^{(o)} \oplus (2 \cdot 3^n) \mathbb{1}_x \oplus (b_n - 2) \mathbb{1}_y.$$

(Recall Remark 3.5.) We will use (25) in the final reflection step below.

Now we indicate the stabilization steps. The first step is based on the count $4 \cdot 3^{n+1} = 4 \cdot 3^n + 4(2 \cdot 3^n)$ and the induction hypothesis:



The final reflection step requires justification. Observe that we need to send the remaining excess chips to the sinks ∂G_{n+1} . Since b_n is odd (resp. even) when n is odd (resp. even), we separately prove that



Recalling (25), we apply the reflection Lemma 3.11 with $\alpha = 2 \cdot 3^n$ and $\beta = b_n - 2$, and verify that (20) is satisfied with $k_x = b_n - 2$, $k_y = b_n - 1$, $p_0 = -1$, $p_1 = 1$ and $p_2 = 0$. This proves the case when n is even. For the case when n is odd, the argument is the same except that 1 chip is removed from x . The number of chips 3^n received by the sink can be inferred directly.

In either case, once we glue back the resulting configuration, there will be 3 chips on each junction vertex in ∂G_n . This leads to the claimed final configuration shown above, with each sink vertex in ∂G_{n+1} receiving $b_n + 3^n = b_{n+1}$ chips.

Finally, topple on ∂G_{n+1} , making sure that every topple on ∂G_{n+1} also triggers a topple at every vertex in $G_{n+1}^{(s)}$ according to Lemma 3.1. \square

We can now establish the existence of explosion at mass $4 \cdot 3^n$.

Corollary 3.15. *For $n \geq 2$, $\max\{m \in \mathbb{N} : r_m = 2^n\} = 4 \cdot 3^n - 1$. Moreover, $r_{4 \cdot 3^n} - r_{4 \cdot 3^{n-1}} \geq 2$ for each $n \geq 3$.*

Proof. The first statement is a consequence of Propositions 3.13 and 3.14, together with the fact that $b_n \geq 4$ for $n \geq 2$. For the second statement, note that Propositions 3.14 and 3.2 imply that $r_{4 \cdot 3^n} = 2^n + r_{b_n-2}$. When $n \geq 3$, $r_{b_n-2} \geq 2$, so $r_{4 \cdot 3^n} - r_{4 \cdot 3^{n-1}} \geq (2^n + 2) - 2^n = 2$. \square

Corollary 3.16 (Periodicity of sandpile patterns). *Let $m \geq 4 \cdot 3^n$. Then for each $k \in \mathbb{N}$ and $k \leq n$, $(m \mathbb{1}_o)^\circ|_{G_k^{(s)}} = ((m + 2 \cdot 3^k) \mathbb{1}_o)^\circ|_{G_k^{(s)}}$.*

Proof. The condition $m \geq 4 \cdot 3^n$ is to ensure that $(m \mathbb{1}_o)^\circ|_{G_n^{(s)}}$ is a recurrent configuration (but see Remark 3.25). The claim then follows from Proposition 3.7. \square

Having identified the main explosions, we can now identify the secondary explosions occurring at mass $6 \cdot 3^n$, $8 \cdot 3^n$, and $10 \cdot 3^n$.

Proposition 3.17. *For each $n \in \mathbb{N}$ and $p \in \{0, 1, 2, 3\}$,*

$$(((4 + 2p)3^n - 2) \mathbb{1}_o)^\circ = \left(\begin{array}{c} \text{triangle with vertices } 1+p \cdot 3^n, 1+p \cdot 3^n, \text{ and } M_n \\ \text{with an arrow from } M_n \text{ to the bottom vertex} \end{array} \right)^\circ ; ((4 + 2p)3^n \mathbb{1}_o)^\circ = \left(\begin{array}{c} \text{triangle with vertices } m'_{n,p}, m'_{n,p}, \text{ and } e_n \\ \text{with an arrow from } e_n \text{ to the bottom vertex} \end{array} \right)^\circ,$$

where $m'_{n,p} = b_n + p \cdot 3^n = (p + \frac{1}{2}) 3^n + \frac{3}{2}$. It follows that

$$r_{(4+2p)3^n-2} = 2^n + r_{p \cdot 3^{n-1}} \quad \text{and} \quad r_{(4+2p)3^n} = 2^n + r_{(p+\frac{1}{2})3^{n-\frac{1}{2}}}.$$

Proof. The diagrams follow directly from Propositions 3.13, 3.14 and 3.7. The radial identities are a consequence of Proposition 3.2, Item (2). \square

We can use Proposition 3.17 and induction to obtain an easy consequence.

Corollary 3.18. *For every $m \in [10 \cdot 3^{n-1}, 4 \cdot 3^n]$:*

- (1) $r_m = 2^n$.
- (2) $(m\mathbb{1}_o)^\circ$ has 1 chip on each vertex in the boundary set ∂G_n .

Proof. To prove Part (1), we note by Corollary 3.15 that $r_m \leq 2^n$. To show that $r_m = 2^n$, it is enough to show that $r_{10 \cdot 3^{n-1}} = 2^n$ by induction on n . When $n = 1$, $r_{10 \cdot 3^0} = r_{10} = 2$. Suppose $r_{10 \cdot 3^{n-1}} = 2^n$. Then using Proposition 3.17 we have

$$r_{10 \cdot 3^n} = 2^n + r_{(3+\frac{1}{2})3^{n+1}-\frac{1}{2}} \geq 2^n + r_{10 \cdot 3^n} = 2^n + 2^n = 2^{n+1}.$$

Combined with $r_{10 \cdot 3^n} \leq 2^{n+1}$ this implies $r_{10 \cdot 3^n} = 2^{n+1}$.

To prove Part (2), note that since the receiving set $((10 \cdot 3^{n-1})\mathbb{1}_o)^\circ$ is an exact ball and has full support in G_n , each vertex in ∂G_n must receive at least 1 chip. Meanwhile, Proposition 3.13 states that $((4 \cdot 3^n - 1)\mathbb{1}_o)^\circ$ also has full support in G_n and carries 1 chip on each vertex in ∂G_n . The claim follows from the fact that the number of chips on ∂G_n increases monotonically with m . \square

3.5. Enumeration of radial jumps (I): analysis of sandpile tiles. In the next two subsections we complete the proof of Theorem 5. We present the proofs in the following order:

- “ $4\frac{2}{3}^-$ ” and “ $5\frac{1}{3}^-$,” followed by “ $4\frac{2}{3}^-$.”
- “ $4\frac{4}{9}$ ” and “ $5\frac{1}{3}$,” which are proved in tandem.
- “ $e + 2$,” followed by “ $4\frac{4}{9}$.”

The first two items are based on tiling ideas and are proved in this subsection. The last item is proved in the next subsection.

To establish “ $4\frac{2}{3}^-$,” we introduce another family of sandpile tiles.

Lemma 3.19. *The following stabilization holds:*

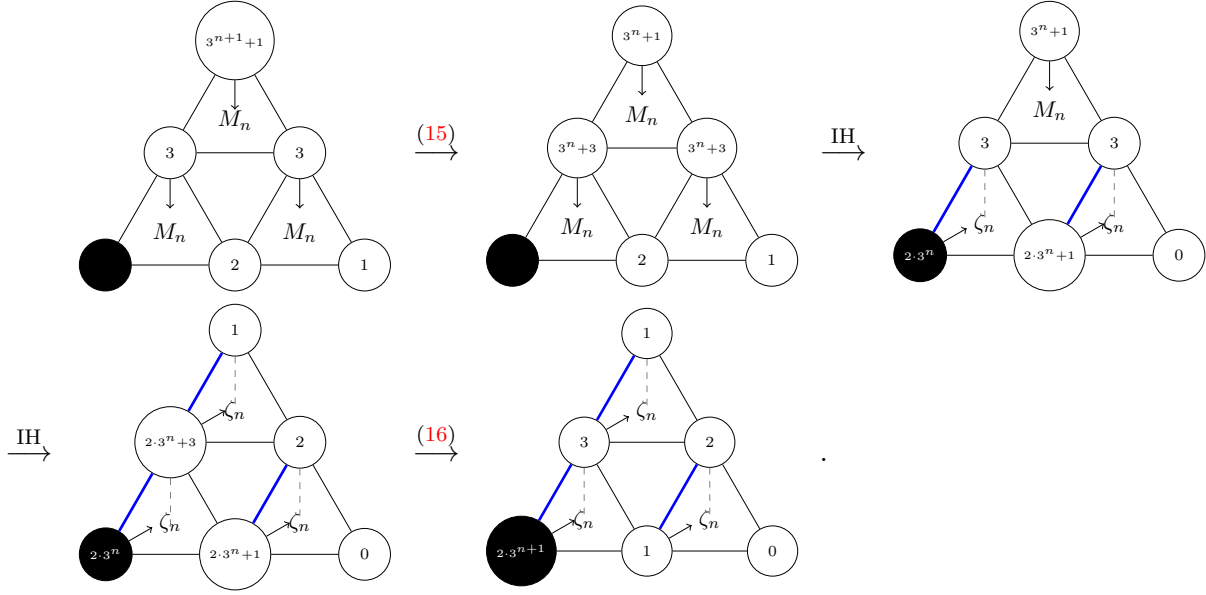
$$(27) \quad \begin{array}{c} \text{Diagram 1: A triangle with vertices } 3^{n+1} \text{ (top), } 1 \text{ (bottom right), and a black dot (bottom left). An arrow labeled } M_n \text{ points from } 3^{n+1} \text{ to } 1. \\ \text{Diagram 2: A triangle with vertices } 1 \text{ (top), } 0 \text{ (bottom right), and } 2 \cdot 3^n \text{ (bottom left, black dot). An arrow labeled } \zeta_n \text{ points from } 1 \text{ to } 2 \cdot 3^n. \end{array} \quad \longrightarrow$$

where $\begin{array}{c} \text{Diagram 3: A triangle with vertices } 1 \text{ (top), } 0 \text{ (bottom right), and } 0 \text{ (bottom left, black dot). An arrow labeled } \zeta_1 \text{ points from } 1 \text{ to } 0. \\ \text{Diagram 4: A triangle with vertices } 3 \text{ (top), } 2 \text{ (bottom right), } 1 \text{ (bottom left), and } 0 \text{ (bottom left, black dot). Arrows labeled } \zeta_1 \text{ point from } 3 \text{ to } 2 \text{ and } 3 \text{ to } 1. \end{array} =$, and for $n \geq 1$, ζ_{n+1} is constructed by gluing three copies of ζ_n according to the rule

$$\begin{array}{c} \text{Diagram 5: A triangle with vertices } 1 \text{ (top), } 0 \text{ (bottom right), and } 0 \text{ (bottom left, black dot). A blue line connects the top vertex to the bottom left vertex. An arrow labeled } \zeta_{n+1} \text{ points from the top vertex to the blue line.} \\ \text{Diagram 6: A triangle with vertices } 3 \text{ (top), } 2 \text{ (bottom right), } 1 \text{ (bottom left), and } 0 \text{ (bottom left, black dot). Three blue lines connect the top vertex to the bottom left vertex, the bottom left vertex to the bottom right vertex, and the bottom right vertex to the top vertex. Arrows labeled } \zeta_n \text{ point from } 3 \text{ to } 2, 3 \text{ to } 1, \text{ and } 2 \text{ to } 1. \end{array} =$$

(For emphasis: Every vertex along the blue line carries 3 chips.)

Proof. The $n = 1$ case is verified directly. Assume that the claim holds at level n . At level $n + 1$ we have the following series of stabilizations:

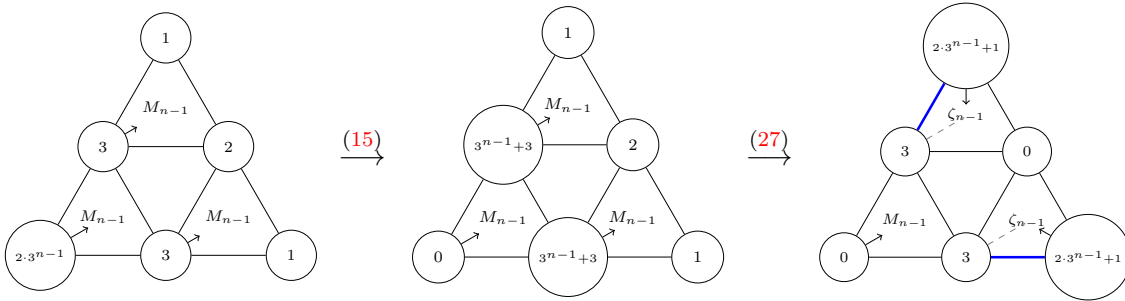


□

Proposition 3.20 ($4\frac{2}{3}^-$).

$$((4\frac{2}{3} \cdot 3^n - 2)\mathbb{1}_o)^\circ = \left(\begin{array}{c} m'_n \\ \nearrow \eta(m) \\ m'_n \end{array} \right)^\circ, \text{ where } m'_n = 2 \cdot 3^{n-1} + 1.$$

Proof. We start with the configuration $((4 \cdot 3^n - 2)\mathbb{1}_o)^\circ$ and add to it $\frac{2}{3} \cdot 3^n = 2 \cdot 3^{n-1}$ chips at o . The resulting stabilization is



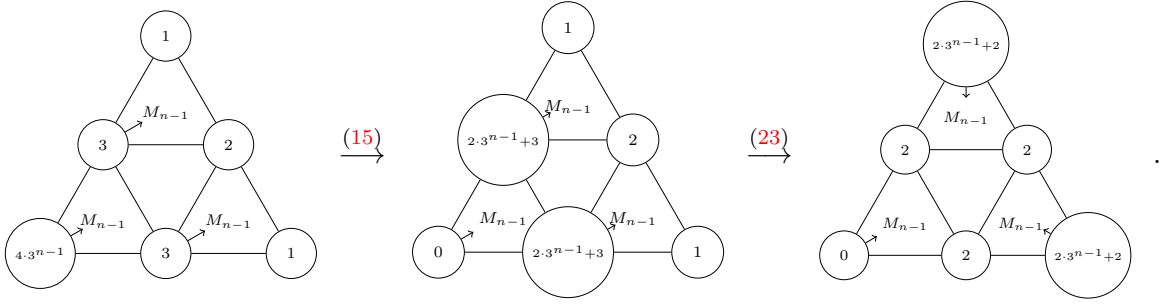
□

Proposition 3.21 (“ $5\frac{1}{3}^-$ ”).

$$\left((5\frac{1}{3} \cdot 3^n - 2) \mathbb{1}_o \right)^\circ = \left(\begin{array}{c} \text{Diagram} \end{array} \right)^\circ, \text{ where } \ell'_n = 2 \cdot 3^{n-1} + 2.$$

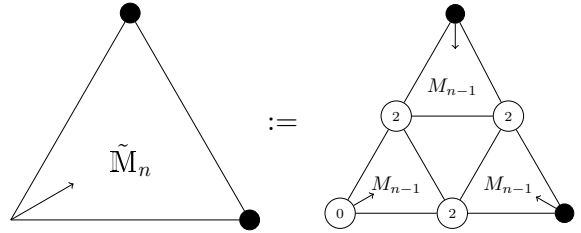
Proof. We start with the configuration $((4 \cdot 3^n - 2) \mathbb{1}_o)^\circ$, established in Proposition 3.13, and add to it $1\frac{1}{3} \cdot 3^n = 4 \cdot 3^{n-1}$ chips at o . The stabilization then proceeds as follows:

(28)



□

It will be helpful to introduce a shorthand for the tile

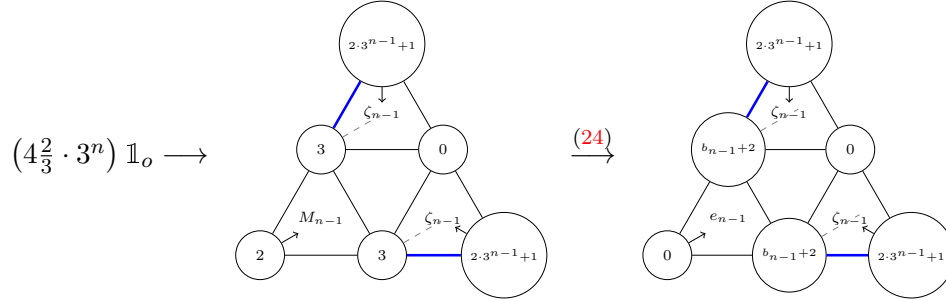


Proposition 3.22 (“ $4\frac{2}{3}$ ”).

$$\left((4\frac{2}{3} \cdot 3^n) \mathbb{1}_o \right)^\circ = \left(\begin{array}{c} \text{Diagram} \end{array} \right)^\circ, \text{ where } \ell'_n = 2 \cdot 3^{n-1} + 2.$$

Proof. Using Propositions 3.20 and 3.21, we can infer that the number of chips received at the sink is at least $2 \cdot 3^{n-1} + 1$ and at most $2 \cdot 3^{n-1} + 2$. To see that it is the latter count, we add 2 chips at

o to the diagram for $((4\frac{2}{3} \cdot 3^n - 2)\mathbb{1}_o)^\circ$:



We then topple both cut vertices in ∂G_{n-1} . Thanks to the line of 3's that connects ∂G_{n-1} to the sink ∂G_n , this triggers a “chain reaction” of topplings down the line and delivers extra chips to ∂G_n . \square

Next we prove “ $4\frac{4}{9}$ ” and $5\frac{1}{3}$ ” in tandem.


Proposition 3.23 (“ $4\frac{4}{9}$ ”).


$$((4\frac{4}{9} \cdot 3^n)\mathbb{1}_o)^\circ = \left(\begin{array}{c} \text{Diagram: A triangle with vertices } m'_n \text{ (top), } m'_n \text{ (bottom right), and an unlabeled vertex (bottom left). An arrow labeled } \eta(m) \text{ points from the bottom left vertex to the bottom right vertex.} \end{array} \right)^\circ, \text{ where } m'_n = 2 \cdot 3^{n-1} + 1.$$

Proposition 3.24 (“ $5\frac{1}{3}$ ”).

$$((5\frac{1}{3} \cdot 3^n)\mathbb{1}_o)^\circ = \left(\begin{array}{c} \text{Diagram: A triangle with vertices } 1+3^n \text{ (top), } 1+3^n \text{ (bottom right), and an unlabeled vertex (bottom left). An arrow labeled } \eta(m) \text{ points from the bottom left vertex to the bottom right vertex.} \end{array} \right)^\circ.$$

The figure shows a sequence of four triangular graphs, each with vertices labeled 1, 2, and 3. The graphs are connected by arrows labeled (15), (16), and (27). The first graph has edges labeled M_{n-1} and vertices labeled 1, 2, 3. The second graph has vertices labeled 1, 2, 3 and edges labeled M_{n-1} , with a large circle at vertex 1 containing $2 \cdot 3^{n-2} + 4$. The third graph has vertices labeled 1, 2, 3 and edges labeled M_{n-1} , with a large circle at vertex 1 containing $3^{n-1} + 3$. The fourth graph has vertices labeled 1, 2, 3 and edges labeled M_{n-1} , with a large circle at vertex 1 containing $2 \cdot 3^{n-1} + 1$. The edges are labeled with M_{n-1} , \tilde{M}_{n-1} , $\tilde{\eta}_{n-1}$, and ζ_{n-1} .

(29) 

(30) 

Finally, we have the stabilization (Mb_n) , which is established via induction on n :

$$(31) \quad \begin{array}{ccc} \begin{array}{c} \text{---} b_n - 1 \text{---} \\ \diagup \quad \diagdown \\ \bullet \quad \quad 1 \end{array} & \xrightarrow{(Mb_n)} & \begin{array}{c} \text{---} 0|1 \text{---} \\ \diagdown \quad \diagup \\ \bullet \quad \quad 1 \end{array} \end{array}$$

M_n ψ_n

The $n = 1$ case is verified directly. Suppose (31) holds at level n . Then in conjunction with (22) we deduce that for $k \in [b_n - 1, 3^n]$,

$$(32) \quad \begin{array}{ccc} \begin{array}{c} \text{---} k \text{---} \\ \diagup \quad \diagdown \\ \bullet \quad \quad 1 \end{array} & \longrightarrow & \begin{array}{c} \text{---} \quad \quad \quad \\ \diagdown \quad \diagup \\ \bullet \quad \quad \quad \end{array} \end{array}$$

M_n $\eta_n(k)$

where $\eta_n(k) \in \mathcal{R}_n^{(o)}$. The induction step then proceeds as follows, noting that $b_{n+1} = b_n + 3^n$, and $b_n - 2 = \frac{3}{2}(3^{n-1} + 1) - 2 \in [\frac{4}{9} \cdot 3^n, \frac{2}{3} \cdot 3^n]$:

$$\begin{array}{ccccc} \begin{array}{c} \text{---} b_{n+1} - 1 \text{---} \\ \diagup \quad \diagdown \\ \text{---} 3 \text{---} \quad \text{---} 2 \text{---} \\ \diagup \quad \diagdown \quad \diagup \quad \diagdown \\ \bullet \quad \quad 3 \quad \quad 3 \quad \quad 1 \end{array} & \xrightarrow{(22)} & \begin{array}{c} \text{---} b_n \text{---} \\ \diagdown \quad \diagup \\ \text{---} 3^n + 2 \text{---} \quad \text{---} 2 \text{---} \\ \diagup \quad \diagdown \quad \diagup \quad \diagdown \\ \bullet \quad \quad 3 \quad \quad 3 \quad \quad 1 \end{array} & \xrightarrow{(\mathcal{Q}_n) + \text{Prop. 3.20}} & \begin{array}{c} \text{---} 0|1 \text{---} \\ \diagdown \quad \diagup \\ \text{---} 3^n + 2 \cdot 3^{n-1} + 2 \text{---} \quad \text{---} 2 \cdot 3^{n-1} + 2 \text{---} \\ \diagup \quad \diagdown \quad \diagup \quad \diagdown \\ \bullet \quad \quad 3 \quad \quad 3 \quad \quad 1 \end{array} \\ \xrightarrow{(32)} \downarrow & & \downarrow & & \\ \begin{array}{c} \text{---} 0|1 \text{---} \\ \diagdown \quad \diagup \\ \text{---} 3^n + 2 \text{---} \quad \text{---} 2 \text{---} \\ \diagup \quad \diagdown \quad \diagup \quad \diagdown \\ \bullet \quad \quad B_n \quad \quad B_n \quad \quad 1 \end{array} & \xrightarrow{(16)} & \begin{array}{c} \text{---} 0|1 \text{---} \\ \diagdown \quad \diagup \\ \text{---} 2 \text{---} \quad \text{---} 2 \text{---} \\ \diagup \quad \diagdown \quad \diagup \quad \diagdown \\ \bullet \quad \quad B_n \quad \quad B_n \quad \quad 1 \end{array} & & \end{array}$$

In the above, A_n and B_n are two recurrent configurations whose patterns are complicated to describe, according to our sandpile simulations.

Proof of Propositions 3.23 and 3.24. Looking at (29), (30), and (31) and how they are established diagrammatically, it suffices to prove the following trio of implications, where “OC” denotes “other conditions” that have already been established independently:

$$\begin{aligned} (\tilde{M}_n) + \text{OC} &\implies (\mathcal{Q}_{n+1}), \\ (Mb_n) + \text{OC} &\implies (\tilde{M}_{n+1}), \\ (Mb_n) + (\mathcal{Q}_n) + \text{OC} &\implies (Mb_{n+1}). \end{aligned}$$

The proof by induction on n is straightforward. □

Remark 3.25. We observe from our numerical computations that $((10 \cdot 3^{n-1})\mathbb{1}_o)^\circ|_{G_n^{(s)}}$ is a recurrent configuration. If this observation can be proved directly, then “ $5\frac{1}{3}$ ” can be established without resort to diagrams, since $5\frac{1}{3} \cdot 3^n = 10 \cdot 3^{n-1} + 2 \cdot 3^n$, and we can use Corollary 3.18 and the $(2 \cdot 3^n)$ -periodicity to deduce that each sink in ∂G_n receives $3^n + 1$ chips.

3.6. Enumeration of radial jumps (II): analysis of traps along the space-filling curve.

It remains to prove “ $e + 2$ ” and “ $4\frac{4}{9}$.” For these we take advantage of the structure of the identity element e_n , namely, the space-filling curve along which every vertex carries 3 chips. See Figure 10.

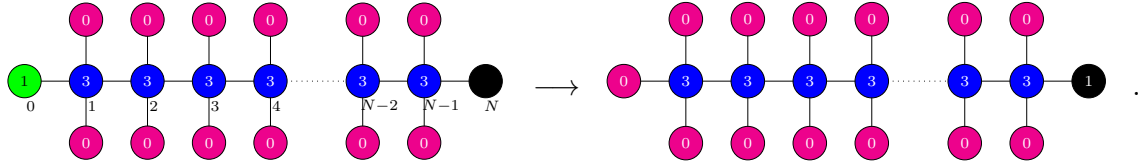
Proposition 3.26 (“ $e + 2$ ”). *For every $n \in \mathbb{N}$, adding $2\mathbb{1}_o$ to e_n and then stabilizing results in 1 chip received by each sink in ∂G_n . Therefore*

$$((4 \cdot 3^n + 2)\mathbb{1}_o)^\circ = \left(\begin{array}{c} \text{Diagram of a triangle with vertices } b_{n+1}, \text{ and } \eta(m), \text{ and } b_{n+1} \text{ at the bottom.} \\ \end{array} \right)^\circ.$$

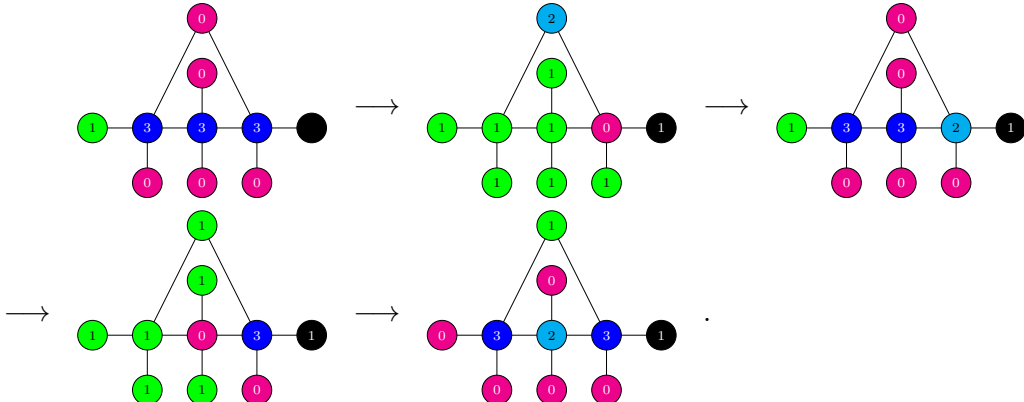
Proof. Given the configuration e_n , adding 2 chips at o triggers a chain of topplings along each space-filling curve, thereby sending 1 chip to each sink vertex. That no more chips can drop into the sink is implied by Proposition 3.28 below. \square

Our next task is to analyze the configuration $e_n \oplus 2\mathbb{1}_o$ in $G_n^{(s)}$, and explain how traps appear along the space-filling curve. As a warm-up exercise let us work through two toy examples.

First consider a “line graph.” Take a positive integer $N \geq 2$. Consider the graph whose vertex set is $(0,0) \cup \{1, \dots, N-1\} \times \{-1, 0, 1\} \cup (N,0)$, and whose edge set consists of edges of the form $(x,0) \sim (x+1,0)$, $0 \leq x \leq N-1$; $(x,1) \sim (x,0)$, $1 \leq x \leq N-1$; and $(x,-1) \sim (x,0)$, $1 \leq x \leq N-1$. Designate $(0,0)$ as the origin, $(N,0)$ as the sink, and suppose on every vertex $(x,0)$ along the line carries the maximal number of chips (3), and every vertex elsewhere carries 0 chips. It is easy to verify that the 1 chip at the origin is transmitted all the way to the sink without changing the configuration on and off the line:



Next we modify the above graph by identifying vertices off the line. For simplicity, take $N = 4$ and identify the vertices $(1,1)$ and $(3,1)$. We then carry out the stabilization systematically by alternating stabilizations on and off the line.



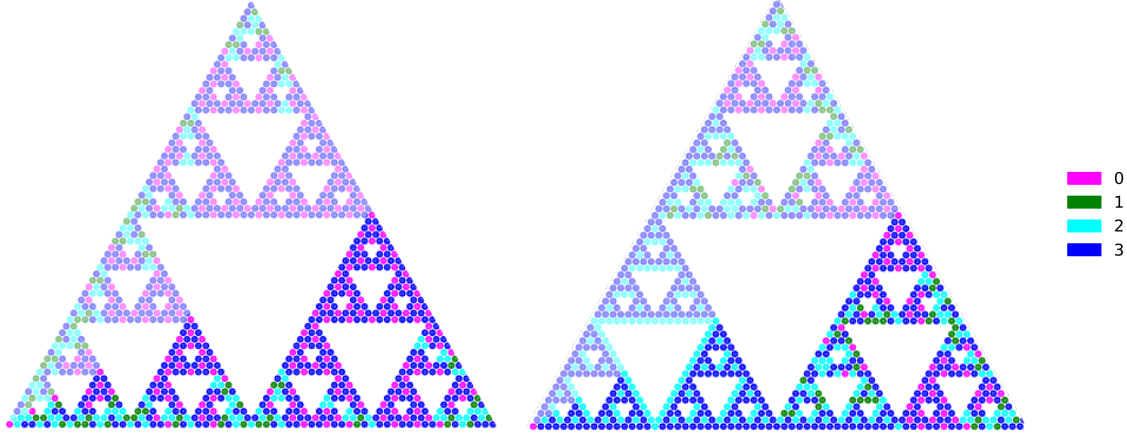


FIGURE 15. The configuration $e_5 \oplus 2\mathbb{1}_o$ (left) and $e_5 \oplus (4 \cdot 3^{5-2}) \mathbb{1}_o$ (right). Blotches of 1's and 2's are “traps,” which appear in well-defined locations.

Observe the appearance of the vertex “2” on the line: this forms a “trap” in the sense that the next chip to travel down the line will be stopped by it. To “re-open” the line of communication requires additional chips at the origin. Of course this does not preclude additional chip(s) from traveling down the “sky hook,” origin–3–1–3–sink. At any rate, we emphasize that *the identification of off-line vertices results in the formation of traps on the line*.

Having explained the trap mechanism in the simple setting, we now proceed to the actual analysis. Parametrize one half of $G_n^{(s)}$ by the length of the space-filling curve. Starting with 2 chips at the origin, we carry out the stabilization systematically. Due to the identifications of the off-line vertices, this triggers a series of topplings backwards along the curve, resulting in the creation of a finite number of well-separated *traps*, represented by blotches of 1's and 2's; see the left configuration in Figure 15. Figure 16 shows the precise mechanism of trap creation in the case e_3 .

A key observation is that whenever the on-line propagation stops in the middle of a “*sky hook*”—where (far-away) vertices on-line are connected to the same off-line vertex—this results in the creation of a trap at the start of the hook. See the transition from (c) to (e), and from (g) to (i), in Figure 16. This leaves the configuration in some portion of the space-filling curve unchanged. Thus after stabilization is complete, the space-filling curve contains several traps, and connecting two adjacent traps is a *corridor*: each vertex on the corridor carries 3, and off it, 0 chip.

Given the landscape of traps, the goal is to add enough chips at o so that they can overcome one trap after another. Keep in mind, however, that whenever a chip lands on a corridor but is stopped by the next trap, the aforementioned argument implies that additional traps may be created along the corridor.

Now that we have laid out the key observations, it is time to establish the following comparison lemma, which says that over the configuration e_n , it is “easier” to send chips down the axial direction than the oblique direction.

Lemma 3.27. *If*

does not result in more than 1 chip received by each sink, then

neither does

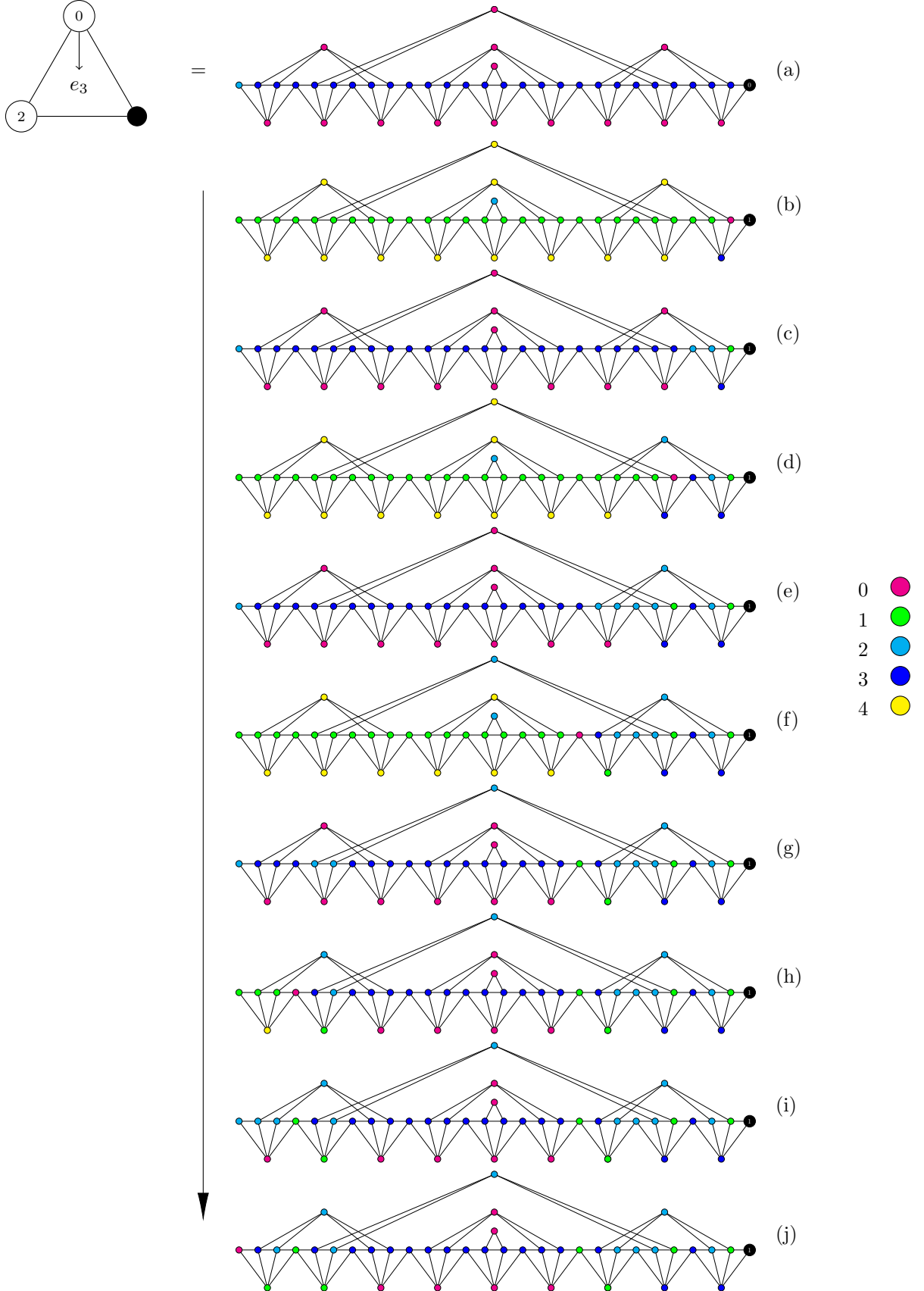
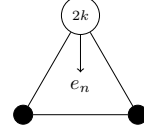


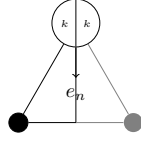
FIGURE 16. Stabilization after adding 2 chips at the start of the space-filling curve in e_3 . This is carried out systematically by alternating stabilizations on and off the space-filling curve. The final configuration consists of two traps and a corridor.

Proof. First note that by the axial symmetry, it is enough to split



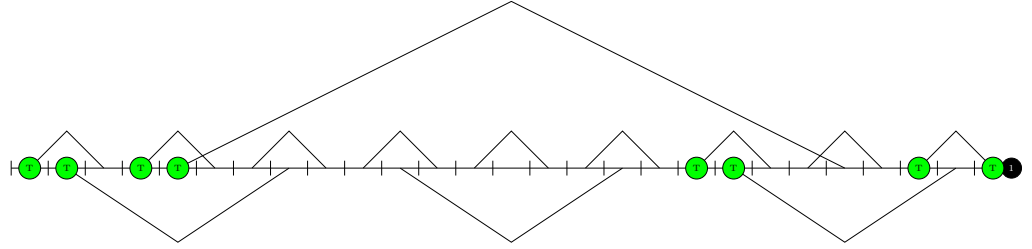
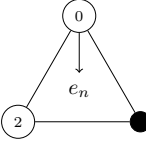
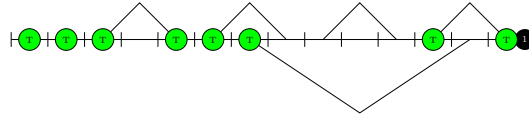
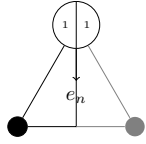
in two halves, and

consider whether

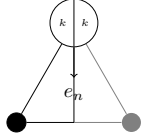


results in more than 1 chip received by the sink. With this proviso

we now parametrize the two configurations in the statement by the length of the space-filling curve. When the origin topples once, the resulting landscape of traps (●) is shown below. (In the right-hand diagrams, each tick mark represents distance 3^{n-3} in the graph metric along the space-filling curve. For clarity, traps, corridors, and sky hooks of length scale $< 3^{n-3}$ are omitted from the diagrams.)

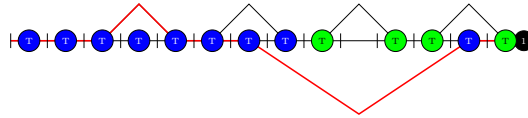


Suppose



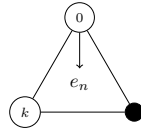
does not result in more than 1 chip received by each sink. In the best-case,

or most greedy, scenario, chips topple along the shortest path (marked in **thick red line**) in such a way that all but the final trap has been overcome. Traps which are guaranteed to be overcome in this scenario are denoted by ●. Observe that there are 7 traps along the shortest path which are overcome.



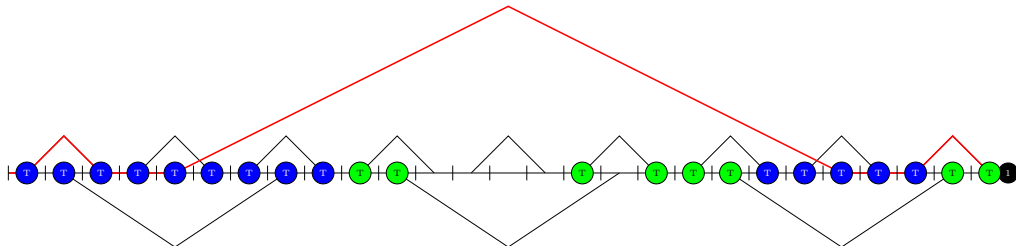
(33)

As a result, when we stabilize



we also expect, in the best-case scenario, no more than

7 traps overcome along the shortest path, as indicated in the diagram below:



(34)

In fact, since the graph in (34) has additional branching compared to the graph in (33), the diagram (34) overrepresents the number of topplings than the actual case. Nevertheless it does indicate that no more than 1 chip can drop into the sink. \square

Proposition 3.28 ($4\frac{4}{9}^-$).

$$\left((4\frac{4}{9} \cdot 3^n - 2)\mathbb{1}_o\right)^\circ = \left(\begin{array}{c} \text{triangle with } b_{n+1} \text{ at top and } b_{n+1} \text{ at bottom} \\ \text{edge from top to bottom-left labeled } \eta(m) \end{array} \right)^\circ.$$

Proof. This is equivalent to the stabilization

$$(35) \quad \begin{array}{c} \text{triangle with } 0 \text{ at top, } 0 \text{ at bottom-right, and } \frac{4}{9} \cdot 3^n - 2 \text{ at bottom-left} \\ \text{edge from top to bottom-left labeled } e_n \end{array} \longrightarrow \begin{array}{c} \text{triangle with } 1 \text{ at top, } 1 \text{ at bottom-right, and } 0 \text{ at bottom-left} \\ \text{edge from top to bottom-left labeled } \#_n \end{array},$$

which we prove by induction on n . The base case is verified directly. Assume (35) holds at level $n-1$. Observe that to obtain $((4\frac{4}{9} \cdot 3^n - 2)\mathbb{1}_o)^\circ$, we start with the configuration $((4 \cdot 3^n - 2)\mathbb{1}_o)^\circ$ and add to it $\frac{4}{9} \cdot 3^n = 4 \cdot 3^{n-2}$ chips at o .

$$\begin{array}{ccc} \begin{array}{c} \text{triangle with } 1 \text{ at top, } 2 \text{ at bottom-right, and } 4 \cdot 3^{n-2} \text{ at bottom-left} \\ \text{edges } M_{n-1} \end{array} & \xrightarrow{(28)} & \begin{array}{c} \text{triangle with } 1 \text{ at top, } 2 \text{ at bottom-right, and } 2 \cdot 3^{n-2} + 4 \text{ at bottom-left} \\ \text{edges } M_{n-1} \end{array} \\ \begin{array}{c} \text{triangle with } b_{n-1} \text{ at top, } 2b_{n-1} \text{ at bottom-right, and } 2 \cdot 3^{n-2} + 2 \text{ at bottom-left} \\ \text{edges } e_{n-1} \end{array} & \xrightarrow{(26)} & \begin{array}{c} \text{triangle with } b_n \text{ at top, } b_n \text{ at bottom-right, and } b_{n-2} + 1 \text{ at bottom-left} \\ \text{edges } e_{n-1} \end{array} \end{array}$$

(24) (26)

In the next step we topple the $b_{n-2} + 1$ chips at the cut point in ∂G_n . Recall that in e_{n-1} there is a path connecting ∂G_{n-1} and ∂G_n along which every vertex carries 3 chips, cf. Proposition 3.26. Thus the first topple will trigger a chain of topplings which sends 1 chip to the sink in ∂G_n . We now claim that no additional chips can drop into ∂G_n , i.e.,

$$\begin{array}{c} \text{triangle with } 0 \text{ at top, } 0 \text{ at bottom-right, and } b_{n-2} - 1 \text{ at bottom-left} \\ \text{edge from top to bottom-right labeled } e_{n-1} \end{array} \longrightarrow \begin{array}{c} \text{triangle with } 0 \text{ at top, } 1 \text{ at bottom-right, and } 0|1 \text{ at bottom-left} \\ \text{edge from top to bottom-right labeled } \S_{n-1} \end{array}.$$

Since $b_{n-2} - 1 = \frac{3}{2}(3^{n-3} + 1) - 1 = \frac{1}{6} \cdot 3^{n-1} + \frac{1}{2} < \frac{1}{2} \left(\frac{4}{9} \cdot 3^{n-1} - 2 \right)$, the claim follows from the induction hypothesis (35) at level $n - 1$ and the comparison Lemma 3.27. We thus verify (35) at level n . \square

Proof of Theorem 5. So far we have proved the results for $p = 0$. To obtain the result for $p \in \{1, 2, 3\}$, we just add to every existing diagram $2p \cdot 3^n$ chips at o . By (15), stabilization results in adding $p \cdot 3^n$ chips to each sink in ∂G_n . \square

3.7. Recursive formula for the cluster radius.

Proof of Theorem 6. We combine the results in Theorem 5 with Proposition 3.2, Item (2). Specifically, given $m' - 2$, we identify the numbers c and d such that the $r(x)$ is constant on $[c, d)$ and $m' - 2 \in [c, d)$. This then leads to the claimed radial recursions (see also Figure 11), as well as the complete characterization of the radial jumps. The reason that we specify the results for $n \geq 3$ (or $n \geq 4$) is due to jumps for $n \in \{1, 2, 3\}$ which do not follow the periodicity stated in Theorem 5, cf. Table 3 and Figure 6. \square

3.8. Cluster growth asymptotically follows a power law modulated by log-periodic oscillations. The goal of this subsection is to prove Theorem 2, Part (2). The proof employs the renewal theorem, which is widely used in the study of fractal geometry, see e.g. [23, 39, 42, 51]. The key input is

Proposition 3.29 (Remainder estimate). *For all $m \in \mathbb{N}$, $|r_{3m} - 2r_m| \leq 1$.*

Proof. Theorem 6 states that given $a \in [4, 12)$, there exists $b \in [4, 12)$ such that

$$\text{either } r_{a \cdot 3^n} = 2^n + r_{b \cdot 3^{n-2}} \text{ for } n \geq 4, \text{ or } r_{a \cdot 3^n} = 2^n + r_{b \cdot 3^{n-1}} \text{ for } n \geq 3.$$

This implies that

(36)

$$\text{either } r_{a \cdot 3^{n+1}} - 2r_{a \cdot 3^n} = r_{b \cdot 3^{n-1}} - 2r_{b \cdot 3^{n-2}} \text{ for } n \geq 4, \text{ or } r_{a \cdot 3^{n+1}} - 2r_{a \cdot 3^n} = r_{b \cdot 3^n} - 2r_{b \cdot 3^{n-1}} \text{ for } n \geq 3.$$

So it is enough to check that for every $b \in [1, 4 \cdot 3^3)$, $|r_{3b} - 2r_b| \leq 1$, cf. Table 3, and then apply (36) inductively. \square

For our purposes the following version of the renewal theorem will suffice. Denote by \mathcal{F} the space of Borel measurable functions $f : \mathbb{R} \rightarrow \mathbb{R}$ such that $\lim_{t \rightarrow -\infty} f(t) = 0$ and such that f is bounded on $(-\infty, a]$ for every $a \in \mathbb{R}$. A Borel measure μ is said to be τ -**arithmetic** if $\tau > 0$ is the largest number such that the support of μ is contained in the additive subgroup $\tau\mathbb{Z}$. If no such τ exists then we say that μ is **non-arithmetic**.

Lemma 3.30 (Renewal theorem, cf. [23, Proposition 7.1 and Theorem 7.2]). *Let $g : \mathbb{R} \rightarrow \mathbb{R}$, and μ be a Borel probability measure supported on $[0, \infty)$, Suppose:*

$$(R1) \quad \lambda := \int_0^\infty t d\mu(t) < \infty.$$

$$(R2) \quad \int_0^\infty e^{-at} d\mu(t) < 1 \text{ for every } a > 0.$$

$$(R3) \quad g \text{ has a discrete set of discontinuities, and there exist } c, \alpha > 0 \text{ such that } |g(t)| \leq ce^{-\alpha|t|} \text{ for all } t \in \mathbb{R}.$$

*Then there is a unique $f \in \mathcal{F}$ which solves the **renewal equation***

$$f(t) = g(t) + \int_0^\infty f(t-y) d\mu(y) \quad (t \in \mathbb{R})$$

and the solution is

$$f(t) = \sum_{k=0}^{\infty} (g * \mu^{*k})(t),$$

where $(g * \mu)(t) = \int_0^\infty g(t-y) d\mu(y)$ denotes the convolution of g and μ , and μ^{*k} denotes the k -fold convolution of μ .

Furthermore,

- If μ is **non-arithmetic**, then

$$\lim_{t \rightarrow \infty} f(t) = \frac{1}{\lambda} \int_{-\infty}^{\infty} g(y) dy.$$

- If μ is **τ -arithmetic**, then for all $y \in [0, \tau)$,

$$\lim_{k \rightarrow \infty} f(k\tau + y) = \frac{\tau}{\lambda} \sum_{j=-\infty}^{\infty} g(j\tau + y).$$

Proof of Theorem 2, Part (2). We extend $m \mapsto r_m$ to a function $r : [0, \infty) \rightarrow \mathbb{N}$ via $r(x) = r_{\lfloor x \rfloor}$. It is easy to verify that Proposition 3.29 extends to the function r . For the rest of the proof we designate the remainder function

$$(37) \quad R : [0, \infty) \rightarrow \{-1, 0, 1\}, \quad R(x) = r(x) - 2r\left(\frac{x}{3}\right).$$

Since $r_1 = 0$, it follows that $R(x) = 0$ whenever $x \leq 1$.

Making the change of variables $x = e^t$ in (37) we obtain

$$r(e^t) = 2r\left(\frac{e^t}{3}\right) + R(e^t) = 2r(e^{t-\log 3}) + R(e^t).$$

Multiplying both sides by e^{-t/d_H} yields the renewal equation

$$(38) \quad f(t) = f(t - \log 3) + g(t) = \int_0^\infty f(t-y) \delta_{\log 3}(dy) + g(t),$$

where

$$(39) \quad f(t) := e^{-t/d_H} r(e^t) \quad \text{and} \quad g(t) := e^{-t/d_H} R(e^t).$$

It is clear that $f \in \mathcal{F}$.

To ensure that f is the unique solution to (38), we verify Conditions (R1) through (R3) of Lemma 3.30. Firstly $\mu = \delta_{\log 3}$, so $\lambda = \log 3$, verifying (R1). (R2) is validated by noting that the relevant integral equals $e^{-a \log 3} = 3^{-a} < 1$ for $a > 0$. Last but not least, since $x \mapsto R(x)$ has only jump discontinuities at the positive integers, it is straightforward to deduce that the set of discontinuities of g is discrete. In addition $g(t)$ decays exponentially in $|t|$, i.e.,

$$|g(t)| \begin{cases} \leq e^{-t/d_H}, & t > 0, \\ = 0, & t \leq 0. \end{cases}$$

This verifies (R3).

By Lemma 3.30, f is the unique solution to (38). As μ is a delta mass, we are in the τ -arithmetic case with $\tau = \log 3$, which implies the limit statement

$$\lim_{k \rightarrow \infty} f(k \log 3 + y) = \sum_{j=-\infty}^{\infty} g(j \log 3 + y) \quad \text{for all } y \in [0, \log 3),$$

which can be rewritten in terms of r and R as follows:

$$(40) \quad \lim_{k \rightarrow \infty} (3^k e^y)^{-1/d_H} r(3^k e^y) = \sum_{j=-\infty}^{\infty} (3^j e^y)^{-1/d_H} R(3^j e^y) \quad \text{for all } y \in [0, \log 3).$$

To deduce (3) we will replace $3^k e^y$ by x . This triggers a change of variables on the RHS of (40) and yields

$$x^{-1/d_H} r(x) = \sum_{j=-\infty}^{\infty} (3^j \tilde{x})^{-1/d_H} R(3^j \tilde{x}) + o(1) \quad \text{as } x \rightarrow \infty,$$

where $\tilde{x} := \tilde{x}(x) \in [1, 3)$ is the unique number such that $\log \tilde{x} \equiv \log x \pmod{\log 3}$. Note that since $R(x) = 0$ for $x \leq 1$, the terms with negative values of j do not contribute to the Fourier series. Hence we obtain (3) with

$$(41) \quad \mathcal{G}(\log x) = \mathcal{G}(\log \tilde{x}) = \sum_{j=0}^{\infty} (3^j \tilde{x})^{-1/d_H} R(3^j \tilde{x}).$$

Since $R(x)$ has a finite number of jump discontinuities on $[0, 4 \cdot 3^4)$, and it has a well-defined number of jumps on $[4 \cdot 3^n, 4 \cdot 3^{n+1})$, $n \geq 4$, at $a \cdot 3^n$, where $a \in \{4 + 2p, 4\frac{4}{9} + 2p, 4\frac{2}{3} + 2p, 5\frac{1}{3} + 2p \mid p \in \{0, 1, 2, 3\}\}$, it follows that $\mathcal{G}(\log x)$ has a finite number of jump discontinuities.

To obtain the identity (4), we restrict to $x \in [\frac{10}{9}, \frac{4}{3})$, in which case $\tilde{x} = x$. By Corollary 3.18 it follows that $R(3^j x) = 0$ for all $j \geq 2$. Meanwhile, $R(3^j x) = 1$ when $j = 1$, and $R(3^j x) = 0$ when $j = 0$. So $\mathcal{G}(\log x) = (3x)^{-1/d_H} = \frac{1}{2} x^{-1/d_H}$.

The proof of the global estimate (5) is given in §3.9. \square

Remark 3.31. Computing the \mathcal{G} function (41) for $\tilde{x} \in [1, \frac{10}{9})$ requires knowing $R(3^j \tilde{x})$ for all j , which can be obtained using Theorem 6, cf. Figure 11. This is a relatively tedious exercise, so we opt for a more geometric approach in making the global estimate (5).

3.9. Geometric estimate of sandpile growth. In this subsection we estimate the growth of the abelian sandpile cluster on SG , using only information about volumes of subsets of SG . The techniques described below have been applied to other graphs [11, 22], and appear to give close-to-optimal global lower bound on SG , cf. Figure 6. However these do not yield the necessary remainder estimate to produce the log-periodic oscillations shown in the previous subsection §3.8.

To be precise, we prove

Proposition 3.32. *For every $m \in \mathbb{N}$ we have*

$$\frac{(r_m)^{d_H} + 1}{m} \geq \frac{2}{9} \quad \text{and} \quad \frac{(r_m - 1)^{d_H}}{m} \leq \left(\frac{3}{4}\right)^{d_H}.$$

The bounds (5) follow from taking the limits $m \rightarrow \infty$ of the inequalities in this proposition.

Recall from Proposition 3.2, Part (1) that $B_o(r_m - 1) \subset A(m) \subset S(m) = B_o(r_m)$, where $A(m)$ and $S(m)$ are, respectively, the firing set and the receiving set corresponding to $(m\mathbb{1}_o)^\circ$.

Proof of Proposition 3.32, lower bound. Since $S(m) = B_o(r_m)$, and the maximal stable configuration has 3 chips everywhere (except at o where a max of 1 chip is allowed, but WLOG we may assume that m is even, so o carries 0 chip), we have

$$\frac{m}{3} \leq \#(\text{vertices in } B_o(r_m) \text{ occupied with a chip}) \leq |B_o(r_m)|.$$

So it suffices to give a good upper bound for $|B_o(r_m)|$.

Suppose $r_m = (1 - \epsilon)2^k$ for some $k \in \mathbb{N}$ and $2^{-p} \leq \epsilon < 2^{-(p-1)}$, $p \in \{2, \dots, k\}$. Observe that $B_o(r_m) \subset B_o((1 - 2^{-p})2^k)$, and that $B_o(2^k) \setminus B_o((1 - 2^{-p})2^k)$ is the union of 2^p copies of the graph G_{k-p} excluding the head vertex. Since $|V(G_k)| = \frac{3}{2}(3^k + 1)$, we deduce that

$$\begin{aligned} |B_o(r_m)| &\leq |B_o((1 - 2^{-p})2^k)| = \frac{3}{2}(3^k + 1) - 2^p \left[\frac{3}{2}(3^{k-p} + 1) - 1 \right] \\ &< \frac{3}{2} \left[3^k \left(1 - \left(\frac{2}{3} \right)^p \right) + 1 \right] < \frac{3}{2} \left[(r_m)^{d_H} \frac{1 - \epsilon^{d_H-1}}{(1 - \epsilon)^{d_H}} + 1 \right]. \end{aligned}$$

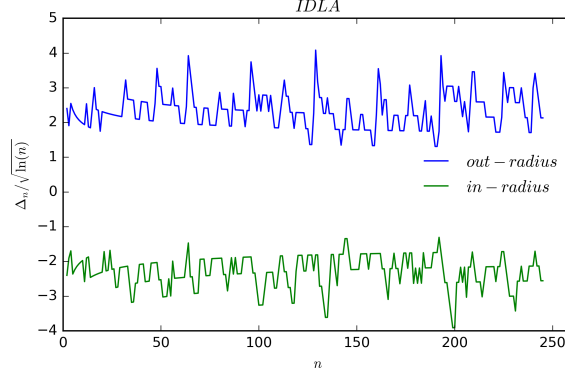


FIGURE 17. Maximal out-radius and minimal in-radius vs. the expected radius for 1000 realizations of the IDLA on SG .

Since

$$\sup_{\epsilon \in (0, \frac{1}{2})} \frac{1 - \epsilon^{d_H - 1}}{(1 - \epsilon)^{d_H}} = 1,$$

we conclude that

$$m \leq 3|B_o(r_m)| < \frac{9}{2}((r_m)^{d_H} + 1).$$

□

To prove the upper bound we invoke a result of Rossin [61].

Lemma 3.33 ([61, Lemme 15]). *Let X be a connected subgraph of G . The minimum number of grains needed for every vertex of X to topple at least once is equal to $|\text{in}(X)| + |C_G(X)|$, where $\text{in}(X)$ is the set of (internal) edges in X , $C_G(X) = \{(i, j) : i \in X, j \in V \setminus X\}$, and $|\cdot|$ denotes the cardinality of the edge set.*

Proof of Proposition 3.32, upper bound. Since $S(m) = B_o(r_m) \supset A(m)$, we can bound the mass needed to fill $B_o(r_m)$ from below by the mass needed to topple everywhere in $A(m)$.

Suppose $r_m = (1 - \epsilon)2^k + 1$ for some $k \in \mathbb{N}$ and $2^{-(p+1)} \leq \epsilon < 2^{-p}$, $p \in \{1, 2, \dots, k\}$. Since $A(m) \supset B_o(r_m - 1) \supset B_o((1 - 2^{-p})2^k)$, according to Lemma 3.33, we have

$$(42) \quad m \geq |\text{in}(A(m))| + |C_G(A(m))| \geq |\text{in}(B_o(r_m - 1))| \geq |\text{in}(B_o((1 - 2^{-p})2^k))|.$$

It is direct to check that $B_o(2^k) \setminus B_o((1 - 2^{-p})2^k)$ is the union of 2^p copies of the graph G_{k-p} . Since G_k has 3^{k+1} edges, we deduce that the RHS of (42) equals

$$3^{k+1} - 2^p 3^{k-p+1} = 3 \left(\frac{r_m - 1}{1 - \epsilon} \right)^{d_H} \left(1 - \left(\frac{2}{3} \right)^p \right) \geq 3(r_m - 1)^{d_H} \frac{1 - (2/3)^p}{(1 - 2^{-(p+1)})^{d_H}}.$$

Therefore

$$(43) \quad \frac{(r_m - 1)^{d_H}}{m} \leq \frac{1}{3} \frac{(1 - 2^{-(p+1)})^{d_H}}{1 - (2/3)^p}.$$

It can be checked explicitly that the function $x \mapsto \frac{(1 - 2^{-(x+1)})^{d_H}}{1 - (2/3)^x}$ is decreasing on $(0, \infty)$, and tends to 1 as $x \rightarrow \infty$. For a uniform estimate we can take $p = 1$ in (43) to obtain the claimed upper bound. □

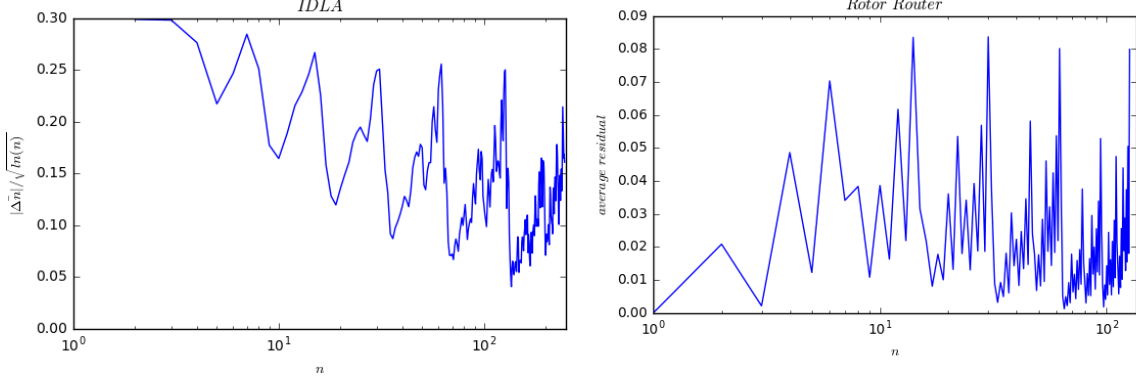


FIGURE 18. Sample average of the absolute value of the radial fluctuations about the expected radius, for 1000 realizations of the IDLA (left) and of rotor-router aggregation (right) on SG .

4. FLUCTUATIONS OF THE IDLA CLUSTER ON SG

In this section we present numerical results concerning fluctuations of the IDLA cluster. Proposition 1.1 implies that the limit shape is a ball in the graph metric, without quantifying the order of the fluctuations about the limit shape. In the case of \mathbb{Z}^d , it is proved that the fluctuations are of order $\sqrt{\log n}$ when $d = 2$, and of order $\log n$ when $d \geq 3$, cf. [2, 3, 35]. The second-named author has written the Python program “AutomataSG” [40] and performed simulations of IDLA on SG , which strongly suggest the following

Conjecture 4.1. *There exists $C > 0$ such that*

$$B_o(n - C\sqrt{\log n}) \subset \mathcal{I}(|B_o(n)|) \subset B_o(n + C\sqrt{\log n})$$

for all n , with probability 1.

To prove the $\sqrt{\log n}$ fluctuation one needs to show that growing a tentacle of length ℓ has a probability of order $\exp(-c\ell^2)$, which is the case on \mathbb{Z}^d , $d \geq 3$ [2, 3, 35], and on the comb lattice [4]. On SG we expect the proof techniques to go beyond what were used in [15], and involves careful potential theoretic analysis on SG .

Another salient feature we see numerically are the log-periodic oscillations in the rescaled radial fluctuations (by $\sqrt{\log n}$). These are present in both the sample maximum (Figure 17) and in the sample mean, rescaled by the expected radius $\sqrt{\log n}$, with the latter being more pronounced. We also simulated rotor-router aggregation where the rotor mechanisms are identical and fixed for all vertices, but the initial rotor configuration is randomized by choosing, independently for every vertex, each of the 4 (or 2 at o) possible rotor directions with equal probability. The resulting *unscaled* radial fluctuations also exhibits log-periodic oscillations (Figure 18).

Open Question 1. Prove the existence of log-periodic oscillations shown in Figures 17 and 18. Even better, characterize the almost-sure properties of the log-periodic oscillation (*e.g.* it contains a dense set of jump discontinuities).

We also expect a corresponding central limit theorem for the rescaled space-time fluctuations, though here we only investigate it numerically. Following [36] we Poissonize the IDLA process. Let $\{N(t) : t \geq 0\}$ be a rate-1 simple Poisson process, and consider the continuous-time IDLA process $\{\mathcal{I}(N(t)) : t \geq 0\}$ started from o . We pick a radius $r = \epsilon 2^k$ for $k \in \mathbb{N}$ and $\epsilon \in 1 - 2^{-p}$, $p \in \mathbb{N}$; observe that the sphere $S_o(r) = \{x \in SG : d(o, x) = r\}$ is an interval when $p = 1$, and is a union of disjoint intervals which is a pre-fractal approximation of the Cantor set when $p \geq 2$.

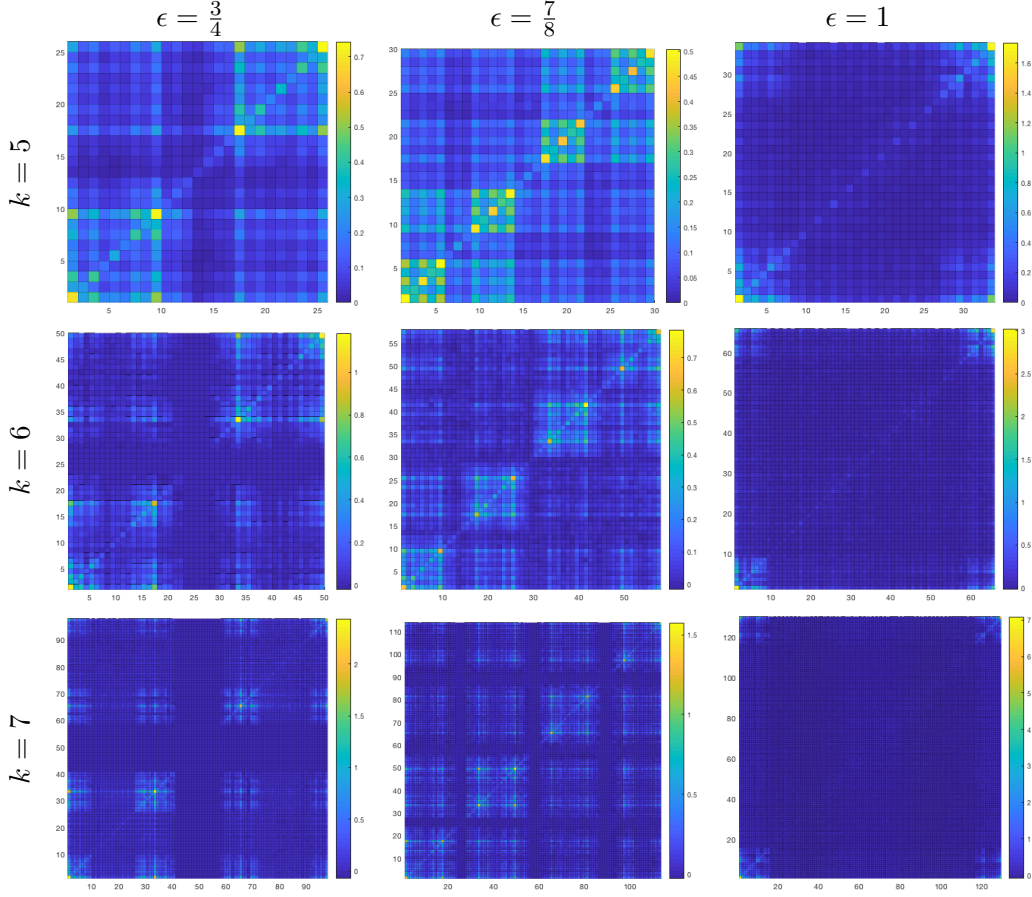


FIGURE 19. Simulations showing the covariance of the continuous-time IDLA height fluctuations $\text{Cov}\left(\frac{h(x)}{\sqrt{\log r}}, \frac{h(y)}{\sqrt{\log r}}\right)$ for $x, y \in S_o(r)$, where $r = \epsilon 2^k$ with $\epsilon \in \{\frac{3}{4}, \frac{7}{8}, 1\}$ and $k \in \{5, 6, 7\}$. Each plot is generated with 1000 simulations.

By Proposition 1.1, $\mathcal{I}(N(B_o(r)))$ is close to $B_o(r)$, so we consider radial fluctuations of the former about the sphere $S_o(r)$ by introducing the function $h : S_o(r) \rightarrow \mathbb{Z}$, $h(x) = A(x) - r$, where $A(x)$ is the height of the “tentacle” in the cluster $\mathcal{I}(N(B_o(r)))$ measured transversally from the sphere $S_o(r)$. (Our function h is related to the “lateness function” introduced by [36].) By the FKG inequality [26], the covariance of $h(x)$ and $h(y)$ is always nonnegative. In Figure 19 we present simulations of the covariance of the rescaled h function (by $\sqrt{\log n}$). From the data it appears that the covariance is higher when x and y are taken to lie in the same connected component of $SG \cap S_o(r)$, and furthermore, local maxima of the covariance occur when x and y are both cut points. This may be explained by the fact that tentacles are rooted from the cut points.

5. OPEN QUESTIONS

We close this paper with some outstanding questions and future directions.

Extensions to nested fractals. In light of Theorem 3, it is natural to ask if there are other examples where the limit shapes of the four Laplacian growth models coincide. Some potential candidates are the Vicsek tree (Figure 20a), the planar Sierpinski gaskets $SG(m)$ (Figure 20b, whereupon rotor walks are studied in [27]), and higher-dimensional Sierpinski simplices (Figure 20c), all of which are **nested fractals** as defined by Lindström [52].

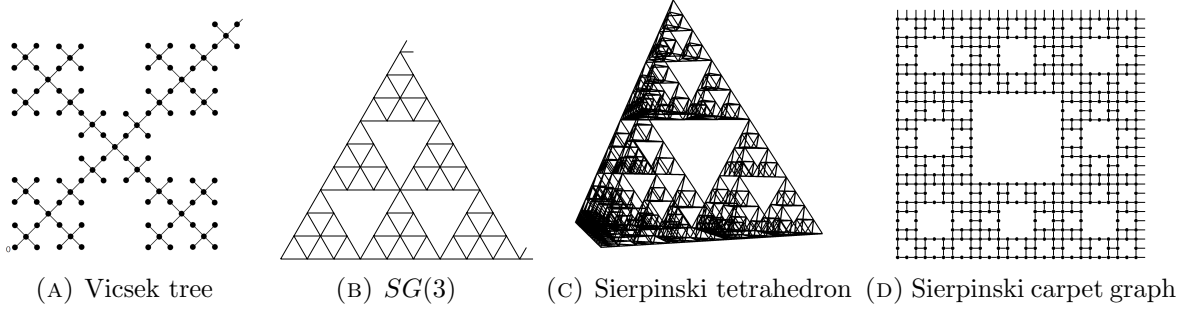


FIGURE 20. A sample of self-similar fractal graphs.

Conjecture 5.1. *Limit shape universality of single-source Laplacian growth models holds on nested fractal graphs, if the starting vertex o is chosen such that all balls $B_o(n)$ in the graph metric have spatial symmetry.*

Open Question 2. To what extent can one establish log-periodic oscillations in Laplacian growth models on nested fractal graphs?

Recent simulations by Ilias Stitou suggest that Conjecture 5.1 holds on the Vicsek tree and on $SG(3)$. In particular, log-periodic oscillations are present in the sandpile growth.

From a rigorous perspective, we expect Conjecture 5.1 to hold amongst divisible sandpiles, IDLA, and rotor-router aggregation at the least. Since the harmonic measure on the sphere (in the graph metric) is approximately uniform, this should imply a spherical shape theorem for the divisible sandpiles. Consequently, we can use the same strategy outlined in §1.4.1 to obtain the same limit shapes for the IDLA or rotor-router cluster, respectively.

The more delicate question concerns the abelian sandpile model. For tree nested fractal graphs, this can be addressed using results from [45]. For non-tree nested fractal graphs, the problem appears to be open to the best of our knowledge. (See also [22] for numerical results of the sandpile model on various gasket-type fractal graphs.)

Explosions in sandpile growth. An unexpected feature of the sandpile growth on SG is the presence of radial explosions, which do not appear on \mathbb{Z}^d or trees.

Open Question 3. Does radial explosion of sandpile growth appear on other non-tree nested fractal graphs?

It would seem that the explosion comes from a combination of the loop and the cut point structures of the fractal graph. However, Stitou’s simulations show there is *no* explosion on $SG(3)$ (Figure 20b), despite it having the stated properties. It thus appears that SG may be an exception rather than the rule, even among this class of fractal graphs. A careful study of the corresponding sandpile group may provide clues to resolving this question.

Open Question 4. Study Laplacian growth models and the single-source abelian sandpile model on the Sierpinski tetrahedron (Figure 20c). In particular, what does the cluster (and in the case of the abelian sandpile model, the sandpile configuration) look like when restricted to a cross-section of the tetrahedron that is isomorphic to the two-dimensional gasket?

Scaling limits of the sandpile patterns on SG . The appearance of self-similar sandpile tiles (Figure 9) suggests that there is a scaling limit of the abelian sandpile patterns restricted to the “bulk.” A plausible limit statement is as follows: For a fixed $k \in [4, 12)$, the sequence of configurations $\left\{ 2^{-n} (k \cdot 3^n \mathbb{1}_o)^\circ|_{G_n^{(s)}} \right\}_{n=1}^\infty$ converges to a height function on the limit fractal K . Furthermore, we conjecture that this convergence takes place in the weak- $*$ $L^\infty(K, \nu)$ topology (ν is the standard

self-similar measure on K) along the full sequence indexed by mass $m \rightarrow \infty$. Roughly speaking this says that local averages of the pattern colors in the bulk converges to a function on K . The conjecture is inspired by the elliptic PDE arguments of Pegden and Smart [57] showing the sandpile pattern convergence on \mathbb{Z}^d .

Other single-source and multi-source growth models on SG . Throughout this paper we assumed that particles are launched from a single corner vertex o of SG . One may ask what happens if they are launched from a fixed vertex which is not o , or from multiple vertices. (In the case of \mathbb{Z}^d see [49].) This is very much an analytic problem as it is probabilistic and combinatorial, requiring fine analysis of the Dirichlet (or obstacle) problem on subsets of SG . We expect that recent results of Qiu, Strichartz, and collaborators [29, 60] may be applicable for this purpose.

Another interesting initial condition to explore is the product Bernoulli $\{4 - \delta, 4 + \delta\}$ cluster: that is, start with a nonempty subset of SG (say, $B_o(r)$ for some $r \in \mathbb{N}$) wherein every vertex independently carries either $4 - \delta$ or $4 + \delta$ chips with probability $\frac{1}{2}$. According to simulations by Ahmed Bou-Rabee (Figure 21), it is conjectured that the sandpile cluster exhibit a two-phase pattern structure, where the patterns in the inner ball (the support of the initial cluster) becomes noisy, while the outer annulus carries patterns reminiscent of those in the deterministic single-source sandpile.

Sandpile Markov chain on fractal graphs. In this paper we solved the deterministic abelian sandpile growth problem from a single source. A related, but different, problem is to study the Markov chain on \mathcal{R}_G under stationarity. Recalling that (\mathcal{R}_G, \oplus) is a finite abelian group, it is a standard fact that the stationary distribution is a uniform on \mathcal{R}_G . Besides the works of Daerden *et al.* [17, 18] and Matter [55, Chapter 5] mentioned in Remark 1.4, it would be interesting to exploit the burning bijection and make connections with recent results on spanning trees and Laplacian determinants on fractal graphs [1, 13, 14, 16, 65]. A yet unsolved problem is to compute the average number of chips per vertex, or the sandpile density, on subgraphs of SG under stationarity.

Laplacian growth models on the Sierpinski carpet. One may also perform the same analysis on the Sierpinski carpet graph SC (see Figure 20d), an infinitely ramified fractal. For concreteness we discuss only the case where m particles are launched from the bottom-left corner vertex of SC . Wilfried Huss has performed simulations on both the rotor-router aggregation and the IDLA, *cf.* [32, Figures 8.2 and 8.3]. (Both sandpile problems on SC are open.) His key observations were that given a fixed number of particles, the cluster shapes of the two models look qualitatively similar. However, as m increases, a periodic family of limit shapes, as opposed to a single limit shape, appears to develop in both models. Due to the difficulty in the analysis on the Sierpinski carpet (see [8] for a summary of the state of the art, and references therein for details), we are unable to address Huss' observations rigorously at the moment.

Do limit shapes coincide on different graphs approximating the same space? We end the paper with the following semi-vague question.

Open Question 5. Let $(G_n^{(1)})_n$ and $(G_n^{(2)})_n$ be two sequences of bounded-degree unweighted graphs rooted at a common point o . Assume that both sequences converge, in the pointed Gromov-Hausdorff sense (or is there a better mode of convergence?), to the same metric measure space (X, d, μ) rooted at o . Prove or disprove (with possibly extra conditions) that the clusters associated with any of the Laplacian growth models on $\bigcup_{n \geq 1} G_n^{(1)}$ and $\bigcup_{n \geq 1} G_n^{(2)}$ started from o have the same limit shape.

As an example, take $G_n^{(1)} = (n^{-1}\mathbb{Z})^2$ and $G_n^{(2)}$ to be the hexagonal lattice rooted at o with lattice spacing $1/n$. Another example is to take $G_n^{(1)}$ to be the level- n Sierpinski gasket graph, and $G_n^{(2)}$ to be the level- n Hanoi tower graph (Figure 7). Both sequences of graphs are rooted at the corner vertex o and scaled such that their diameters stay constant.

It will be useful to investigate this problem for the divisible sandpile model first.

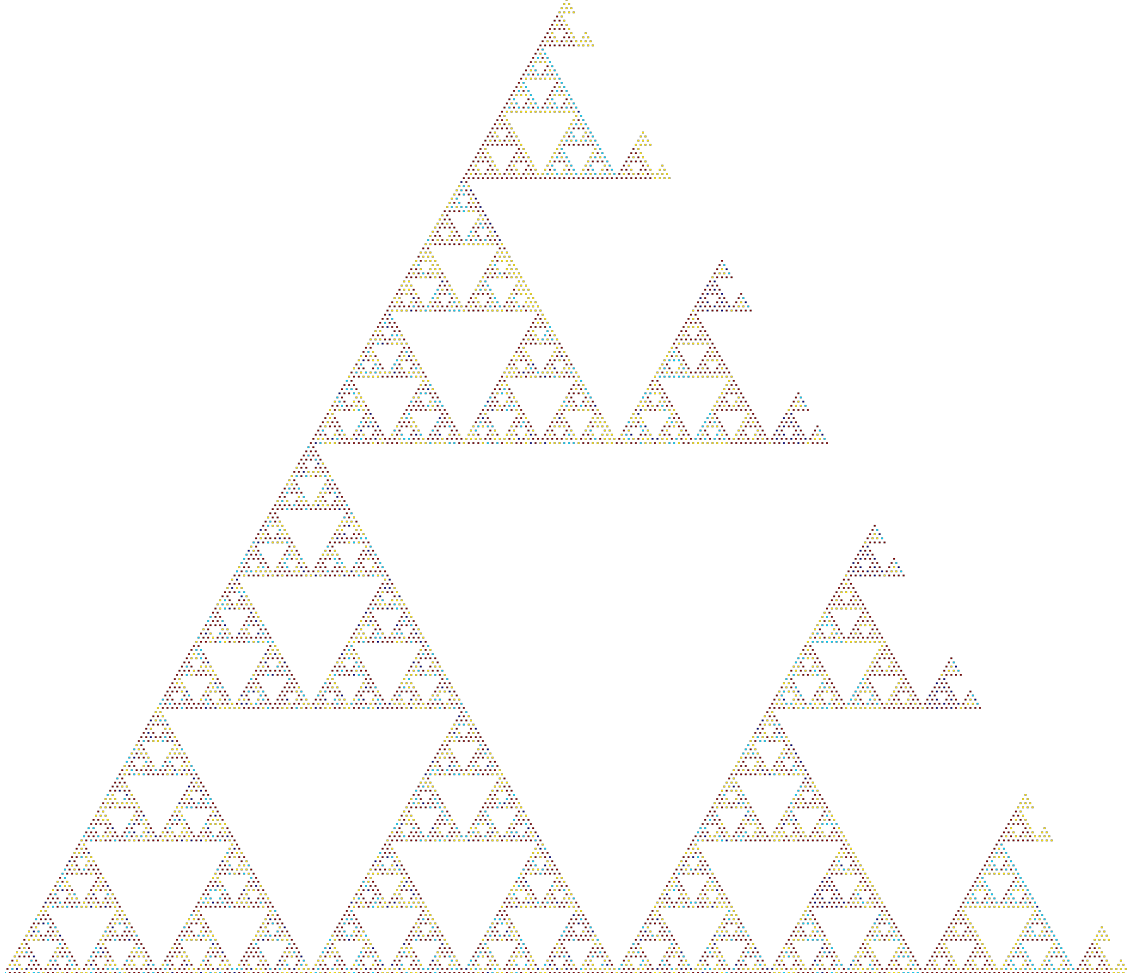


FIGURE 21. A realization of the abelian sandpile configuration starting from the product Bernoulli 3-5 initial configuration on $B_o(160)$. The stable configuration exhibits a two-phase pattern structure: noisy patterns on the inner ball (the support of the initial configuration), and patterns reminiscent of the deterministic single-source sandpile on the outer annulus. Image courtesy of Ahmed Bou-Rabee.

Acknowledgements. JPC would like to thank Lionel Levine for providing many useful suggestions and feedbacks; Ilias Stitou for running computations which helped clarify the mechanisms described in the paper; Ahmed Bou-Rabee for useful discussions concerning the open questions in §5; and Elmar Teufl for bringing to his attention the history behind the Sierpinski arrowhead curve. He also acknowledges inspiring conversations with Richard Kenyon, Tatiana Nagnibeda, Ecaterina Sava-Huss, Robert Strichartz, Alexander Teplyaev, and Wolfgang Woess. JKF would like to thank Patrick Crotty for his help in setting up simulations on the Ho Computer Cluster at Colgate University.

REFERENCES

- [1] Jason A. Anema and Konstantinos Tsougkas, *Counting spanning trees on fractal graphs and their asymptotic complexity*, J. Phys. A **49** (2016), no. 35, 355101, 21, DOI 10.1088/1751-8113/49/35/355101. MR3537208 ↑50
- [2] Amine Asselah and Alexandre Gaudillièr, *From logarithmic to subdiffusive polynomial fluctuations for internal DLA and related growth models*, Ann. Probab. **41** (2013), no. 3A, 1115–1159, DOI 10.1214/12-AOP762. MR3098673 ↑8, 47

- [3] ———, *Sublogarithmic fluctuations for internal DLA*, Ann. Probab. **41** (2013), no. 3A, 1160–1179, DOI 10.1214/11-AOP735. MR3098674 ↑8, 47
- [4] Amine Asselah and Houda Rahmani, *Fluctuations for internal DLA on the comb*, Ann. Inst. Henri Poincaré Probab. Stat. **52** (2016), no. 1, 58–83, DOI 10.1214/14-AIHP629 (English, with English and French summaries). MR3449294 ↑47
- [5] Per Bak, Chao Tang, and Kurt Wiesenfeld, *Self-organized criticality: An explanation of the $1/f$ noise*, Phys. Rev. Lett. **59** (1987), no. 4, 381–384, DOI 10.1103/PhysRevLett.59.381. ↑2
- [6] ———, *Self-organized criticality*, Phys. Rev. A (3) **38** (1988), no. 1, 364–374, DOI 10.1103/PhysRevA.38.364. MR949160 ↑2
- [7] Martin T. Barlow, *Diffusions on fractals*, Lectures on probability theory and statistics (Saint-Flour, 1995), Lecture Notes in Math., vol. 1690, Springer, Berlin, 1998, pp. 1–121, DOI 10.1007/BFb0092537. MR1668115 ↑9
- [8] ———, *Analysis on the Sierpinski carpet*, Analysis and geometry of metric measure spaces, CRM Proc. Lecture Notes, vol. 56, Amer. Math. Soc., Providence, RI, 2013, pp. 27–53. MR3060498 ↑50
- [9] Norman L. Biggs, *Chip-firing and the critical group of a graph*, J. Algebraic Combin. **9** (1999), no. 1, 25–45, DOI 10.1023/A:1018611014097. MR1676732 ↑10
- [10] Benjamin Bond and Lionel Levine, *Abelian networks I. Foundations and examples*, SIAM J. Discrete Math. **30** (2016), no. 2, 856–874, DOI 10.1137/15M1030984. MR3493110 ↑4
- [11] Yvan Le Borgne and Dominique Rossin, *On the identity of the sandpile group*, Discrete Math. **256** (2002), no. 3, 775–790, DOI 10.1016/S0012-365X(02)00347-3 (English, with English and French summaries). LaCIM 2000 Conference on Combinatorics, Computer Science and Applications (Montreal, QC). MR1935788 ↑45
- [12] Sergio Caracciolo, Guglielmo Paoletti, and Andrea Sportiello, *Deterministic Abelian sandpile and square-triangle tilings*, Combinatorial methods in topology and algebra, Springer INdAM Ser., vol. 12, Springer, Cham, 2015, pp. 127–136. MR3467337 ↑3
- [13] Shu-Chiuan Chang and Lung-Chi Chen, *Structure of spanning trees on the two-dimensional Sierpinski gasket*, Discrete Math. Theor. Comput. Sci. **12** (2010), no. 3, 151–176. MR2786472 ↑50
- [14] Shu-Chiuan Chang, Lung-Chi Chen, and Wei-Shih Yang, *Spanning trees on the Sierpinski gasket*, J. Stat. Phys. **126** (2007), no. 3, 649–667, DOI 10.1007/s10955-006-9262-0. MR2294471 ↑50
- [15] Joe P. Chen, Wilfried Huss, Ecaterina Sava-Huss, and Alexander Teplyaev, *Internal DLA on Sierpinski gasket graphs*, Analysis and Geometry on Manifolds and Graphs, London Mathematical Society Lecture Notes, Cambridge University Press (2019+). To appear. Also available at <https://arxiv.org/abs/1702.04017>. ↑4, 5, 8, 9, 47
- [16] Joe P. Chen, Alexander Teplyaev, and Konstantinos Tsoungkas, *Regularized Laplacian determinants of self-similar fractals*, Lett. Math. Phys. **108** (2018), no. 6, 1563–1579, DOI 10.1007/s11005-017-1027-y. MR3797758 ↑50
- [17] Frank Daerden, Vyacheslav B. Priezzhev, and Carlo Vanderzande, *Waves in the sandpile model on fractal lattices*, Physica A: Statistical Mechanics and its Applications **292** (2001), no. 14, 43–54, DOI 10.1016/S0378-4371(00)00553-7. ↑7, 50
- [18] Frank Daerden and Carlo Vanderzande, *Sandpiles on a Sierpinski gasket*, Physica A: Statistical Mechanics and its Applications **256** (1998), no. 3, 533–546. ↑7, 50
- [19] Deepak Dhar, *Self-organized critical state of sandpile automaton models*, Phys. Rev. Lett. **64** (1990), 1613–1616, DOI 10.1103/PhysRevLett.64.1613. ↑10
- [20] Persi Diaconis and William Fulton, *A growth model, a game, an algebra, Lagrange inversion, and characteristic classes*, Rend. Sem. Mat. Univ. Politec. Torino **49** (1991), no. 1, 95–119 (1993). Commutative algebra and algebraic geometry, II (Italian) (Turin, 1990). MR1218674 ↑4
- [21] Hugo Duminil-Copin, Cyrille Lucas, Ariel Yadin, and Amir Yehudayoff, *Containing internal diffusion limited aggregation*, Electron. Commun. Probab. **18** (2013), no. 50, 8, DOI 10.1214/ECP.v18-2862. MR3078013 ↑9
- [22] Samantha Fairchild, Ilse Haim, Rafael G. Setra, Robert S. Strichartz, and Travis Westura, *The Abelian Sandpile Model on Fractal Graphs*, arXiv preprint (2016). Available at <https://arxiv.org/abs/1602.03424>. ↑3, 7, 11, 12, 13, 45, 49
- [23] Kenneth Falconer, *Techniques in fractal geometry*, John Wiley & Sons, Ltd., Chichester, 1997. MR1449135 ↑43
- [24] ———, *Fractal geometry: Mathematical foundations and applications*, 3rd ed., John Wiley & Sons, Ltd., Chichester, 2014. MR3236784 ↑4
- [25] Anne Fey, Lionel Levine, and Yuval Peres, *Growth rates and explosions in sandpiles*, J. Stat. Phys. **138** (2010), no. 1-3, 143–159, DOI 10.1007/s10955-009-9899-6. MR2594895 ↑8
- [26] Cees M. Fortuin, Pieter W. Kasteleyn, and Jean Ginibre, *Correlation inequalities on some partially ordered sets*, Comm. Math. Phys. **22** (1971), 89–103. MR0309498 ↑48
- [27] Uta Freiberg and Christoph Thäle, *Exact computation and approximation of stochastic and analytic parameters of generalized Sierpinski gaskets*, Methodol. Comput. Appl. Probab. **15** (2013), no. 3, 485–509. MR3085876 ↑48
- [28] Tobias Friedrich and Lionel Levine, *Fast simulation of large-scale growth models*, Random Structures Algorithms **42** (2013), no. 2, 185–213, DOI 10.1002/rsa.20412. MR3019397 ↑9, 17, 18, 19

- [29] Zijian Guo, Rachel Kogan, Hua Qiu, and Robert S. Strichartz, *Boundary value problems for a family of domains in the Sierpinski gasket*, Illinois J. Math. **58** (2014), no. 2, 497–519. MR3367660 ↑50
- [30] David Hilbert, *Ueber die stetige Abbildung einer Linie auf ein Flächenstück*, Math. Ann. **38** (1891), no. 3, 459–460, DOI 10.1007/BF01199431 (German). MR1510683 ↑14
- [31] Alexander E. Holroyd, Lionel Levine, Karola Mészáros, Yuval Peres, James Propp, and David B. Wilson, *Chip-firing and rotor-routing on directed graphs*, In and out of equilibrium. 2, Progr. Probab., vol. 60, Birkhäuser, Basel, 2008, pp. 331–364. MR2477390 ↑4
- [32] Wilfried Huss, *Internal aggregation models*, PhD Thesis, Technische Universität Graz, 2010. Available at <https://www.math.tugraz.at/~huss/new/publications/phdthesis.pdf>. ↑50
- [33] Wilfried Huss and Ecaterina Sava-Huss, *Divisible sandpile on Sierpinski gasket graphs*, Fractals **27** (2019), no. 3, 1950032, 14, DOI 10.1142/S0218348X19500324. MR3957187 ↑4, 5, 8, 9, 17, 19, 20
- [34] Antal A. Járai, *Sandpile models*, Probab. Surv. **15** (2018), 243–306, DOI 10.1214/14-PS228. MR3857602 ↑9, 10
- [35] David Jerison, Lionel Levine, and Scott Sheffield, *Logarithmic fluctuations for internal DLA*, J. Amer. Math. Soc. **25** (2012), no. 1, 271–301, DOI 10.1090/S0894-0347-2011-00716-9. MR2833484 ↑8, 47
- [36] ———, *Internal DLA and the Gaussian free field*, Duke Math. J. **163** (2014), no. 2, 267–308, DOI 10.1215/00127094-2430259. MR3161315 ↑8, 47, 48
- [37] Nikita Kalinin and Mikhail Shkolnikov, *Tropical curves in sandpiles*, C. R. Math. Acad. Sci. Paris **354** (2016), no. 2, 125–130, DOI 10.1016/j.crma.2015.11.003 (English, with English and French summaries). MR3456886 ↑3
- [38] Jun Kigami, *Analysis on fractals*, Cambridge Tracts in Mathematics, vol. 143, Cambridge University Press, Cambridge, 2001. MR1840042 ↑9
- [39] Jun Kigami and Michel L. Lapidus, *Weyl’s problem for the spectral distribution of Laplacians on p.c.f. self-similar fractals*, Comm. Math. Phys. **158** (1993), no. 1, 93–125. MR1243717 ↑43
- [40] Jonah Kudler-Flam, *AutomataSG*, posted on 2018, DOI 10.5281/zenodo.1246802. Available at <https://github.com/jkudlerflam/AutomataSG>. ↑5, 47
- [41] Brigita Kutnjak-Urbanc, Stefano Zapperi, Sava Milošević, and H. Eugene Stanley, *Sandpile model on the Sierpinski gasket fractal*, Phys. Rev. E **54** (1996), 272–277, DOI 10.1103/PhysRevE.54.272. ↑7
- [42] Steven P. Lalley, *Renewal theorems in symbolic dynamics, with applications to geodesic flows, non-Euclidean tessellations and their fractal limits*, Acta Math. **163** (1989), no. 1-2, 1–55, DOI 10.1007/BF02392732. MR1007619 ↑43
- [43] Gregory F. Lawler, *Subdiffusive fluctuations for internal diffusion limited aggregation*, Ann. Probab. **23** (1995), no. 1, 71–86. MR1330761 ↑8, 9
- [44] Gregory F. Lawler, Maury Bramson, and David Griffeath, *Internal diffusion limited aggregation*, Ann. Probab. **20** (1992), no. 4, 2117–2140. MR1188055 ↑2, 8, 9
- [45] Lionel Levine, *The sandpile group of a tree*, European J. Combin. **30** (2009), no. 4, 1026–1035, DOI 10.1016/j.ejc.2008.02.014. MR2504661 ↑49
- [46] Lionel Levine, Wesley Pegden, and Charles K. Smart, *Apollonian structure in the Abelian sandpile*, Geom. Funct. Anal. **26** (2016), no. 1, 306–336, DOI 10.1007/s00039-016-0358-7. MR3494492 ↑2
- [47] ———, *The Apollonian structure of integer superharmonic matrices*, Ann. of Math. (2) **186** (2017), no. 1, 1–67, DOI 10.4007/annals.2017.186.1.1. MR3664999 ↑2
- [48] Lionel Levine and Yuval Peres, *Strong spherical asymptotics for rotor-router aggregation and the divisible sandpile*, Potential Anal. **30** (2009), no. 1, 1–27, DOI 10.1007/s11118-008-9104-6. MR2465710 ↑2, 5, 8, 9
- [49] ———, *Scaling limits for internal aggregation models with multiple sources*, J. Anal. Math. **111** (2010), 151–219, DOI 10.1007/s11854-010-0015-2. MR2747064 ↑50
- [50] ———, *Laplacian growth, sandpiles, and scaling limits*, Bull. Amer. Math. Soc. (N.S.) **54** (2017), no. 3, 355–382, DOI 10.1090/bull/1573. MR3662912 ↑2, 4, 8, 9
- [51] Michael Levitin and Dmitri Vassiliev, *Spectral asymptotics, renewal theorem, and the Berry conjecture for a class of fractals*, Proc. London Math. Soc. (3) **72** (1996), no. 1, 188–214, DOI 10.1112/plms/s3-72.1.188. MR1357092 ↑43
- [52] Tom Lindstrøm, *Brownian motion on nested fractals*, Mem. Amer. Math. Soc. **83** (1990), no. 420, iv+128, DOI 10.1090/memo/0420. MR988082 ↑48
- [53] Dino Lorenzini, *Smith normal form and Laplacians*, J. Combin. Theory Ser. B **98** (2008), no. 6, 1271–1300, DOI 10.1016/j.jctb.2008.02.002. MR2462319 ↑10
- [54] Satya N. Majumdar and Deepak Dhar, *Height correlations in the Abelian sandpile model*, J. Phys. A: Math. Gen. **24** (1991), L357. ↑10
- [55] Michel Matter, *Abelian Sandpile Model on randomly rooted graphs*, PhD Thesis, Université de Genève, 2012. Available at <https://archive-ouverte.unige.ch/unige:21849>. ↑7, 50
- [56] Giuseppe Peano, *Sur une courbe, qui remplit toute une aire plane*, Math. Ann. **36** (1890), no. 1, 157–160, DOI 10.1007/BF01199438 (French). MR1510617 ↑14

- [57] Wesley Pegden and Charles K. Smart, *Convergence of the Abelian sandpile*, Duke Math. J. **162** (2013), no. 4, 627–642, DOI 10.1215/00127094-2079677. MR3039676 ↑2, 50
- [58] ———, *Stability of patterns in the Abelian sandpile*, arXiv preprint (2017). Available at <https://arxiv.org/abs/1708.09432>. ↑3
- [59] David Perkinson, Jacob Perlman, and John Wilmes, *Primer for the algebraic geometry of sandpiles*, Tropical and non-Archimedean geometry, Contemp. Math., vol. 605, Amer. Math. Soc., Providence, RI, 2013, pp. 211–256, DOI 10.1090/conm/605/12117. MR3204273 ↑9
- [60] Hua Qiu and Robert S. Strichartz, *Mean value properties of harmonic functions on Sierpinski gasket type fractals*, J. Fourier Anal. Appl. **19** (2013), no. 5, 943–966, DOI 10.1007/s00041-013-9279-0. MR3110587 ↑50
- [61] Dominique Rossin, *Propriétés combinatoires de certaines familles d’automates cellulaires*, PhD Thesis, Ecole Polytechnique X, 2000. Available at <https://pastel.archives-ouvertes.fr/tel-00011297/file/THESE.pdf>. ↑46
- [62] Waclaw Sierpinski, *Sur une courbe dont tout point est un point de ramification*, Compt. Rend. Acad. Sci. Paris **160** (1915), 302–305. ↑14
- [63] Robert S. Strichartz, *Some properties of Laplacians on fractals*, J. Funct. Anal. **164** (1999), no. 2, 181–208. MR1695571 ↑20
- [64] ———, *Differential equations on fractals: A tutorial*, Princeton University Press, Princeton, NJ, 2006. MR2246975 ↑9
- [65] Elmar Teufl and Stephan Wagner, *The number of spanning trees in self-similar graphs*, Ann. Comb. **15** (2011), no. 2, 355–380, DOI 10.1007/s00026-011-0100-y. MR2813521 ↑50

(Joe P. Chen) DEPARTMENT OF MATHEMATICS, COLGATE UNIVERSITY, HAMILTON, NY 13346, USA.

E-mail address: `jpchen@colgate.edu`

URL: <http://math.colgate.edu/~jpchen>

(Jonah Kudler-Flam) KADANOFF CENTER FOR THEORETICAL PHYSICS, THE UNIVERSITY OF CHICAGO, CHICAGO, IL 60637, USA.

E-mail address: `jkudlerflam@uchicago.edu`